This thesis entitled

Dynamics of message interchange between stochastic units in the contexts of human communication behaviour and spiking neurons

Written by

Andreas Kaltenbrunner

And directed by

Prof. Dr. Vicente López

Has been approved by the Department of Information and Communications Technologies

Barcelona, September 2007

A thesis submitted in partial fulfillment of the requirements for the Degree of *Doctor per la Universitat Pompeu Fabra*

Para Yolanda y Nikolas

Agradecimientos

Quisiera agradecer a mi tutor de tesis, Vicente López, el haber confiado en mi cuando me presenté en su despacho hace cuatro años, diciéndole que quería hacer un doctorado, sin saber ni dónde me metía ni qué significaba hacer ciencia. Por darme esa oportunidad de crecimiento personal, profesional e intelectual que significa hacer un doctorado. No solo ha estado siempre disponible para compartir conmigo sus amplios conocimientos, sino que ha sabido transmitirme lo esencial de la ciencia: los mecanismos básicos para a la generación y presentación de nuevos conocimientos.

También quisiera agradecer a quienes han contribuido en la realización de este trabajo: Ayman Moghnieh, Rodrigo Meza, Josep Blat y sobre todo a Vicenç Gómez por un sinfín de discusiones y por estar siempre disponible para ayudar en la solución de cualquier problema.

Tampoco puedo olvidarme de quienes me han ayudado con sus comentarios a mejorar el trabajo presentado: Alberto Suárez, Serge Thill, Adan Garriga, Ernest Montbrió, Anders Ledberg, Alex Roxin y Gustavo Deco.

Muchas gracias también a los organizadores de mi estancia en la University of Leicester: Ralph Andrzejak y sobre todo a Rodrigo Quian Quiroga, por su cordial acogida.

Gracias a mis compañeros de doctorado por compartir buenos y malos momentos y por acompañarme en una parte tan importante de mi vida.

Y por ultimo, aunque sin restarles por ello protagonismo, doy las gracias a mis padres y a mis hermanos Martin y Karin, y de manera muy especial a Nikolas por llenar mi vida con sus risas y a Yolanda por apoyarme siempre.

Es ist Unsinn
sagt die Vernunft
Es ist was es ist
sagt die Liebe

Es ist Unglück
sagt die Berechnung
Es ist nichts als Schmerz
sagt die Angst
Es ist aussichtslos
sagt die Einsicht
Es ist was es ist
sagt die Liebe

Es ist lächerlich
sagt der Stolz
Es ist leichtsinnig
sagt die Vorsicht
Es ist unmöglich
sagt die Erfahrung
Es ist was es ist
sagt die Liebe

Erich Fried.

Abstract

This thesis deals with two different subjects concerning dynamics of message interchange between stochastic units.

First, we discuss a theoretical model of an ensemble of stochastic non-leaky integrate-and-fire neurons with global, delayed and excitatory coupling and a small refractory period. Simulations with adiabatic changes of the coupling strength indicate the presence of a phase transition accompanied by a hysteresis around a critical coupling strength. Below the critical coupling production of spikes in the ensemble is governed by the stochastic dynamics whereas for coupling greater than the critical value the stochastic dynamics looses its influence and the units organize into several clusters with self-sustained activity. All units within one cluster spike in unison and the clusters themselves are phase-locked. Theoretical analysis leads to upper and lower bounds for the average inter-spike interval of the ensemble valid for all possible coupling strengths. The bounds allow to calculate the limit behavior for large ensembles and characterize the phase transition analytically. These results may be extensible to pulse coupled oscillators.

The second part is focused on the analysis of human communication behavior. We examine the many-to-many social communication activity on the popular technology-news website Slashdot. To find regular patterns in the activity we have concentrated in the dynamics of message production without considering semantic relations. Regular temporal patterns have been found in the reaction times of both the community and single users to a news-post. The statistics of these activities follow log-normal distributions. Daily and weekly oscillatory cycles, which cause slight variations of this simple behavior, are identified. The findings are remarkable since the distribution of the number of comments per users, which is also analyzed, indicates a great amount of heterogeneity in the community. The reader may find surprising that only a few parameters, allow a detailed description, or even prediction, of social many-to-many information exchange in this kind of popular public spaces.

Resumen

En esta tesis trata de dos temas diferentes referente a la dinámica de intercambio de mensajes entre unidades estocásticas.

Primero, discutimos un modelo teórico de un conjunto de neuronas estocásticas tipo integración-y-disparo con integración sin pérdidas, un pequeño periodo refractario, y con acoplamiento global y retardado. Simulaciones con cambios adiabáticos de la fuerza del acoplamiento indican la presencia de una transición de fase acompañada por una histéresis alrededor de un valor crítico de la fuerza del acoplamiento. Por debajo del acoplamiento crítico la producción de disparos es gobernada por la dinámica estocástica, mientras que por encima del valor crítico la dinámica estocástica pierde su influencia y las unidades se organizan en varios subgrupos con actividad auto-sostenida. Todas las unidades de un subgrupo disparan al unísono y los subgrupos entre sí están sincronizados fuera de fase. Un análisis teórico lleva a cotas superiores e inferiores para el promedio del tiempo entre dos disparos de la población. Estas cotas son válidas para todos los posibles valores de la fuerza del acoplamiento. Las cotas permiten calcular el comportamiento límite para conjuntos grandes y caracterizar la transición de fase analíticamente. Estos resultados pueden ser extensibles a osciladores acoplados por pulsos.

La segunda parte se centra en el análisis de patrones de comportamiento en comunicación humana. Examinamos la actividad causada por comunicación entre comunidades de usuarios en Slashdot, un popular sitio web de noticias relacionados con tecnología. Para encontrar patrones regulares en la actividad nos hemos concentrado en la dinámica de producción de mensajes sin considerar relaciones semánticas. Se han encontrado patrones regulares en el tiempo de reacción a una nueva noticia tanto para la comunidad como para usuarios individuales. La estadística de estas actividades sigue distribuciones log-normales. Se identifican ciclos oscilatorios diarios y semanales, que causan variaciones leves de este simple comportamiento. Los resultados son notables puesto que la distribución del número de comentarios por usuarios, también analizada en este estudio, indica una gran cantidad

de heterogeneidad en la comunidad. El lector puede encontrar sorprendente que pocos parámetros, permiten una descripción detallada y pueden permitir la predicción del intercambio social de información entre multitudes en esta clase de espacios públicos populares.

Contents

List of Figures

List of Tables

Outline of Dissertation

This thesis is organized into three parts. Part I gives an introduction into some of the theoretical background needed for understanding this tesis. Part II and III form each of them an autonomous component which can be read independently from the other. Both deal with different aspects of the dynamics of message interchange between stochastic units. The first mainly treats of ensembles of stochastic integrate-and-fire model neurons and the second one analyses the communication patterns in a large online community. An introduction and motivation of the different problems can be found at the beginning of each part. In what follows, we give a detailed description of the contents of each chapter.

PART I: Theoretical Background

Chapter 1: This chapter explains the terminology used in this work when referring to locking and synchronization phenomena in networks of weakly and pulse coupled oscillators. A short introduction into those two concepts is given as well.

Chapter 2: We give an introduction into the diffusion process and its role in neural dynamics and models of human reaction times. The stochastic integrate-and-fire neuron, its relation with pulse coupled oscillators and the model used in Part II of this thesis are explained.

PART II: Neural populations

Chapter 3: A short introduction into the study of synchronization in networks of neuron-like elements which interchange messages is given and the relation of our findings with those in the literature is discussed.

Chapter 4: In this chapter we introduce a discrete time version of a non-leaky integrate-and-fire neuron which will be further studied in the next chapters. We also explain the methodology used in this study.

Chapter 5: We present results of numerical experiments with adiabatic changes of the coupling strength in homogeneous populations of stochastic non-leaky integrate-and-fire neurons with delayed, pulsed coupling and a small refractory period. Analytical approximations of the expected behavior of the population are given.

Chapter 6: The results of the previous chapter are extend to heterogeneous networks.

Chapter 7: In this chapter we show that the obtained results are independent if either parallel or sequential updating is used.

Chapter 8: The results obtained in Part II and their possible applications and consequences are discussed.

PART III: Human communication behavior

Chapter 9: In this chapter we first give an overview of recent findings about human population dynamics placing emphasis on results which report heavy tailed probability distributions. Then the class of heavy tailed distributions is formally defined and two exponents of this class (power-law and log-normal distributions) are explained in more detail and set in contrast with each other.

Chapter 10: We describe the popular technology news-platform Slashdot and the crawling-process used to obtain data from this website. Then some basic magnitudes of the obtained data are presented and the observed activity cycles are described.

Chapter 11: A detailed analysis of the temporal behavior patterns of the users commenting the news posts on Slashdot is given. It is shown that user-behavior can be well approximated with log-normal distributions. An even further improvement can be achieved if the log-normal distributions are modified according to the circadian rhythm of the populations.

Chapter 12: In this chapter we first study the distribution of activity among all the users participating in the debates, which is shown to be well approximated by a truncated log-normal distribution. We then focus on the temporal activity patterns of single users, which are similar to those of the entire community and can be modelled as well by log-normal distributions.

Chapter 13: The results obtained in Part III and their possible applications and relations with other studies are discussed.

Conclusions and Future Research: In the last chapter of the dissertation we give the main conclusions of this work and describe its perspectives and possibilities for future research.

APPENDIX:

Appendix A: In this Appendix we give a proof of the periodic pattern condition, which enables us to calculate the minimum number of neurons per cluster to allow a repetitive firing pattern with a given period. This condition is the basis of the theoretical results of section 5.4.

Appendix B: Theoretical upper and lower bounds for the inter-spike interval of populations of stochastic non-leaky integrate-and-fire neurons are derived. A sharper lower bound for the expectation of the inter-spike interval over is also given.

Appendix C: In this Appendix the thermodynamic limits of the bounds of Appendix B are calculated, These limits are applied in subsection 5.4.3 to show the change in behavior of the system around the critical coupling strength.

Appendix D: A graphical explanation of the lower bound for the expectation of the inter-spike interval is given. The expression is interpreted as the sides of a right triangle whose acute angles experience a phase transition at the critical coupling strength.

Part I

Theoretical Background

Chapter 1

Synchronization

In this chapter we explain the terminology used in this work when referring to locking and synchronization. We introduce briefly the concepts of weakly and pulse coupled oscillators and concentrate on locking and synchronization phenomena in networks of such types of oscillators. The following is based mainly on the textbooks of Pikovsky, Rosenblum and Kurths (2001) and Izhikevich (2007). Whenever there was a discrepancy between the two works we favored the latter.

1.1 Introduction

Synchronization is a phenomena that can be found in many areas such as natural sciences, engineering and social life and has a long history in science. Christian Huygens was probably the first to describe a synchronization phenomena as early as in the seventeenth century when he observed the synchronization of two clocks hanging on a wall. A reprint of letters to his father mentioning this discovery can be found in (Pikovsky et al., 2001). The word "synchronous" originates from the Greek words σύν (*syn*, meaning the same, common) and χρόνος (*chronos*, meaning time), which in a direct translation would mean something like "sharing the same time" or "occurring in the same time". Nowadays synchronization is understood as an *adjustment of rhythms of oscillating objects due to their weak interaction* (Pikovsky et al., 2001). An oscillator is an active system that contains an internal source of energy which is transformed into oscillatory movement. Being isolated the oscillator continues to generate the same rhythm until the source of energy expires.

1.2 Forms of locking and synchronization in periodic oscillators

In what follows we restrict ourselves only on the description of locking and synchronization phenomena of periodic oscillators. More general forms of synchronization, such as **complete** and

generalized synchronization can occur in chaotic oscillators, but a description of these phenomena is beyond the scope of this thesis. (See for example Pikovsky et al., 2001 for an introduction on synchronization of chaotic oscillators).

1.2.1 Weakly coupled oscillators

Periodic oscillators generate a periodic process $x(t)$ and can be characterized by their phase $\phi(t)$ and amplitude $R(t)$. The phase $\phi(t)$ increases continuously in time (usually by 2π during a period T of the oscillator) and the amplitude $R(t)$ can be written in terms of $\phi(t)$. We consider now a system of N interacting periodic oscillators of the form:

$$\frac{dx_i(t)}{dt} = f_i\big(x_i(t)\big) + \varepsilon \sum_{j=1}^{N} g_{ij}\big(x_i(t), x_j(t)\big) \tag{1.1}$$

with functions $g_{i,j}$ being periodic in both arguments. For weak coupling $\varepsilon \ll 1$ the above system can be reduced to the phase model for coupled oscillators (Kuramoto, 1984; Hoppensteadt and Izhikevich, 1997):

$$\frac{d\phi_i(t)}{dt} = \omega_i + \varepsilon \sum_{j=1}^{N} Q_{ij}\big(\phi_i(t), \phi_j(t)\big) \tag{1.2}$$

being ϕ_i the phase of oscillator i and w_i its frequency. The Q_{ij} are 2π-periodic functions in both arguments. Intuitively, the above reduction can be performed since periodic oscillators can be described by a stable limit cycle and weak perturbations (or couplings) influence only the phase of an oscillator but not its amplitude (Pikovsky et al., 2001).

With the phase reduction of equation (1.2) we can write a system of two weakly coupled oscillators in the following general form:

$$\begin{aligned} \frac{d\phi_1(t)}{dt} &= h_1\big(\phi_1(t), \phi_2(t)\big), \\ \frac{d\phi_2(t)}{dt} &= h_2\big(\phi_1(t), \phi_2(t)\big). \end{aligned} \tag{1.3}$$

Again h_1 and h_2 are 2π-periodic functions in both arguments.

The phases $\phi_{1,2}(t) \bmod 2\pi$ of the two oscillators are defined on circles. Their state-space is thus a torus and the system (1.3) performs a trajectory on this torus. According to the form of this trajectory we can separate different forms of locking and synchronization of the two oscillators:

Frequency locking: The oscillators are frequency-locked if there exists a periodic trajectory on the state space. If during this trajectory ϕ_1 performs p oscillations and ϕ_2 during the same time q, we speak of $p:q$ frequency-locking (p and q are relatively prime integers).

Entrainment: A $1:1$ frequency locking is called entrainment.[1]

[1] Note that in the literature the terms entrainment and synchronization are often used as synonyms. Here we we follow the nomenclature of Izhikevich (2007) and define them separately.

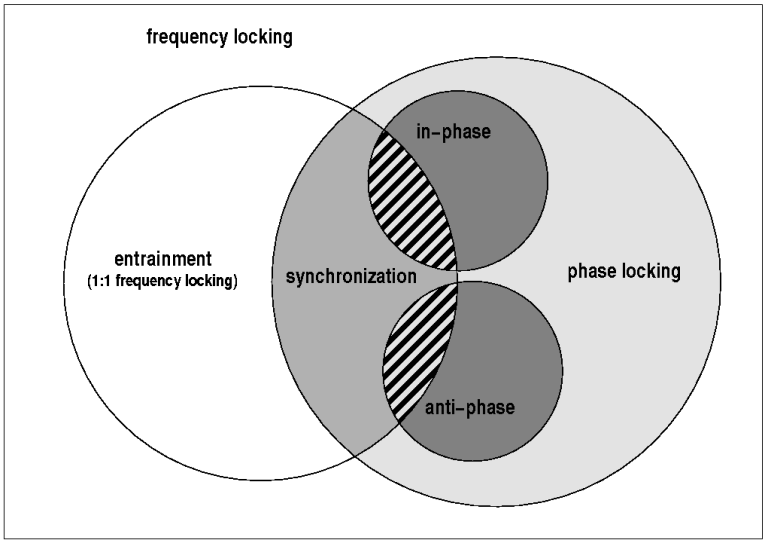

Figure 1.1: Degrees of locking for oscillators (Figure inspired by Izhikevich, 2007)

Phase-locking If the oscillators are $p:q$ frequency-locked and their phases fulfill

$$q\phi_1(t) - p\phi_2(t) = \text{const} \tag{1.4}$$

we speak of $p:q$ phase-locking. Depending on the value of the constant we can separate the following forms of phase locking: **in-phase** (const $= 0$), **anti-phase** const $= \pm\pi$, or **out-of-phase**.

The case of $1:1$ phase-locking is usually referred to as synchronization, and we have analogous to the above separation the following nomenclature:

In-phase synchronization: The oscillators do not only share a single common frequency, but also tend to oscillate with a common phase angle. i.e. the phase difference is zero.

Anti-phase synchronization The oscillators share the same frequency but oscillate in anti-phase, i.e. $\phi_1(t) - \phi_2(t) = \pm\pi$

Phase-locked synchronization: The most general case $\phi_1(t) - \phi_2(t) = \text{const} \neq 0$. The oscillators share the same frequency but oscillate with a constant phase difference.

Figure 1.1 shows in a Venn-like diagram the relationships of the above described types of synchronizations and locking. Those types can also be found in networks of $N > 2$ oscillators, where their occurrence is equivalent to pairwise frequency-locking, entrainment or phase-locking of the oscillators in the network. However, more complex phenomena, such as phase-locked clusters or partial synchronized regions, can be observed in networks and will partly be described in Part II of this thesis.

1.2.2 Pulse coupled oscillators

If the coupling between oscillators happens at discrete times (via a pulse) and can be described as an effect multiplied by a delta function, we speak of pulse coupled oscillators (Canavier and Achuthan, 2007). Their phase is usually taken to be proportional to the time between the emission of two consecutive pulses. That is if T is this period, the phase $\phi(t)$ fulfills $\phi(t+T) = \phi(t) + 2\pi$. The coupling between units in this case is pulse like. In its most simple form, i.e. without considering delays nor refractory periods, a system of two pulse coupled oscillators can be written as following way:

$$\begin{aligned} \frac{dx_1(t)}{dt} &= f_1\big(x_1(t)\big) + \varepsilon_1 \sum_k^{\infty} \delta\big(t - t_{2,k}\big) \\ \frac{dx_2(t)}{dt} &= f_2\big(x_1(t)\big) + \varepsilon_2 \sum_k^{\infty} \delta\big(t - t_{1,k}\big) \end{aligned} \tag{1.5}$$

where $\delta(t)$ is the Dirac delta function and $\{t_{i,k} | k \in \mathbb{N}\}$ is the sequence of pulses emitted by oscillator i, i.e. its **pulse train**.

Contrary to weakly coupled oscillators, in the definition of locking and synchronization phenomena between pulse coupled oscillators their phase difference is not required to be constant. It only has to be bounded and is allowed to oscillate around some value. This is justified by the fact that usually, e.g. in the case of spiking neurons, one is only interested in the pulse trains the two oscillators generate.

Formally we require:

$$|q\phi_1(t) - p\phi_2(t)| < \text{const} \tag{1.6}$$

for $p : q$ **phase locking**. This is equivalent to the definition of frequency locked oscillators, which implies that there is no separation between frequency and phase locking for pulse coupled oscillators. Again we speak of **synchronization** in the case of $1 : 1$ phase locking.

Since the phase difference is no longer constant in the above condition, it is convenient to define the different types of synchronization over the time-difference between two consecutive pulses of the oscillators. That is, if the period of oscillation is T, the oscillators are synchronized **in-phase** if they emit a pulse exactly at the same time (or within a very narrow time-window). We speak of synchronization in **anti-phase** if one oscillator emits a pulse $T/2$ time units after the other.[2] Any other time-difference is referred to as **phase-locked** or **out-of-phase synchronization**.[3] As in the case of weakly coupled oscillators the definitions extend to networks via pairwise locking.

[2] Note that contrary to weakly coupled oscillators we do not speak of in-phase or anti-phase $p : q$ phase-locking.

[3] Some authors (Pikovsky et al., 2001) use the phase difference in these definitions, requiring either $\phi_1(t) - \phi_2 \approx 0$ or $\phi_1(t) - \phi_2 \approx \pm\pi$. For our purposes the above definition is more useful.

Chapter 2

Diffusion models

In this chapter we give a brief introduction into different models of neural dynamics and human behavior which are based on a stochastic accumulation process (SAP). The following was mainly inspired by the reviews of Smith (2000) and Burkitt (2006).

2.1 Wiener Process

Before we start with the definition of a SAP, we first give a brief description of the Wiener Process, a continuous stochastic process which was introduced in 1923 by Norbert Wiener as a rigorous mathematical model of the Brownian motion and is sometimes also referred to as Brownian motion process. It is the continuous limit of a simple random walk (Cox and Miller, 1965) and can be defined in the following way (Ross, 2003):

Definition 1 *A stochastic process* $\{W(t), t \geq 0\}$ *is said to be a Wiener process if*

(i) $W(0) = 0$*;*

(ii) $\{W(t), t \geq 0\}$ *has stationary*[1] *and independent increments*[2]*;*

(iii) for every $t > 0$*.* $W(t)$ *is normally distributed with mean* 0 *and variance* $\sigma^2 t$*.*

For $\sigma = 1$, we speak of a standard Wiener process. Some interesting properties which follow immediately from this definition are: the variance of a standard Wiener process in an interval is equal to the length of the interval, i.e. $E\left(\left(W(t_1) - W(t_2)\right)^2\right) = |t_1 - t_2|$, and its correlation function $E\left(W(t_1)W(t_2)\right) = \min(t_1, t_2)$.

[1] Stationary means that $W(t+s) - W(t)$ does not depend on t.
[2] Its increments in successive non-overlapping intervals are independent.

2.2 Stochastic accumulation process

The time evolution of neural potentials or the information accumulation process in decision making tasks can be described in a general form as solution of the following SDE:

$$dX(t) = \mu\big(X(t),t\big)dt + \sigma\big(X(t),t\big)\xi(t) \tag{2.1}$$

where $X(t)$ is a random variable which represents the amount of accumulated information at time t and $dX(t)$ is the random change in the process $X(t)$ that occurs in an infinitesimally small time interval dt. The stochasticity is introduced in the equation by $\xi(t)$ representing Gaussian white noise, which is equivalent to the first derivative of a standard Wiener process $W(t)$. Equation (2.1) includes linear as well as nonlinear processes of arbitrary order. If we restrict ourselves to a linear first order version of (2.1), we can rewrite it as

$$dX(t) = \Big(\mu(t) + b(t)X(t)\Big)dt + \Big(\sigma(t) + c(t)X(t)\Big)\xi(t) \tag{2.2}$$

where $\mu(t)$,$b(t)$,$\sigma(t)$ and $c(t)$ are continuous functions of time. We can distinguish two important special cases of 2.2.

$$dX(t) = \Big(\mu(t) - \gamma X(t)\Big)dt + \sigma\xi(t) \tag{2.3}$$

$$dX(t) = \mu(t)dt + \sigma\xi(t) \tag{2.4}$$

which are obtained setting $\sigma(t) = \sigma$ constant, $c(t) = 0$ and $b(t) = -\gamma$ or $b(t) = 0$. The diffusion process of Equation (2.3) is called the Ornstein-Uhlenbeck process, and (2.4) a Wiener Process with drift. Both have great importance for theory and applications in the explanation of response times in simple information processing tasks (Smith, 2000) or for neural modelling (Burkitt, 2006).

2.3 The diffusion process in human and animal behavior models

Diffusion models are often used to explain the response time (RT) distribution of decisions of human or animal test subjects in simple perceptual and cognitive tasks. The models are based on the premise of noisy stimulus representation in the central nervous system and the necessity to accumulate successive samples of the noisy stimulus until a decision-threshold is reached (Ratcliff and Smith, 2004). Correspondence between this models and the growth of stimulus information in neural firing data has been reported (Smith and Ratcliff, 2004).

The solution $X(t)$ of the SDE (2.1) describes in a general form the amount of accumulated stimulus information at time t. Depending on the type of task, either one or two sided first passage

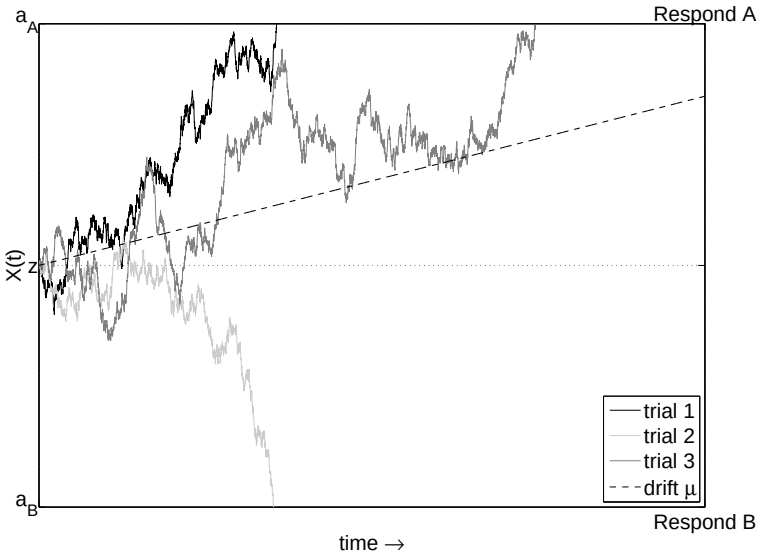

Figure 2.1: Diffusion model as explanation of response time in a two-choice task (Figure inspired by Ratcliff and Smith, 2004)

time problems of the diffusion process $X(t)$ are of interest to model the reaction time. Two sided problems are used when modelling cognitive tasks where a test subject has to choose between two different responses according to the stimulus presented, while one sided problems can model tasks where the decision is between performing a response or do nothing.

One sided problems involve a single random variable T, which stands for the time where the accumulate information $X(t)$ first reaches the in the general case time dependent decision threshold $a_A(t)$. T is defined as

$$T = \inf\{t|X(t) \geq a_A(t)\}; \quad X(t_0) = z < a_A(t_0), \tag{2.5}$$

with the diffusion process starting at time t_0 at $X(t_0) = z$.

The two sided problem involves a pair of random variables T_A and T_B, which represent the time where $X(t)$ first exceeds the threshold $a_A(t)$ or falls below $a_B(t)$. Again both threshold may be time-dependent and can be interpreted as decision criteria of competing responses. We can formally define T_A and T_B in the following way:

$$T_A = \inf\{t|X(t) \geq a_A(t) \wedge X(\tau) \geq a_B(\tau) \text{ for all } t < \tau\}, \tag{2.6}$$

$$T_B = \inf\{t|X(t) \leq a_B(t) \wedge X(\tau) \leq a_A(\tau) \text{ for all } t < \tau\}, \tag{2.7}$$

with $a_B(t_0) < X(t_0) = z < a_A(t_0)$ and $a_B(t) < a_A(t)$ for all $t \leq t_0$. The statistics of interest are now the first passage time distributions of T or T_A and T_B respectively, which for certain restrictions on the parameters of (2.1) and the decision criteria can written in closed form. See Smith (2000) and Ratcliff and Smith (2004) for more details and examples.

An example of three different trajectories towards the decision thresholds in a two decision task model is given by Figure 2.1. The decision criteria a_A and a_B are set to be constant and the diffusion process $X(t)$ is a Wiener process with a constant drift, i.e. the solution of (2.4) with $\mu(t) = \mu$. The drift parameter determines the preferred direction of the diffusion process, indicated by the dashed line in Figure 2.1. While the trials 1 (black) and 3 (dark gray) reach a_A leading to the preferred response A. The trajectory of trial 2 (light gray) falls below a_B, implying that the corresponding realization of the task lead to response B.

If we had a one sided first passage time problem, the later trajectory would not stop at a_B and $X(t)$ would eventually increase again to reach a_A at a later time, or in the oposite case the trajectory would correspond to a no response trial.

2.4 The diffusion process in neural models

2.4.1 The stochastic integrate and fire model

In neural dynamics one is interested in modeling the evolution of the membrane potential $v(t)$ of a neuron in time. The membrane potential is modified by excitatory or inhibitory synaptic inputs form other neuron. If the membrane potential exceeds a fixed threshold, an output spike is generated and the membrane potential relaxes to a resting potential V_0. In other words, a neuron sums up inputs and fires if they exceed a certain value, which explain the name of integrate-and-fire. Often a leaky term is included in this mechanisms, since the membrane potential of real neurons decreases if no new inputs arrive. A deterministic version of the leaky integrate-and-fire neural model is often written in the following form:

$$C_m \frac{dv(t)}{dt} = -\frac{C_m}{\tau_m}(v(t) - V_0) + I_s(t) + I_{inj}(t), \tag{2.8}$$

The first term on the right hand side of the equation describes the current due to passive leak of the membrane, i.e. the leak current. The rest of the variables are described in Table 2.1.

C_m	...	the membrane capacitance.
$I_s(t)$	...	the synaptic input current to the neuron.
$I_{inj}(t)$	...	a current injected into the neuron, by an intra-cellular electrode.
τ_m	...	the passive membrane time constant, which is related with $\tau_m = R_m Cm$ to C_m and the leak resistance R_m.
V_0	...	the resting potential.

Table 2.1: Explanation of variables used in equation (2.8).

The arrival times of the synaptic input are often modelled as Poisson processes (Cox and Miller,

1965), which is reasonable if we consider a large number of independent synaptic inputs. If we differentiate between excitatory and inhibitory synaptic inputs, we can rewire the synaptic input current as:

$$I_s(t) = C_m\left(\varepsilon_E S_E(t) - \varepsilon_I S_I(t)\right), \tag{2.9}$$

Where S_E and S_i are the Poisson processes of excitatory and inhibitory inputs with rates λ_E and λ_I, and $\varepsilon_E > 0$ and $\varepsilon_I > 0$ the changes in current due to a single synaptic event. Using (2.9) in (2.8) and setting $I_{inj}(t) = 0$ leads to the so called Stein model (1965):

$$\tau_m \frac{dv(t)}{dt} = -\Big(v(t) - V_0\Big) + \varepsilon_E S_E(t) - \varepsilon_I S_I(t). \tag{2.10}$$

which can be approximated by a continuous diffusion model, namely the Ornstein-Uhlenbeck model (Uhlenbeck and Ornstein, 1930), assuming that the discrete evolution of the potential is sufficiently small (Redner, 2001) and is then usually written as (compare with equation 2.3):

$$\frac{dv(t)}{dt} = -\frac{v(t) - V_0}{\tau_m} + \mu + \sigma\xi(t). \tag{2.11}$$

where $\xi(t)$ is Gaussian white noise and the intensity coefficient σ and the drift μ relate with the parameters of the Poisson process in the following way:

$$\mu = \varepsilon_E\lambda_E - \varepsilon_I\lambda_I, \tag{2.12}$$

$$\sigma = \sqrt{\varepsilon_E^2\lambda_E + \varepsilon_I^2\lambda_I}. \tag{2.13}$$

If we omit the leaky term in Eq. 2.11 we get a SDE equivalent to eq. (2.4) with $\mu(t) = \mu$ constant, which can be solved easily. The result is the perfect integrator or non-leaky integrate-and fire neuron model, one of the first neural models to be analyzed (Gerstein and Mandelbrot, 1964). We get that

$$v(t) = v_0 + \mu t + \sigma W(t), \quad t > 0 \tag{2.14}$$

where $v_0 = v(0)$ and $W(t)$ is the standard Wiener process described in section 2.1.

2.4.2 Pulse coupled oscillators

The deterministic integrate-and-fire model of equation (2.8) can be simplified using a phase reduction technique (Winfree, 2001) in the following way. We set the resting potential $V_0 = 0$ and rescale the membrane potential $v(t)$ to eliminate the constants, which results in a voltage like state variable $x(t)$ with the threshold at 1. We get

$$\frac{dx}{dt} = \alpha - \gamma x \tag{2.15}$$

for $0 \leq x \leq 1$ and $\gamma > 0$. If $x \geq 1$ then the neuron fires and x is reset to zero. The external input to the neuron is given by α.

If the external input is strong enough ($\alpha > \gamma$), an individual neuron fires repetitively even in the absence of coupling with other neurons and we have an integrate-and-fire oscillator. A combination of N such oscillators, with pulsed coupling has been used to model the self synchronization of the cardiac pacemaker (Peskin, 1975). Every unit i that reaches threshold increases all other units state by an amount ε. If m neurons fire simultaneously the states of all other neurons are increased by $m\varepsilon$. Such a system of pulsed coupled oscillators always synchronizes for almost all initial conditions of the system. (Mirollo and Strogatz, 1990).

2.4.3 Discrete integrate-and-fire model

The simplified leaky integrate-and-fire model of (2.15) can be discretized (van Vreeswijk and Abbott, 1993), which allows to study the effect of transmission delays analytically. Integration of equation (2.15) over one time-step leads to

$$\begin{aligned} a_i(t+1) &= \lambda a_i(t) + \alpha + \varepsilon m(t) && \text{if } a_i(t) < 1, \\ a_i(t+1) &= 0 && \text{if } a_i(t) \geq 1. \end{aligned} \tag{2.16}$$

where $\lambda = exp(-\beta)$ and $m(t)$ stands for the number of neurons which reach threshold at time t. The transmission delay of the above system is 1, it takes one time-step for a spike to reach all the other neurons. The units of system (2.16) also experience a refractory period, which is a small time period after a neuron has reached its threshold during which it is insensible to incoming synaptic events. This is reflected in the second equation of (2.16) which ignores spikes received from other units.

For the above equations, bounds for regions with self sustained firing patterns of an homogeneous ensemble of N neurons have been derived in van Vreeswijk and Abbott (1993) in the absence of external input to the system, i.e. $\alpha = 0$.

2.4.4 Discrete stochastic integrate-and-fire model

As a variant of system (2.16) Rodríguez, Suárez and López (2001) introduced a stochastic non-leaky integrate-and-fire model. In their model the threshold is set to L and only discrete values are allowed for the state variables $a_i(t)$ and the coupling strength ε. Instead of using a constant input α to the neurons, the state of a unit performs a random walk according to the outcome of a Bernoulli process. The state increases for every success and remains constant in case of failure, being p the probability of success. Combining this with the input from other neurons leads to the following equations:

$$
\begin{aligned}
a_i(t+1) = & \begin{cases} a_i(t)+m(t)\varepsilon+1 & \text{with probability } p \\ a_i(t)+m(t)\varepsilon & \text{with probability } (1-p) \end{cases} && \text{if } a_i(t) < L, \\
a_i(t+1) = & \quad 1+\big(m(t)-1\big)\varepsilon \text{ with probability } 1 && \text{if } a_i(t) \geq L. \qquad (2.17)
\end{aligned}
$$

Again $m(t)$ stands for the number of neurons which reach threshold in time-step t. The above system can be seen as a discrete variant of the diffusion model of Gerstein and Mandelbrot (see equation 2.14), although the monotonically increasing random walk does not exactly coincide with a discrete version of a Brownian motion. Note that the previous system (2.16) treats the refractory period differently, it does not allow any modification of the state variable while equations (2.17) only block the stochastic increases of the states of the units but enable changes due to incoming messages from other neurons during the refractory period.

System (2.17) experiences clustering phenomena for larger values of ε (Rodríguez, Suárez and López, 2002). A more general version of this model will be introduced and further analyzed in Part II of this thesis.

Part II

Neural populations

Chapter 3

Introduction to message interchange in neural populations

The collective dynamics of networks composed of neuron-like elements which interchange messages have been studied in many areas of science. Several models have been developed to simulate and analyze phenomena produced by pacemaker cells in heart (Peskin, 1975), neurons in the brain (Bienenstock, 1995), swarms of fireflies (Buck, 1988; Copeland and Moiseff, 1995) or hand clapping of opera theater attendants (Néda, Ravasz, Brechet, Vicsek and Barabási, 2000). Synchronization of the ensemble units is a common characteristic of these phenomena.

The observed synchronization effects are different according to the model characteristics. Most studies consider only instantaneous coupling (i.e no delay in the message exchange) between the units which simplifies the analysis of the resulting dynamics. Under this restriction Mirollo and Strogatz (1990) demonstrated that certain types of identical leaky oscillators with global coupling synchronize for almost all initial conditions. Their result has been extended by Senn and Urbanczik (2000) allowing non-identical oscillators whose intrinsic frequencies, thresholds and couplings are heterogeneous within a certain range. They showed that non-leaky linear integrate-and-fire neurons synchronize for any initial condition for almost all parameter values of the system and speculate that, using perturbative arguments, their results might be still valid in the presence of a small leakiness. The influence of an absolute refractory period on the Mirollo-Strogatz model has been analyzed by Chen (1994) and Kirk and Stone (1997). The authors of these papers showed that the system approaches synchrony for almost all initial conditions if the refractory period is below a critical value.

If a delay for the message exchange is added more complex forms of synchronization are observed. Gerstner (1996) found than an ensemble of non-leaky oscillators with identical frequencies, converges to periodic phase locked firing but does not necessarily fire in unison, under the restriction that the sum of input due to coupling to each oscillator is constant. Ernst, Pawelzik and Geisel (1995; 1998) report that for both, excitatory and inhibitory coupling, leaky pulse coupled oscillators tend to cluster their activities. All oscillators within a cluster are synchronized and fire in unison whereas

the clusters are phase-locked with constant phase differences. The number of clusters of the system was inversely proportional to the length of the delay for inhibitory coupling. The stability of these clusters was analyzed by Timme, Wolf and Geisel (2002) and Ashwin and Timme (2005). Clusters have also been observed by van Vreeswijk (1996) for coupling with α functions. For very large delays (larger than the period of isolated neurons) Gong and van Leeuwen (2007) found that a network of sparsely connected pulse coupled spiking neurons jumps spontaneously between a large variety of quasi stable phase locked states. Similar phenomena have been proposed as a possible mechanism for neural information coding and processing in the form of synfire chains (Abeles, 1991; Bienenstock, 1995; Diesmann, Gewaltig and Aertsen, 1999; Ikegaya et al., 2004). The importance of delay for neural modeling has recently been addressed by Izhikevich, Gally and Edelman (2004) and Izhikevich (2006), claiming that it allows an unprecedented information capacity, which translates into an increase of stable firing patterns in more realistic neural populations due to heterogeneous delays.

In this study we investigate the influence of variations in the coupling strength on a network of non-leaky integrate-and-fire neurons with delayed, pulsed coupling and a small refractory period. We show that a system of these characteristics exhibits a phase transition with a delay-induced hysteresis. Phase transition phenomena are well known in populations of weakly coupled oscillators, where the onset of synchronization represents a second order phase transition analogous to the formation of a Bose-Einstein condensate (Winfree, 1967; Kuramoto, 1984). Interacting chaotic oscillators also exhibit a special kind of phase transition which closely resembles that seen in spin glasses (Kaneko, 1990). Recent work analyzes the existence of phase transitions for chains (Östborn, 2002) and lattices (Östborn, Åberg and Ohlén, 2003) of pulse-coupled oscillators with a particular, biologically inspired phase response curve. For a review on phase transitions and other critical phenomena in complex networks see Dorogovtsev, Goltsev and Mendes (2007).

Contrary to the former mentioned studies the neurons of the network we analyze are driven by stochastic input, i.e. pulse-coupled oscillators with stochastic frequencies. Such type of model neurons have been introduced in Gerstein and Mandelbrot (1964) and one possible interpretation of the stochasticity is random input form background neurons that are not explicitly modeled (Stein, 1967). The units perform a random walk towards a threshold and, according to the characteristics of the stochastic input, several studies have analyzed the resulting distributions of the inter-spike intervals of single units for the case of non-leaky integrate-and-fire (IF) neurons[1] (Tuckwell, 1988; Fusi and Mattia, 1999; Salinas and Sejnowski, 2002; Middleton, Chacron, Lindner and Longtin, 2003; Lindner, 2004). For a review on those results and the more biological plausible models of leaky IF neurons see (Burkitt, 2006) and the references therein.

Here we are interested in a network of such units which can be interpreted as a simplified model

[1] Sometimes also referred to as leak-less or perfect integrator neurons.

of a pool of globally coupled neurons with similar properties, which receive stochastic input form different regions of the brain (Gerstner, 2000). Such networks have been studied for the cases of inhibitory (Brunel and Hakim, 1999; Brunel and Hansel, 2006) and excitatory coupled (Gerstner, 2000) leaky IF neurons. The later work mainly concentrated on noise in the thresholds or the refractoriness and only makes some comments on the effect of stochastic inputs. A combination of excitatory and inhibitory coupling, where noise leaded to enhanced stability of long distance synchronization, has been analyzed in a realistic heterogeneous neural model (Hodgkin-Huxley) by (McMillen and Kopell, 2003).

A common problem of these more biologically plausible models is that analytical studies are hard to perform especially if delay and refractory period are added. To bypass this problem we base our analysis on a discrete-time model introduced in Rodríguez et al. (2001), of globally coupled, non-leaky integrate-and-fire neurons with a constant transmission delay and a refractory period, where the stochastic inputs to the units are provided by a Bernoulli process. This model allows efficient simulations and a detailed analytical study and is an extension of the discrete model presented in van Vreeswijk and Abbott (1993).

The use of a stochastic model allows to observe that the nature of the dynamics changes abruptly from a regime where the units show noisy, irregular spiking behavior at low coupling to a regime with deterministic, self-sustained and repetitive spiking behavior if the coupling is increased to values greater than the critical coupling strength. There the units organize into several clusters, have all the same inter-spike interval (ISI), fire in-phase with the units of their own cluster and phase-locked with constant time differences to the neurons of other clusters. The clusters are robust to modifications of the rate of the stochastic input. If the coupling strength is increased even more, the number of clusters and the length of the ISI decrease since some clusters merge, but the system continues with the phase-locked firing. If, on the contrary, the coupling is decreased, the units of the population remain firing phase-locked without an increase of the ISI or the number of clusters until the critical coupling strength is reached, where the clusters start to dissolve. Thus a hysteresis effect can be observed.

The phase transition and the hysteresis can be described in detail. Upper and lower bounds for the ISI as well as an approximation for the mean ISI are obtained and the system's behavior for large ensemble sizes (i.e. at its thermodynamic limit) is characterized.

We conjecture that the observed phenomena can potentially occur in rather different models with a refractory period and delayed coupling. The results may be useful to explain certain aspect of animal behavior e.g. synchronized and non-synchronized flashing of North American fireflies (Copeland and Moiseff, 1995), create a simple working-memory (Wang, 2001) and may be applied in information processing.

Chapter 4

Neural model and experimental procedures

In this chapter we explain the model used in this study and the methodology of the simulations and data analysis.

4.1 A discrete model of an stochastic integrate-and-fire neuron

The discrete neural model studied in this work is based on the one introduced by Rodríguez et al. (2001), which is an extension of the work of van Vreeswijk and Abbott (1993). It is composed of a globally coupled network of N non-leaky stochastic integrate-and-fire units. Unlike the model of Rodríguez et al. (2001), where only a finite number of states is allowed, each unit i is at time t in a continuous state $a_i(t) \in [1,\infty)$. Transitions between states can take place only at discrete time-steps and are limited by a threshold L. L is a positive real number and limits the range of excitations in the sense that every state $a_i(t) \geq L$ is meta-stable since it absorbs any further state transitions or incoming messages and relaxes to 1 after the end of a refractory period t_{ref}.
We have two types of state transitions:

1. Stochastic state transitions:

   At every discrete time-step t a single unit can increase its state variable by 1 with probability p if the state of the neuron is below threshold L.

$$\begin{aligned} a_i(t+1) &= \begin{cases} a_i(t)+1 & \text{with probability } p \\ a_i(t) & \text{with probability } (1-p) \end{cases} && \text{if } a_i(t) < L, \\ a_i(t+t_{ref}) &= 1 \text{ with probability } 1 && \text{if } a_i(t) \geq L. \end{aligned} \tag{4.1}$$

2. State transitions due to coupling between units:

   A unit j that reaches the threshold L at time t emits a spike and increases the continuous state variable of an unit i by an amount ε_{ij} at time $t+\delta$, where δ stands for the synaptic delay.

Rodríguez et al. (2001) only allowed positive integer values for ε_{ij}. We will not use this restriction and allow any non-negative real number. The total amount of change of a single unit at time $t+\delta$ is obtained by summing over all neurons which had reached the threshold at time t. This gives us the following transition function due to messages of other units (we have to consider three cases depending on the threshold situation and the relation of t_{ref} and δ):

$$a_i(t+\delta) = \begin{cases} a_i(t) + \sum_{j=1}^{N} \varepsilon_{ij}\Theta_L(a_j(t)) & \text{if } a_i(t) < L, \\ 1 + \sum_{j=1}^{N} \varepsilon_{ij}\Theta_L(a_j(t)) & \text{if } a_i(t) \geq L \text{ and } \delta \geq t_{ref}, \\ 1 & \text{if } a_i(t) \geq L \text{ and } \delta < t_{ref}. \end{cases} \tag{4.2}$$

Notice that $\Theta_L(x) = \Theta(x-L)$ where $\Theta(x)$ is the Heaviside step function whose value is 0 for negative inputs and 1 elsewhere. We use this function to sum only over the neurons which reached threshold L in the previous time-step.

We restrict our analysis to the case of $\delta \geq t_{ref}$. Consequences of other choices are discussed in chapter 8. To keep the simulations simple we set both t_{ref} and δ equal to 1, which allows us to combine these two types of evolution (4.1) and (4.2) into a single equation and we get the following dynamics:

$$\begin{aligned} a_i(t+1) &= \begin{cases} a_i(t) + \sum_{j=1}^{N} \varepsilon_{ij}\Theta_L(a_j(t)) + 1 & \text{with probability } p \\ a_i(t) + \sum_{j=1}^{N} \varepsilon_{ij}\Theta_L(a_j(t)) & \text{with probability } (1-p) \end{cases} && \text{if } a_i(t) < L, \\ a_i(t+1) &= 1 + \sum_{j=1}^{N} \varepsilon_{ij}\Theta_L(a_j(t)) \text{ with probability 1} && \text{if } a_i(t) \geq L. \end{aligned} \tag{4.3}$$

Rodríguez et al. (2001) set all $\varepsilon_{ij} = \varepsilon$ for $i \neq j$ and all $\varepsilon_{ii} = 0$. With these prerequisites the parameter

$$\eta = \frac{L-1}{(N-1)\varepsilon} \tag{4.4}$$

was introduced to characterize the strength of the interactions among the units. The parameter η gives the ratio between the total change in activation needed for a neuron to fire and the one provided by the coupling with the rest of the population. For $\eta \gg 1$ the following expressions approximate well the mean and standard deviation of the ISI of a neuron in the ensemble:

$$\tau_{mf} = t_{ref} + \frac{L-(N-1)\varepsilon-1}{p}, \qquad \sigma_{mf} = \frac{\eta-1}{\eta}\frac{\sqrt{(L-(N-1)\varepsilon-1)(1-p)}}{p}. \tag{4.5}$$

Details and derivations of these equations, which are based on a mean-field approach, replacing the state transitions due to coupling between units by their average, can be found in (Rodríguez et al.,

2001)[1]. Equations (4.5) fail to describe the behavior of the system in regions of high coupling. At $\eta = 1$ they predict one giant cluster containing all the units with an ISI of 1. This would only be true for a system without delay and refractory period. In our system, however, the more important correlations due to the delayed message exchange become (i.e. the smaller becomes η), the bigger is the difference between τ_{mf} and the ISI of the units. This was first reported by Rodríguez et al. (2002), who found that for $\eta = 1$ after an initial transient the system reaches one of a large number of periodic firing patterns, composed of several clusters. The same is true for $\eta < 1$, as can be observed in Figure 4.1, where raster plots of spikes of a system consisting of 100 neurons are shown. The irregular behavior of the system at $\eta = 1.2$ (Figure 4.1a) changes into a regular repetitive spiking pattern at $\eta = 1$ (Figure 4.1b) if the coupling is increased. If increased further some clusters merge but the system continues with the phase-locked clustered firing as shown in Figure 4.1c for $\eta = 0.9$.

[1]Note that (Rodríguez et al., 2001) used $t_{ref} = 1$ in their analysis, which can be easily extended to the general case of t_{ref} variable.

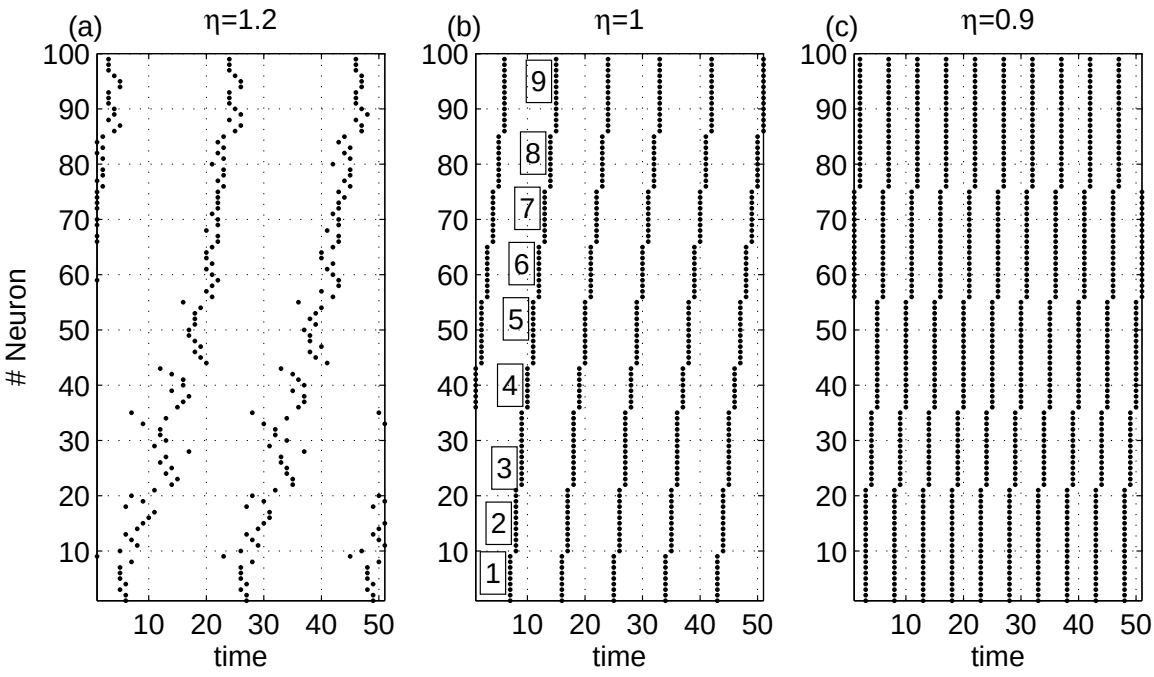

Figure 4.1: Raster plot of spikes (firing patterns) of 100 neurons (noise rate $p = 0.9$ and threshold $L = 100$) for different values of η. Simulation started with a random initial state for every neuron. Coupling strength is slowly increased every 100 time-steps and time was set to 0 after a transient of 50 time-steps. For clarity in the visualization the neurons are re-labeled according to their spike-time at $\eta = 1$. **(a)** We observe irregular firing at $\eta = 1.2$. **(b)** At $\eta = 1$ the neurons organize into 9 phase-locked clusters (labeled by the boxed numbers). **(c)** At $\eta = 0.9$ the number of phase-locked clusters is reduced to 5 since clusters number $1,2$; $4,5$; $6,7$ and $8,9$ merged into new bigger clusters. Note that the length of the ISI coincides with the number of clusters for $\eta = 1$ and $\eta = 0.9$.

4.2 Experimental procedures

To analyze the system described in section 4.1 we use the following experimental procedures. The phase transition and the hysteresis are best understood observing how the system reacts to adiabatic[2] changes of the coupling strength. A simple analogy is useful to understand the procedure. Consider a cloud of particles that is slowly concentrated or diluted by increasing or decreasing the volume. We begin with a very dispersed cloud with little interaction between the particles and start to concentrate it in a stepwise manner. At every concentration step the interaction among the particles increases. At some point the process is inversed and the cloud is diluted again until reaching the original state. We therefore distinguish two different processes in our experiments, to which we refer as *concentration process* and *dilution process*. The particles are in our case the spiking units and the interaction can be measured via the relation of the threshold L and the coupling strength ε multiplied by the number of units N. As explained above (see equation 4.4) this relation is reflected in the parameter η, which in our analogy represents the volume of the system.

In our experiments we choose a fixed set of N neurons with fixed threshold L. The only parameter allowed to change is the global interaction strength ε. We start with units at random initial states and at regions of high η (usually $\eta = 2$) where the system can be described with high accuracy by equations (4.5) and is ergodic in the sense that all accessible micro-states are visited over a long period of time. The units in these regions can be viewed as nearly independent with a threshold lowered by the mean activity induced by messages received from other units. The only difference to real independence is a period focusing effect described by Rodríguez et al. (2001). This results in a slightly lower (by a factor $(\eta - 1)/\eta$ standard deviation than the one of an independent unit with lowered threshold.

Once an experiment is started we let the system evolve enough time-steps to avoid dependence on unnatural initial conditions (i.e. conditions that are not typical of the system) and let the ISI stabilize. Now we can start the concentration process by decreasing η in a stepwise manner. We achieve this via adapting ε. Notice that, although we change η by a constant $\Delta\eta$, the changes of ε are not constant due to the inverse relation of η and ε. After every decrease of η we let the system evolve enough time-steps until the ISI stabilizes again. This procedure is repeated until a value of η in the range between 1 and 0.5 is reached. Then we reverse the procedure and start the dilution process. We increase η in a stepwise manner until we reach again the starting value of η.

To analyze the results we calculate two types of statistics of the ISIs of the units for every value of η.

1. The statistics of the ISI of the units just before the parameters of the system are changed (i.e. ε is increased or decreased). We call the first two moments of these statistics τ and σ (τ denotes the mean ISI of the ensemble and σ their standard deviation).

[2] We use the term *adiabatic* as it is used in quantum mechanics, meaning a "sufficiently slow" change of the system.

2. The statistics of τ and σ of different experiments: We call $\langle\tau\rangle$ the mean and σ_{exp} the standard deviation of the ensemble's mean ISI τ. In the case of σ we only calculate its mean value, which we denote $\langle\sigma\rangle$.

The value of $\langle\sigma\rangle$ gives us an idea of the likelihood to end up firing with phase-locked clusters for the given parameter values. The closer $\langle\sigma\rangle$ is to 0 the bigger is this likelihood. If the units in one experiment have all the same ISI their standard deviation σ equals 0. σ_{mf} of equation (4.5) estimates $\langle\sigma\rangle$.

On the other hand, σ_{exp} measures the influence of the initial conditions and variations in the stochastic state transitions on the mean ISI τ of the ensemble.

Chapter 5

Results for homogeneous networks

In this chapter we first present the outcome of several experiments that reveal the existence of a phase transition phenomenon of the system described in section 4.1 around a critical value of the coupling parameter η. This phenomenon is accompanied by a hysteresis effect which will also be described. We then give analytical bounds for the mean ISI $\langle\tau\rangle$. This description allows us to calculate the behavior of the observed phenomena for $N \to \infty$. We will refer to this limit behavior as thermodynamic limit in the rest of this work.

5.1 Experimental Results

5.1.1 Dependence of the ISI on the coupling strength ε

As explained in section 4.1 one of the quantities we are interested in this work is the ISI. Especially we want to know how it is modified by small changes of the coupling parameter η. We therefore performed several experiments for different ensemble sizes as described in section 4.2 and observed the dependence of the mean value of the ISI $\langle\tau\rangle$ on the coupling parameter η for different values of the rate p of the stochastic evolution. First we analyze only the concentration process, where we slowly increase the amount of coupling between the neurons. Since the coupling parameter η is inverse proportional to the coupling strength an increase of the coupling strength indicates a decrease of η.

Figure 5.1a and 5.1b show the results for 1000 such concentration experiments for noise rates of $p = 0.9$ (solid line) and $p = 0.6$ (dashed line). We used an ensemble size of $N = 1000$ neurons and can observe how the mean ISI $\langle\tau\rangle$ decreases as we increase the coupling. Initially at high values for η there is a clear dependence on the noise rate p which seems to disappear as we reach $\eta = 1$. A closer examination of the mean ISIs of both experiments in this region reveals that their difference for η close to 1 and below decays exponentially to 0 with decreasing η. (Shown in the insets of Figures

5.1a and 5.1b). We will see later in the theoretical analysis that the greater N the faster is this decay and at the thermodynamic limit the mean ISI is independent of p for all values of $\eta < 1$.

When we analyze the deviation of the ISIs we also notice a change in the behavior of the system if we approach $\eta = 1$. The mean deviation $\langle\sigma\rangle$ of several experiments drops to 0 when the critical value of η is reached, indicating that the units organize into clusters and fire phase-locked, all with the same ISI. Figure 5.2a shows this effect for the concentration experiments with the two different noise rates analyzed before. In the inset we notice that for a noise level of $p = 0.9$ (solid line) the onset of phase-locking already happens at $\eta \approx 1.04$. This can also be observed in the deviation σ_{exp} of the

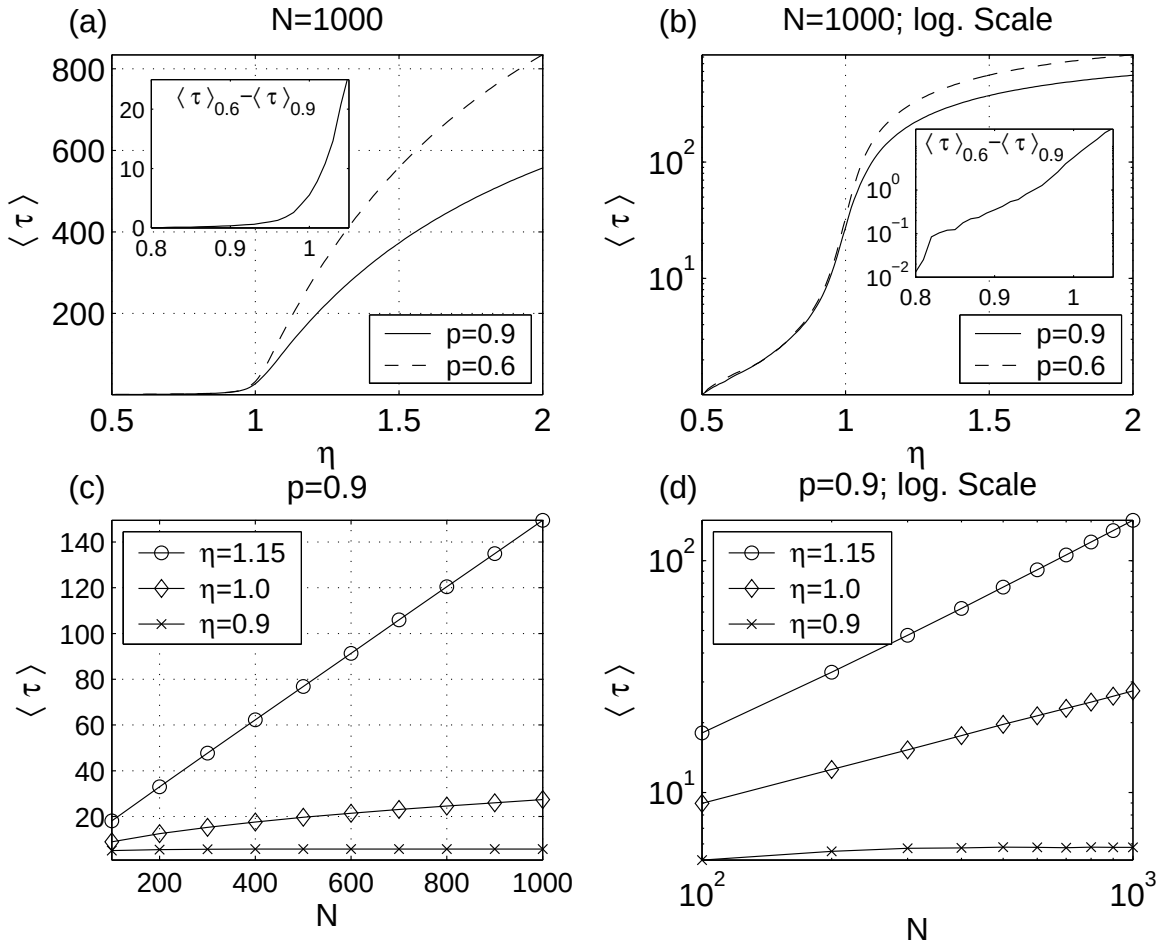

Figure 5.1: Mean ISI: Values of the ISI $\langle\tau\rangle$ over all neurons and 1000 experiments for increasing ε (i.e. decreasing η). Number of neurons $N = 1000$ equals threshold L in all cases. **(a)** Dependence of $\langle\tau\rangle$ on η for two different noise levels p. Inset shows the difference of both curves in the interesting region around $\eta = 1$. **(b)** Same as (a) but in logarithmic scale. **(c)** Dependence of $\langle\tau\rangle$ on N for different values of η and $p = 0.9$. **(d)** Same as (c) but in logarithmic scale. We can see a linear dependence of $\langle\tau\rangle$ on N for $\eta = 1.15$, a square root dependence for $\eta = 1$ and nearly no dependence for $\eta = 0.9$.

experiments ISIs. Figure 5.2b shows the corresponding value of σ_{exp}. Here the onset of phase-locking is marked by an increase of σ_{exp}.

If the units are not phase-locked, σ_{exp} is low since it is the deviation of averages. Although there may be great differences between the ISIs of the units as is reflected by the value of $\langle\sigma\rangle$, once the mean ISI τ of the ensemble is calculated, these fluctuations are just averaged out. But as the units start to organize into phase-locked clusters the ensemble dynamics starts to govern the system. The deviation of the ensemble, σ, equals 0 but the deviation of the experiments, σ_{exp}, increases. The mean ISI τ of the ensemble is now an integer value, which depends on the evolution of all the units since the beginning of the experiment. This gives rise to a broader shape of the ISI distribution. Small

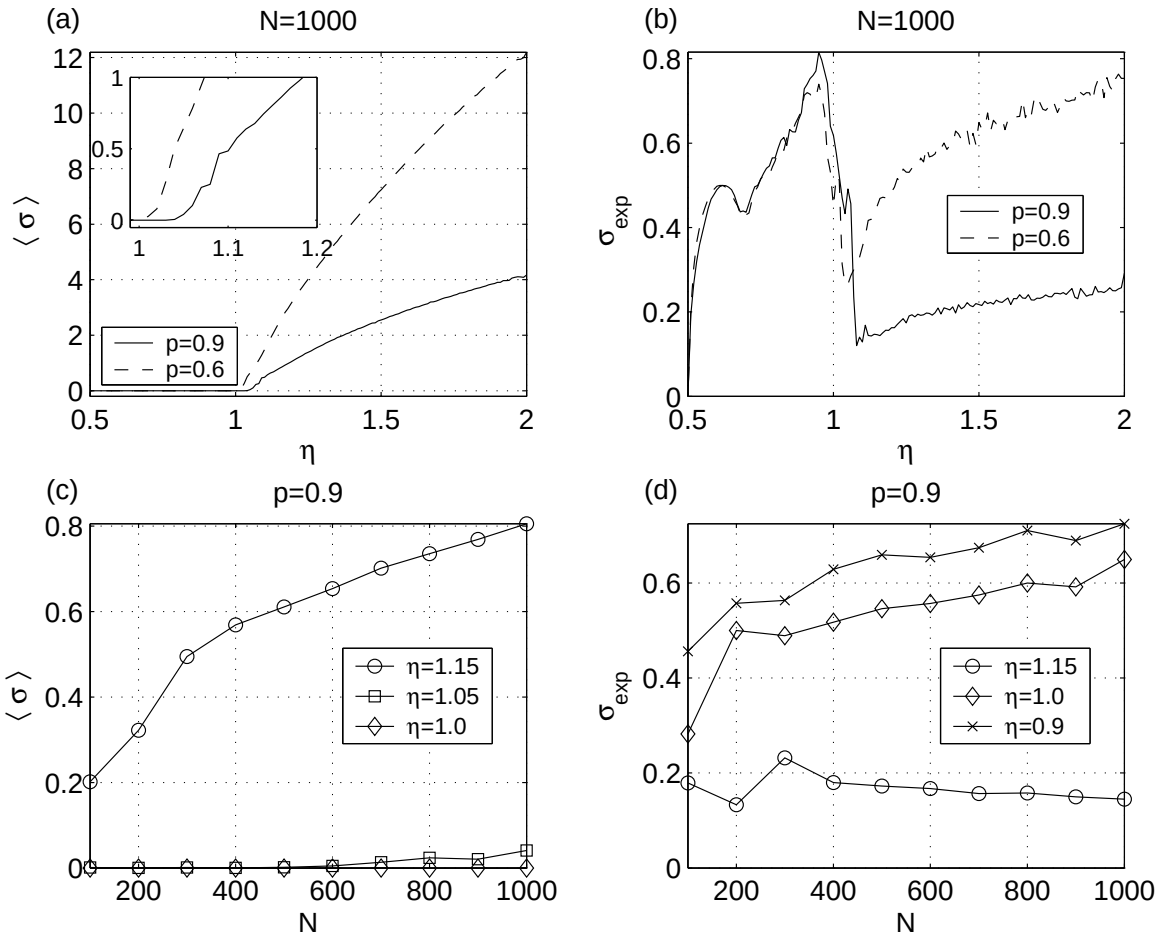

Figure 5.2: Standard Deviations: Values of the deviations of $\langle\sigma\rangle$ and σ_{exp} of the experiments with increasing ε (e.g. decreasing η) presented in Figure 5.1. Number of neurons N equals threshold L in all cases. **(a)** Dependence of $\langle\sigma\rangle$ on η for two different values of p. Inset shows a zoom on the interesting region around $\eta = 1$. **(b)** Same as (a) but for σ_{exp} **(c)** Dependence of $\langle\sigma\rangle$ on N for different values of η and $p = 0.9$. $\langle\sigma\rangle = 0$ for all $\eta < 1$ due to synchronization. **(d)** Dependence of σ_{exp} on N for different values of η and $p = 0.9$.

fluctuations in the evolution of some units can lead to a different ISI of the whole system. Therefore the averaging effect observed before is lost and different experiments, although started with the same initial conditions, can lead to systems with different τ.

The maximum of σ_{exp} is reached when the rate p of the stochastic evolution looses most of its influence on the size of the ISI (Compare with Figure 5.1). In this sense the interval between the local minimum at $\eta > 1$ and maximum at $\eta < 1$ of σ_{exp} marks the transition between an ensemble governed by the stochastic evolution to an ensemble with self-sustained activity where the stochastic evolution does not have much influence on the statistics of the system. We can see that once the local maximum is reached the curves for $p = 0.9$ and $p = 0.6$ are practically identical if the system is further concentrated. (i.e the coupling strength is increased). σ_{exp} reaches a value of 0 at $\eta = 0.5$ when the system consists only of one giant cluster which spikes at every time-step. The strange bump at $\eta \approx 0.7$ can be explained by a probability of nearly 80% of having an ISI of 2 for this value of η. The value of σ_{exp} experiences thus an important decrease, but starts to increase again when the concentration continues and the probability of having an ISI of 1 increases.

5.1.2 Dependence of the ISI on the ensemble size N

Once the properties of the deviations have been described, our analysis focuses again on the mean ISI $\langle\tau\rangle$. The strange shape of the curves in the logarithmic scale of Figure 5.1b suggests that apart from the elimination of the dependency on the noise rate p something else is going on around the value of $\eta = 1$. To investigate this point further we observed the dependence of the ISI $\langle\tau\rangle$ on the ensemble size N.

Figures 5.1c and 5.1d reveal a quite different kind of dependence for different values of the coupling parameter η. For $\eta = 1.15$ (line with circles) we observe a linear dependence of $\langle\tau\rangle$ on N, whereas for $\eta = 0.9$ (line with crosses) the value of the ISI stabilizes once a certain number of neurons is in the ensemble ($N \geq 300$) and does not show any dependence on the ensemble size. At $\eta = 1$ (line with diamonds) another type of relationship is observed. The slope in the double logarithmic scale of Figure 5.1d has nearly exactly a value of 0.5 indicating a relationship of type $\sqrt{N} \sim \langle\tau\rangle$.

The corresponding values of the deviations $\langle\sigma\rangle$ and σ_{exp} for $p = 0.9$ can be seen in Figures 5.2c and 5.2d. As expected for $\eta \leq 1$ the mean deviation $\langle\sigma\rangle = 0$ since the units fire phase-locked. We omit for clarity the line for $\eta = 0.9$ and only show the values for $\eta = 1$ (line with diamonds). For $\eta = 1.15$ (line with circles) we get a linear dependence of $\langle\sigma\rangle$ on $\sqrt{N}$ as predicted by Eq. (4.5). The additional curve for $\eta = 1.05$ (line with squares) allows to observe that the smaller the ensemble the earlier happens the onset of phase-locking in the concentration process. Here the units are phase-locked already for ensemble sizes of $N > 500$.

The dependence of σ_{exp} on N can be observed in Figure 5.2d. For $\eta = 1.15$ (line with circles),

where the stochastic state transitions govern the ensemble, σ_{exp} slightly decreases since an increase of N implies an increase of the number of samples taken for every ISI τ and due to the central limit theorem a decrease of the deviation. For $\eta = 0.9$ (solid line with crosses) and $\eta = 1.0$ (solid line with circles) the σ_{exp} increases as N increases. This behavior changes in the case of $\eta = 0.9$, where σ_{exp} stabilizes for higher values of N and becomes independent of the ensemble size (data not shown).

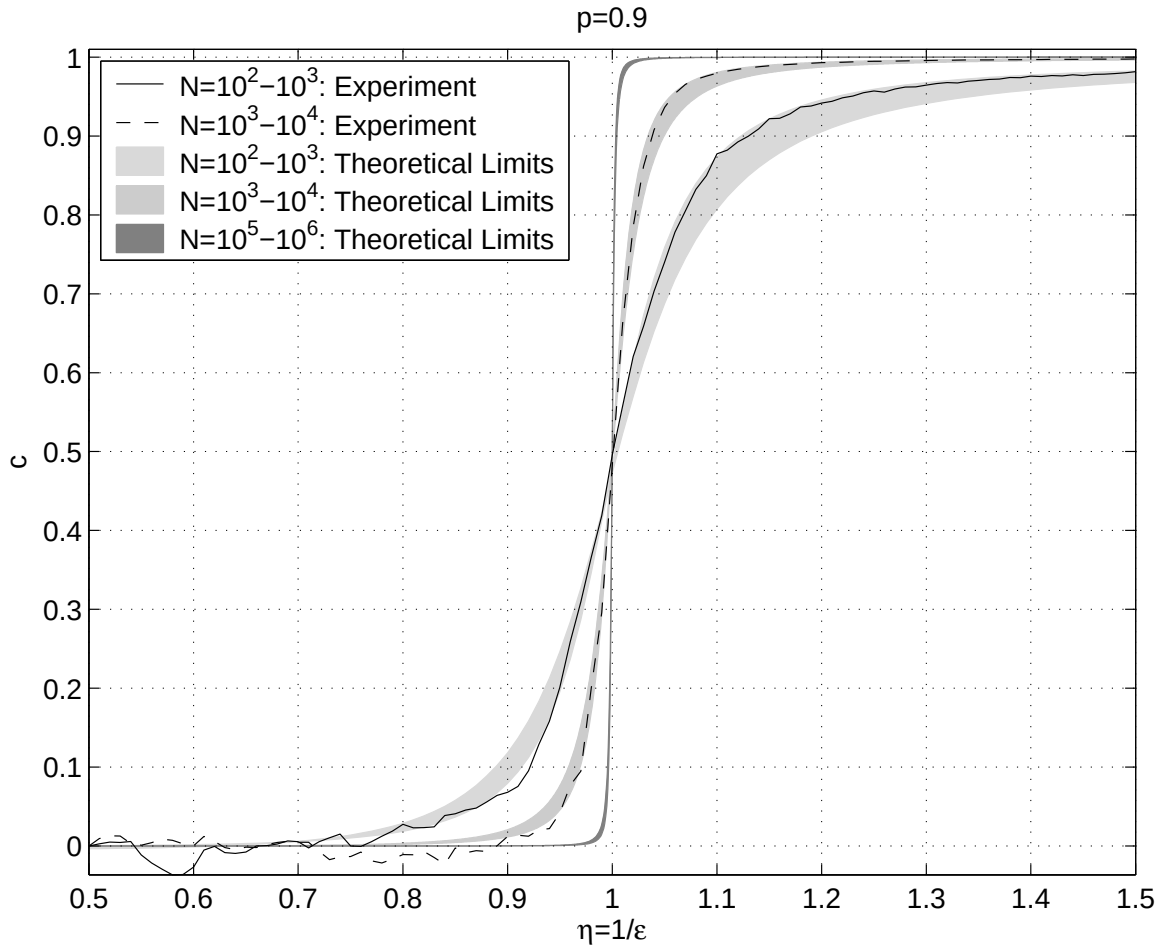

Figure 5.3: Comparison between experimental and theoretical results for the parameter c of the assumption that $\langle\tau\rangle = \alpha N^c$. 10 sets of 1000 experiments with $p = 0.9$ and different values for N were carried out. (Solid line: $N \in \{100, 200, \ldots 1000\}$. Dashed line: $N \in \{1000, 2000, \ldots 10000\}$). The values of c have been obtained by a least squares fit of the experiments with the linear equation $\ln(\langle\tau\rangle) = \ln(\alpha) + c\ln(N)$. The shaded areas show the region of possible values of c obtained by least squares fits of the theoretical bounds for $\langle\tau\rangle$ of equations (5.10) and (5.11) and the assumption. For $N \in \{10^5, \ldots 10^6\}$ (darkest area), the value of c is already very close to its thermodynamic limit. The difference between the values of c of the two bounds is very low.

5.2 Characterization of the Phase Transition

The results of the dependence of the mean ISI $\langle\tau\rangle$ on the ensemble size N for different values of η presented in Figures 5.1c and 5.1d motivate us to investigate if there exists a relation of type

$$\alpha N^c = \langle\tau\rangle \tag{5.1}$$

and analyze the dependence of c and α on the coupling parameter η. Equation (5.1) can be transformed into a linear equation with slope c and y-intercept α

$$\ln(\alpha) + c\ln(N) = \ln(\langle\tau\rangle). \tag{5.2}$$

This allows us to calculate c and α by least squares fits of the simulation data.

The results of these fits are shown in Figures 5.3 and 5.4. In both we see two curves, each represents a set of 10 different values of N. For every value of N the mean ISI $\langle\tau\rangle$ of 1000 concentration processes was calculated. For the solid line N takes values from 100 to 1000 in steps of 100 and for the dashed line values from 10^3 to 10^4. We can see that both c and α experience a sharp change of their value around $\eta = 1$. The higher the value of N the sharper this change is. We can therefore speak of a phase transition around a critical value of $\eta = 1$. We expect that for $N \to \infty$ the value of c should jump from 1 for $\eta > 1$ via 0.5 at $\eta = 1$ to 0 for $\eta < 1$.

The gray areas represent bounds obtained from theoretical analysis and will be discussed in section 5.4.

5.3 Hysteresis effect

After having analyzed the concentration process experimentally and characterized a phase transition phenomenon we are interested in what happens if we invert the process. Instead of increasing the coupling strength we decrease it in a stepwise manner. As described in section 4.2 we call this type of experiment dilution process. If we combine concentration and dilution process to obtain a cyclic process we notice a hysteresis effect comparing the mean ISIs $\langle\tau\rangle$ of both processes for values of η close to 1 and below.

Figure 5.5 shows this effect for 3 different starting points of the dilution process. The dotted line represents the mean ISI $\langle\tau\rangle$ of the concentration process of 1000 experiments. When the concentration process stops and the dilution process is started, τ and therefore also $\langle\tau\rangle$ remain constant until a dilution of $\eta > 1$ is reached. The solid line with circles represents a dilution process stating at $\eta = 0.5$ and the dashed line with $+$ markers one starting at $\eta = 0.9$. In both cases the ISI remains unchanged until $\eta = 1$ where it jumps then to a value slightly higher than the one predicted by the formulas (4.5)

for this case. If we start the dilution process already at $\eta = 0.99$ we observe that $\langle\tau\rangle$ remains constant even for $\eta = 1.01$. Only if we dilute further $\langle\tau\rangle$ increases and starts to coincide with $\langle\tau\rangle$ of the other two dilution processes. Approximately at $\eta = 1.08$ the ISI of the dilution process coincides with the one of the concentration process. To understand this phenomenon in detail we carry out a theoretical analysis which will be presented in the next section.

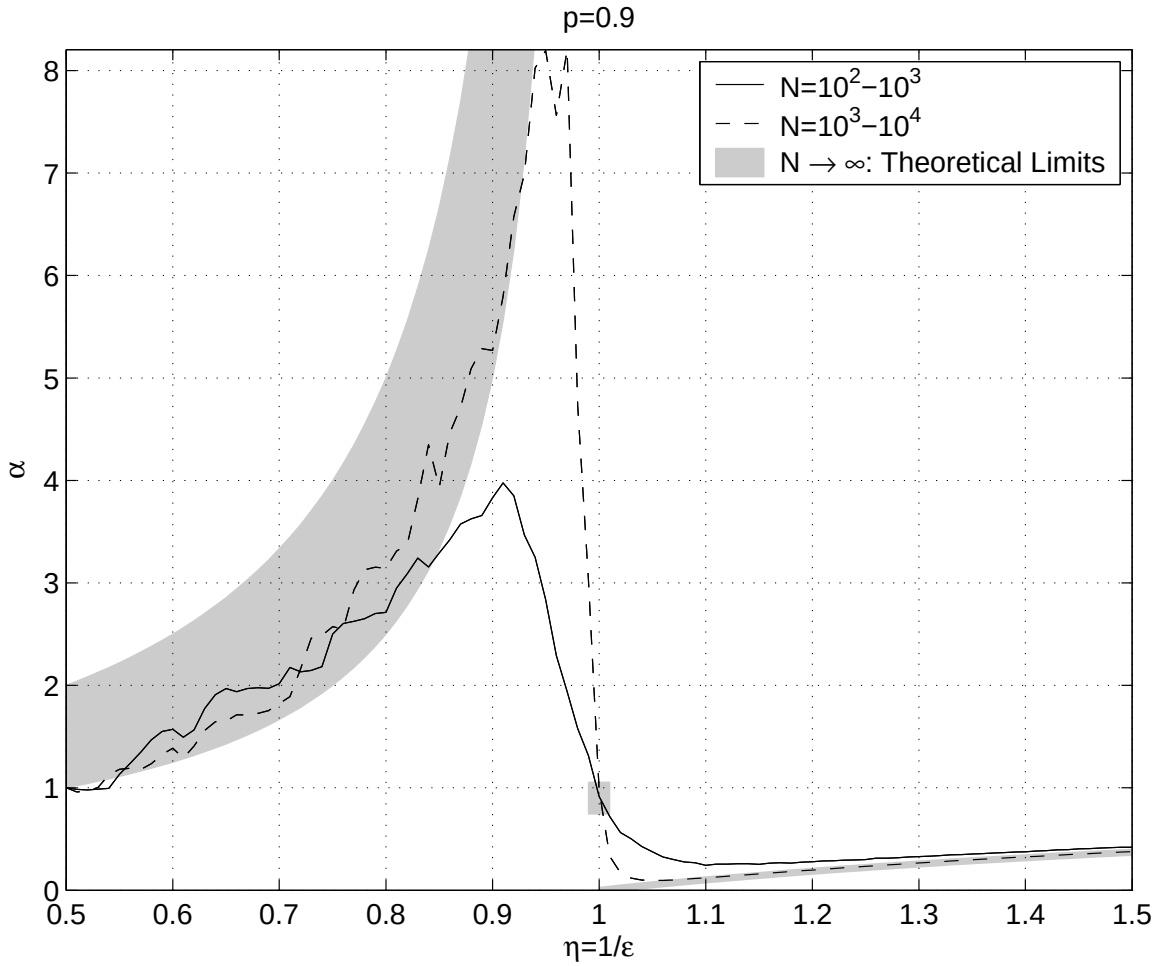

Figure 5.4: Comparison between experimental and theoretical results for the value α under the assumption that $\langle\tau\rangle = \alpha N^c$. 10 sets of 1000 experiments with $p = 0.9$ and different values for N were carried out. (Solid line: $N \in \{100, 200, \ldots 1000\}$. Dashed line: $N \in \{1000, 2000, \ldots 10000\}$). The values of α have been obtained by a least squares fit of the experiments with the equation $\ln(\langle\tau\rangle) = \ln(\alpha) + c\ln(N)$. The shaded areas show the regions of possible values of α for $N \to \infty$ according to equations (5.20).

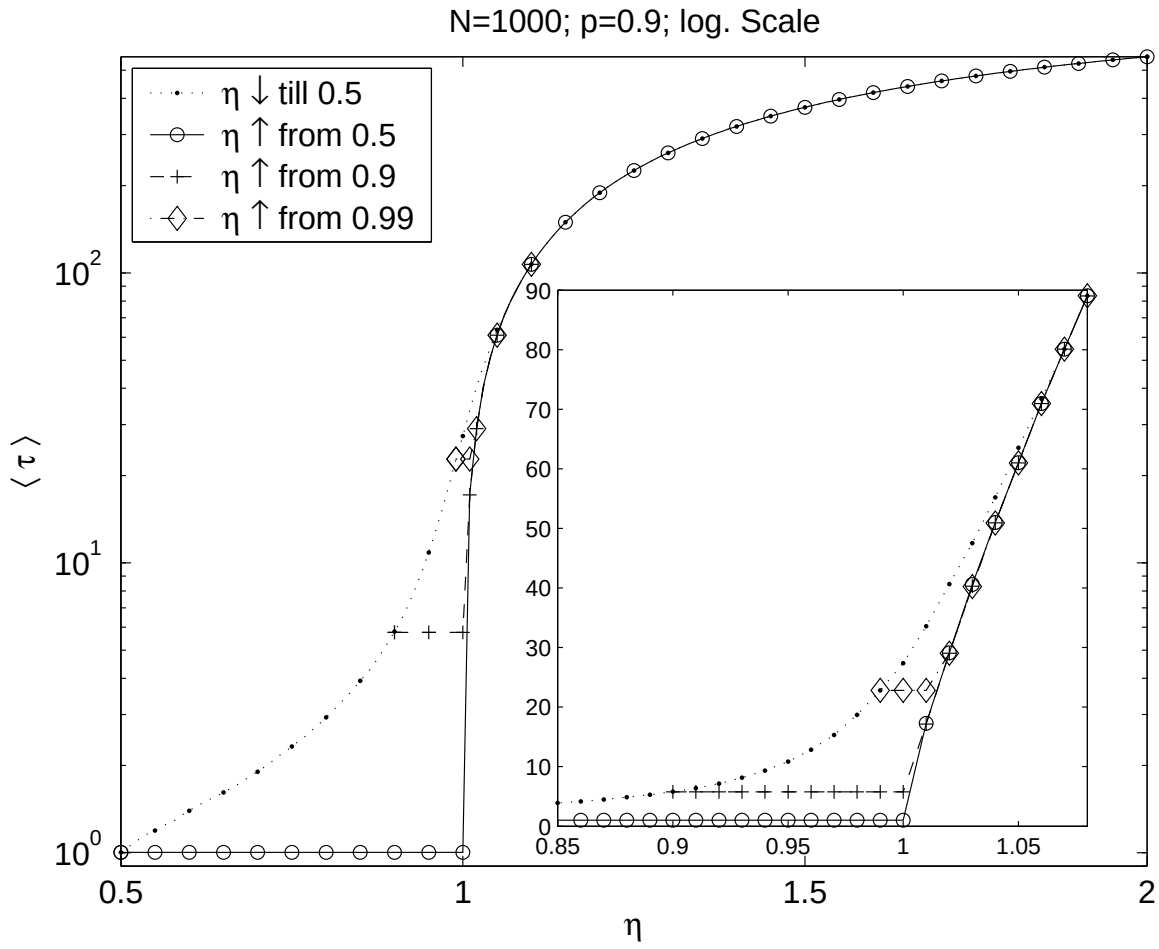

Figure 5.5: Hysteresis effect in the comparison of the dependence of $\langle\tau\rangle$ on η between the concentration and dilution process of the experiments. The y-axis shows $\langle\tau\rangle$ of 1000 experiments in logarithmic scale. Four curves are shown: $\eta\downarrow$ till 0.5: shows the results of the concentration process till $\eta = 0.5$. $\eta\uparrow$ from 0.5 is the corresponding part of 1000 dilution processes starting from $\eta = 0.5$. $\eta\downarrow$ from 0.9 shows the result for the dilution process starting after a concentration till $\eta = 0.9$. And $\eta\downarrow$ from 0.99 the same for a concentration until $\eta = 0.99$. The inset shows a zoom on the interesting region around $\eta = 1$ in linear scale. The number of neurons $N = 1000$ equals threshold L and $p = 0.9$ in all cases.

5.4 Theoretical Description

Once identified the phenomena occurring in the model in experiments we make some theoretical observations to gain further insight. We base these observations on a deterministic approximation of the model where the stochastic evolution (4.1) of a neuron i is simplified into the following deterministic iterative rule:

$$\begin{aligned} a_i(t+1) &= a_i(t)+p \quad \text{if } a_i(t) < L, \\ a_i(t+t_{ref}) &= 1 \qquad\quad \text{if } a_i(t) \geq L. \end{aligned} \tag{5.3}$$

The random walk performed by the units is replaced by their average behavior: a deterministic motion with constant homogeneous velocity p. An equivalent continuous time system but with heterogeneous velocities (frequencies) and without delay and refractory period has been studied by Senn and Urbanczik (2000). In the following we will restrict our analysis to the case where the delay δ of the message exchange is greater than or equal to the refractory period t_{ref}.

After an initial transient the deterministic system shows a periodic pattern of spikes. The period of a pattern is the ISI of the ensemble (Figure 4.1b and 4.1c illustrate such patterns). If we take an arbitrary neuron and start the pattern at a spike of this unit, all units will spike exactly once until the next spike of the same unit. The sequence of these spikes will then start again with exactly the same time differences between the spikes, and this pattern will repeat itself forevermore if the parameters of the system are not changed. One can derive the following condition the system fulfills if it shows a periodic firing pattern.

Theorem 1 (Periodic pattern condition) *A system that consists of κ clusters, where every cluster i consists of k_i elements, shows a periodic firing pattern with ISI τ if for every $i \in \{1,\ldots,\kappa\}$*

$$k_i > k_{min}(\tau) = \begin{cases} (N-1)(1-\eta) + \frac{p(\tau-1-t_{ref})}{\varepsilon} & \text{if } \tau \geq 1+t_{ref} \\ (N-1)(1-\eta) & \text{if } \tau < 1+t_{ref} \end{cases} \tag{5.4}$$

is fulfilled.

For derivation of this rule see Appendix A. Condition (5.4) simply tells us that every cluster (i.e. units that reach the threshold at the same time-step) has to be greater than a certain minimum cluster size which depends on the system's parameter and its ISI.

Before we continue our analysis we make some comments on the validity of this rule for the stochastic system. The firing patterns of the deterministic system may also occur in the stochastic system as can be seen in Figure 4.1b and 4.1c. According to the robustness of these patterns against variations in the stochastic evolution we can distinguish between three types of patterns.

Robust firing patterns are totally insensitive to variations of stochastic state transitions in the sense that, no matter how they evolve, even if they are totally suppressed, the system cannot change its periodic pattern.

Semi-robust firing patterns remain unchanged if one or more units evolve slower than with their mean velocity p, but if they evolve much faster the spiking pattern may change. Since such changes are rare, as will be explained subsequently, and the patterns are robust against at least half of the possible stochastic events, we choose the name semi-robust.

Variable firing patterns may change due to very slow or very fast evolution of one or more units.

At $\eta \leq 1$ we can find only robust and semi-robust patterns. Condition (5.4) gives us the rule for a semi-robust pattern in the stochastic system. To get the condition of a robust pattern in this case we would have to replace p with 1.

A change of a semi-robust pattern of phase-locked clusters implies that one or more units change from one cluster to the one firing directly before it. This increases the robustness of the resulting new firing pattern since the smallest cluster has the highest probability of receiving a neuron and leads to a certain balancing of the sizes of the clusters. Only if we have two small clusters spiking one directly after the other a merge of these two clusters might occur, which would imply a decrease of the ISI. Every decrease of the ISI enhances the robustness of the resulting firing pattern, since it implies a decrease of the minimum cluster size $k_{min}(\tau)$. Such events however are rare especially for large populations and their influence is far below the standard deviation of the experiments. Since we are mainly interested in the ISIs of our system we can neglect them in our analysis. Although we have to state that for an infinite simulation time all semi-robust patterns would transform into robust ones.

For $\eta > 1$ we only find variable firing patterns (Figure 4.1a). In the stochastic system, the higher the value of η the lower is the probability to observe between three consecutive spikes of a certain single unit the same two spiking patterns of the rest of the neurons. It is not even granted that the two ISIs of this unit have the same length. But now, unlike the case of $\eta \leq 1$, the fluctuations of the noise cannot create irreversible effects on the ISI of the system. The mean ISI of the system coincides therefore with the one of the deterministic system, which makes the following analysis valid in this region as well.

Every time the coupling strength is increased, after a short transient, the deterministic system fulfills again condition (5.4). This allows us to make some observations on the ISI of the system. Since the cluster sizes have to be integer numbers we define

$$\hat{k}_{min}(\tau) = \lfloor k_{min}(\tau) + 1 \rfloor \tag{5.5}$$

and have the condition $k_i \geq \hat{k}_{min}(\tau)$. This definition guarantees that $\hat{k}_{min}(\tau) \geq 0$ and is necessary for technical reasons in the derivation of the lower bound we will see later. A system with ISI τ consists of $\kappa = \tau/\delta$ clusters since a spiking cluster at time t provokes the spiking of the next one at time $t+\delta$. With this we calculate another quantity we need to describe our system, the mean cluster size given a certain ISI τ:

$$\bar{k}(\tau) = \frac{N\delta}{\tau} \,. \tag{5.6}$$

We then introduce a new function $g(\tau)$ which gives us the ratio between $\bar{k}(\tau)$ and $\hat{k}_{min}(\tau)$.

$$g(\tau) = \frac{\bar{k}(\tau)}{\hat{k}_{min}(\tau)} \,. \tag{5.7}$$

Intuitively this quantity can be seen as the frequency a system consisting only of clusters with the minimum cluster size $\hat{k}_{min}(\tau)$ has to fire with, to achieve the same ISI as the system with cluster-size $\bar{k}(\tau)$. Note that $g(\tau) > 0$ since $\hat{k}_{min}(\tau) \geq 0$.

Using equation (5.5) of the minimum integer cluster size $\hat{k}_{min}(\tau)$ we arrive after some manipulation to the following inequality (See equation B.15 in Appendix B for details).

$$\frac{N\delta}{\langle\tau\rangle} \leq \langle g\rangle \left(k_{min}(\langle\tau\rangle) + 1\right). \tag{5.8}$$

$\langle g\rangle$ denotes the expectation of $g(\tau)$ with respect to the probability distribution of τ. We will call $\langle g\rangle_{min}$ from now on the minimum value, which $\langle g\rangle$ can take to fulfill inequality (5.8). Using $\langle g\rangle_{min}$ inequality (5.8) can be written as

$$\frac{1}{\langle\tau\rangle} = \langle g\rangle_{min}\zeta\,, \tag{5.9}$$

when we replace $(k_{min}(\langle\tau\rangle)+1)/(N\delta)$ with ζ. If we plot $\langle\tau\rangle$ and ζ in double logarithmic scale we notice a nearly linear dependence between $1/\langle\tau\rangle$ and ζ. This is the reason why by replacing $\langle g\rangle_{min}$ with a constant one can get a good approximation of $\langle\tau\rangle$ as we will see later. Two examples for this nearly linear relation can be seen in Figure 5.6a for noise rates of $p = 0.9$ and $p = 0.6$. The inset shows a comparison between ζ and η for $p = 0.9$. If we take a closer look on $\langle g\rangle_{min}$ however, we notice that the hypothesis of a linear relationship does not hold. In Figure 5.6b we can observe the exact value of $\langle g\rangle_{min}$ for the corresponding two sets of experiments. From empirical evidence we can suppose, that for the values of p and η of our simulations 2 is an upper bound of $\langle g\rangle_{min}$, which allows us to replace $\langle g\rangle$ with 2 in inequality (5.8).

5.4.1 Bounds for τ and $\langle\tau\rangle$

With the results of the last section we can derive upper and lower bounds for τ and the mean ISI $\langle\tau\rangle$. Both bounds of $\langle\tau\rangle$ can be used to approximate $\langle\tau\rangle$.

First we derive a lower bound for $\langle\tau\rangle$ using definition (5.7) and condition (5.8). [1]

$$\langle\tau\rangle_{min} = \frac{(N-1)\varepsilon(\eta-1)-\varepsilon}{2p} + \frac{1+t_{ref}}{2} + \sqrt{\left(\frac{(N-1)\varepsilon(\eta-1)-\varepsilon}{2p} + \frac{1+t_{ref}}{2}\right)^2 + \frac{N\varepsilon\delta}{p\langle g\rangle}} \tag{5.10}$$

In the following we will use (if not stated differently) the empirical upper bound 2 of $\langle g\rangle_{min}$ as explained in the previous section to substitute $\langle g\rangle$ in (5.10) and to calculate the numerical values of $\langle\tau\rangle_{min}$.

To get an upper bound for all possible ISIs we use (5.4) and (5.6):

$$\tau_{max} = \frac{(N-1)\varepsilon(\eta-1)}{2p} + \frac{1+t_{ref}}{2} + \sqrt{\left(\frac{(N-1)\varepsilon(\eta-1)}{2p} + \frac{1+t_{ref}}{2}\right)^2 + \frac{N\varepsilon\delta}{p}} \tag{5.11}$$

[1] Note that if $\langle g\rangle$ is replaced by $\langle g\rangle_{min}$ in (5.10) we get an expression for $\langle\tau\rangle$.

and have that (See Appendix B for details):

$$\langle\tau\rangle_{min} \leq \langle\tau\rangle \leq \tau_{max} \,. \tag{5.12}$$

Note that τ_{max} is an upper bound for all ISIs τ whereas $\langle\tau\rangle_{min}$ is only a lower bound for $\langle\tau\rangle$ but not for τ. Because of this fact $\langle\tau\rangle_{min}$ is much closer to $\langle\tau\rangle$ than τ_{max}, as we can observe in the Figures 5.6c and 5.6d which show the quality of these bounds. The solid line in Figure 5.6c represents $\langle\tau\rangle$ for 1000 concentration processes in logarithmic scale. It lies within a gray area that indicates the interval

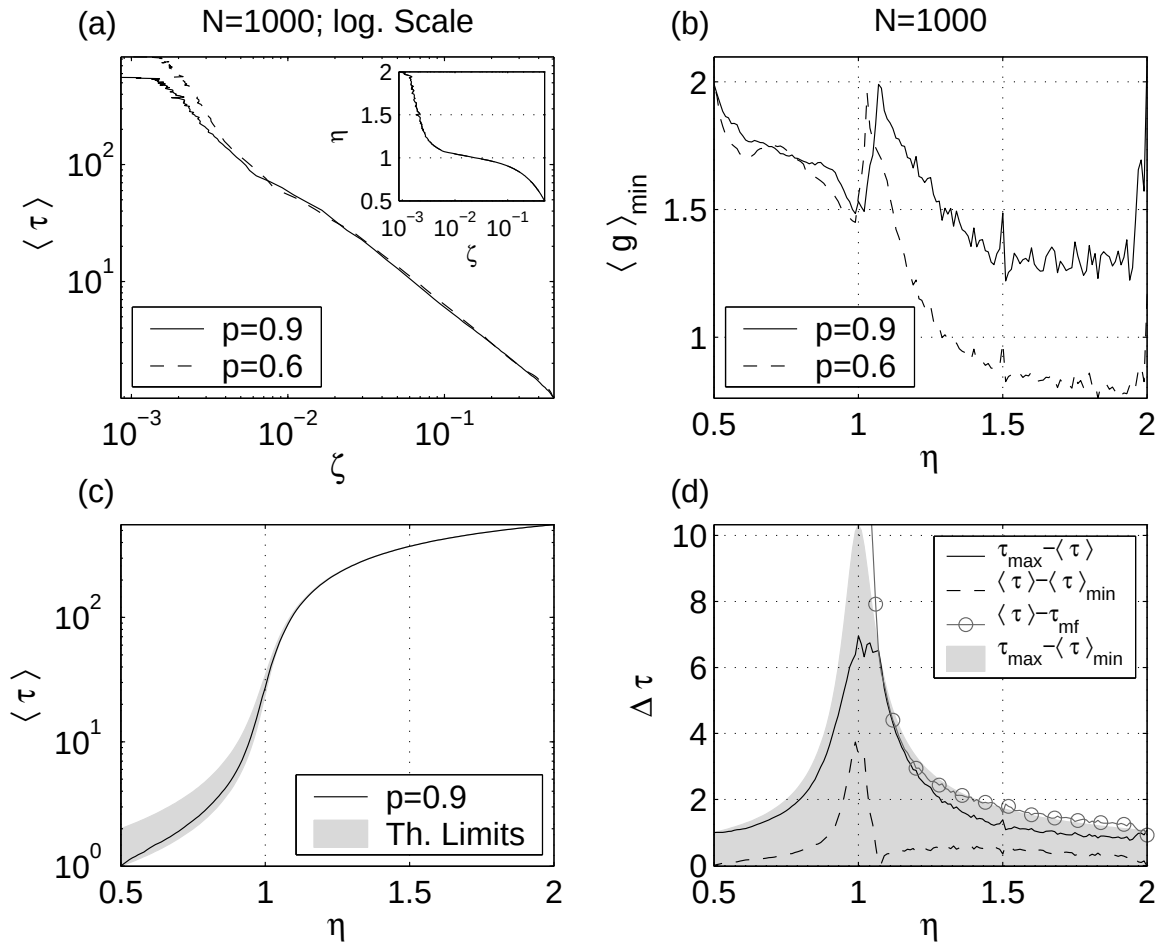

Figure 5.6: **(a)** Relation of $\langle\tau\rangle$ and $\zeta = (k_{min}(\langle\tau\rangle)+1)/(N\delta)$ for two different values of p. **(b)** Dependence of parameter $\langle g\rangle_{min}$ on η for two different values of p. We can observe $\langle g\rangle_{min} \leq 2$. **(c)** The empirical outcome $\langle\tau\rangle$ of the concentration processes of 1000 experiments compared to its theoretical limits τ_{max} and $\langle\tau\rangle_{min}$ (gray area). **(d)** Difference between the theoretical limits τ_{max} and $\langle\tau\rangle_{min}$ (gray area), $\langle\tau\rangle$ and $\langle\tau\rangle_{min}$ (dashed line), τ_{max} and $\langle\tau\rangle$ (black solid line), $\langle\tau\rangle$ and τ_{mf} (gray solid line with circles). τ_{max} has been calculated using equation (5.11) and $\langle\tau\rangle_{min}$ substituting 2 for $\langle g\rangle$ in equation (5.10).

limited by the two bounds $\langle\tau\rangle_{min}$ and τ_{max}.

In section B.2 we derive a lower bound $\tau_{min} \leq \tau$. $\tau_{min} = t_{ref}$ for $\eta < 1$ and coincides with the approximation τ_{mf} (see equation 4.5) for $\eta \geq 1$. We have therefore that

$$\tau_{mf} \leq \tau \leq \tau_{max}. \tag{5.13}$$

The exact difference between $\langle\tau\rangle$ and its bounds is shown in Figure 5.6d. The difference $\langle\tau\rangle - \langle\tau\rangle_{min}$ is indicated by the dashed line, and $\tau_{max} - \langle\tau\rangle$ by the solid line. The gray area shows the width of the interval bounded by $\langle\tau\rangle_{min}$ and τ_{max}. The quantity $\langle\tau\rangle_{min}$ is, for a wide range of values of η, not only a bound but an excellent approximation for $\langle\tau\rangle$. It beats by far the approximation τ_{mf}, whose difference to $\langle\tau\rangle$ is shown by the gray solid line with circles in Figure 5.6d. In spite of this fact the importance of $\langle\tau\rangle_{min}$ and τ_{max} does not only lie in their quality as approximations, but rather in the fact that they are bounds and both experience a similar phase transition effect as $\langle\tau\rangle$. This allows us to derive the thermodynamic limit of $\langle\tau\rangle$.

5.4.2 Thermodynamic Limit

The thermodynamic limits (i.e. the behavior for infinite N and L and finite η) of the bounds from equation (5.10) and (5.11) can be derived after some calculations (See Appendix C for details) and allow to set bounds for the thermodynamic limit of $\langle\tau\rangle$.

$$\begin{aligned}
\lim_{N\to\infty}\langle\tau\rangle &= \delta && \text{if } \eta < 0.5\ , \\
\frac{\delta}{\langle g\rangle(1-\eta)} \leq \lim_{N\to\infty}\langle\tau\rangle &\leq \frac{\delta}{(1-\eta)} && \text{if } 0.5 \leq \eta < 1\ , \\
\sqrt{\frac{\varepsilon\delta}{p\langle g\rangle}} \leq \lim_{N\to\infty}\frac{\langle\tau\rangle}{\sqrt{N}} &\leq \sqrt{\frac{\varepsilon\delta}{p}} && \text{if } \eta = 1\ , \\
\lim_{N\to\infty}\frac{\langle\tau\rangle}{N} &= \frac{\varepsilon(\eta-1)}{p} && \text{if } \eta > 1\ .
\end{aligned} \tag{5.14}$$

The upper bound at $0.5 \leq \eta < 1$ coincides with the one obtained for a model without stochastic input similar to (van Vreeswijk and Abbott, 1993). To characterize the quality of these bounds we examine the quantity $\Delta\tau = \tau_{max} - \langle\tau\rangle_{min}$, especially at its thermodynamic limit. The gray area in Figure 5.6d shows $\Delta\tau$ for the case of $N = 1000$ and $p = 0.9$. From (5.10) and (5.11) we can derive after some

algebra that

$$\lim_{N\to\infty}\Delta\tau=\begin{cases}0 & \text{for } \eta<0.5\ ,\\ \dfrac{\delta}{1-\eta}\left(1-\dfrac{1}{\langle g\rangle}\right) & \text{for } 0.5\le\eta<1\ ,\\ \lim\limits_{N\to\infty}\left(1-\dfrac{1}{\sqrt{\langle g\rangle}}\right)\sqrt{\dfrac{N\varepsilon\delta}{p}} & \text{for } \eta=1\ ,\\ \dfrac{\varepsilon}{p}+\dfrac{\delta}{\eta-1}\left(1-\dfrac{1}{\langle g\rangle}\right) & \text{for } \eta>1\ .\end{cases} \tag{5.15}$$

Since from $\tau_{max}\ge\langle\tau\rangle_{min}$ follows $\Delta\tau\ge 0$, we have that $\langle g\rangle$ and $\langle g\rangle_{min}$ have lower bounds:

$$\lim_{N\to\infty}\langle g\rangle\ge\lim_{N\to\infty}\langle g\rangle_{min}\ge\begin{cases}1 & \text{for } \eta\le 1\ ,\\ \dfrac{p\delta}{p\delta+(\eta-1)\varepsilon} & \text{for } \eta>1\ .\end{cases} \tag{5.16}$$

If we compare $\Delta\tau$ with the difference of τ_{mf} and τ_{max} we get

$$\lim_{N\to\infty}(\tau_{max}-\tau_{mf})=1+\frac{\delta}{\eta-1}\quad\text{for } \eta>1\ . \tag{5.17}$$

For high values of η the limit of this difference tends to 1. Therefore the formulas (4.5) of Rodríguez et al. (2001) really represent a good approximation of the dynamics for $\eta\gg 1$.

Approximation with $\langle\tau\rangle_{min}$ however is always closer to $\langle\tau\rangle$ if $p\ge\varepsilon$. In the case of $p<\varepsilon$ we can derive using $\langle\tau\rangle\ge\tau_{mf}$ an upper bound for $\langle g\rangle_{min}$.

$$\lim_{N\to\infty}\langle g\rangle_{min}\le\frac{p\delta}{(\eta-1)(\varepsilon-p)}\quad\text{if } \eta>1 \text{ and } p<\varepsilon\ . \tag{5.18}$$

As long as we use a value lower than the right hand side of inequality (5.18) to replace $\langle g\rangle$ in (5.10), the approximation of $\langle\tau\rangle$ with $\langle\tau\rangle_{min}$ beats τ_{mf} also for $\eta>1$ and $p<\varepsilon$, and is therefore an improvement to earlier studies for all values of η.

5.4.3 Application of the Thermodynamic Limit

If we suppose a dependence of $\langle\tau\rangle$ on N as in (5.1) ($\alpha N^c\sim\langle\tau\rangle$) we can now derive the thermodynamic limits for α and c from the above results. See Appendix C for details. The value of c is rather straightforward.

$$\lim_{N\to\infty}c=\begin{cases}0 & \text{for } \eta<1\ ,\\ 0.5 & \text{for } \eta=1\ ,\\ 1 & \text{for } \eta>1\ .\end{cases} \tag{5.19}$$

This observation coincides with the experimental results presented in Figure 5.3 and indicates a linear dependence between the ISI and the number of neurons N for $\eta>1$, whereas for $\eta<1$ the ISI does not depend on the amount of units in the ensemble at all. In between at $\eta=1$ the mean value of the

ISI distribution $\langle\tau\rangle$ depends on $\sqrt{N}$.

The thermodynamic limit of α follows straightforward from (5.14). We get:

$$\begin{aligned}
\lim_{N\to\infty}\alpha &= \delta && \text{if } \eta < 0.5\ ,\\
\frac{\delta}{\langle g\rangle(1-\eta)} \le \lim_{N\to\infty}\alpha &\le \frac{\delta}{(1-\eta)} && \text{if } 0.5 \le \eta < 1\ ,\\
\sqrt{\frac{\varepsilon\delta}{p\langle g\rangle}} \le \lim_{N\to\infty}\alpha &\le \sqrt{\frac{\varepsilon\delta}{p}} && \text{if } \eta = 1\ ,\\
\lim_{N\to\infty}\alpha &= \frac{\varepsilon(\eta-1)}{p} && \text{if } \eta > 1\ .
\end{aligned} \tag{5.20}$$

Since we can replace $\langle g\rangle$ with $\langle g\rangle_{min}$ and $1 \le \langle g\rangle_{min} \le 2$ for $\eta \le 1$ we get an excellent approximation for α at the limit of large N. We can observe this in Figure 5.4. The shaded area shows the possible regions of α. Already for low N the experimental data fits well into the theoretical results for the thermodynamic limit, which give an idea what ISI to expect for $\eta < 1$.

A graphical interpretation of the above findings can be found in Appendix D.

5.4.4 Hysteresis

Condition (5.4) for a periodic spiking pattern gives us also the explanation of the hysteresis phenomena. In the dilution process we always start from a robust or semi-robust pattern at $\eta \le 1$ and condition (5.4) is not altered by an increase of η. The inequality gets even sharper, which means that the probability of changing a semi-robust pattern is even lower the more we increase η. In other words: the semi-robust patterns tend to be robust during the dilution process. This changes once we reach $\eta = 1$, since now the stochastic state transitions are needed again to maintain the ISIs. But even for $\eta > 1$ the ISI may remain constant as long as the following condition is fulfilled. (See section B.2 for details and derivation)

$$\tau \ge t_{ref} + \frac{(N-1)\varepsilon(\eta-1)}{p}\ . \tag{5.21}$$

This inequality reflects that the approximations (4.5) of Rodríguez et al. (2001) are a lower bound for the ISI in the dilution process, which have to be fulfilled by the deterministic system. Only when a value of η violating this condition is reached, the system leaves the ISI it has fired with since the beginning of the dilution process and changes to a new ISI which does fulfill the condition. We can observe this in the dashed-dotted line with $\diamond$ markers of Figure 5.5 which shows a dilution process started already at $\eta = 0.99$. In this case $\langle\tau\rangle$ remains constant even for $\eta = 1.01$ since inequality (5.21) is still fulfilled at this point. Only if we dilute further $\langle\tau\rangle$ increases to values fulfilling condition (5.21) and starts to coincide with $\langle\tau\rangle$ of the other two dilution processes. Approximately at $\eta = 1.08$ the mean ISI of dilution processes coincides with the one of the concentration processes, since then the equations (4.5) start to approximate $\langle\tau\rangle$ well again.

Chapter 6

Results for heterogeneous networks

In this chapter we show that the results described in chapter 5 for homogeneous networks can be extended to networks consisting of neurons with heterogeneous coupling strengths and thresholds.

6.1 Generalization of the model

To be able to simulate heterogeneous networks we have to apply the following extensions to the model presented in section 4.1.

- Instead of setting all coupling strengths ε_{ij} equal to an homogeneous coupling strength ε we take the ε_{ij} from a Gaussian distribution with mean $\langle\varepsilon\rangle$.
- We allow heterogeneous thresholds L_i for every unit. Each L_i is taken form a Gaussian distribution with mean $\langle L\rangle$.
- The relation (denominated s) between standard deviations and means of both distributions is fixed.
- To characterize the new extended system we calculate the parameter η in the same way as before but use the mean values $\langle\varepsilon\rangle$ and $\langle L\rangle$ of the distributions instead of L and ε of a homogeneous network. We call this parameter η_{ext}.

$$\eta_{ext} = \frac{\langle L\rangle - 1}{(N-1)\langle\varepsilon\rangle} \; . \tag{6.1}$$

With this model of a heterogeneous network we perform the same type of experiments as described in section 4.2. In the concentration process we start in regions with high η_{ext} and increase the connection strengths of the system adiabatically. As in the experiments with homogeneous networks we increase it by resting a constant value $\Delta\eta_{ext}$ from η_{ext}. We have to calculate the corresponding values of ε_{ij}

after the change by multiplying them by $\eta_{ext}/(\eta_{ext} - \Delta\eta_{ext})$. Thus we achieve that after every change equation (6.1) is still valid.

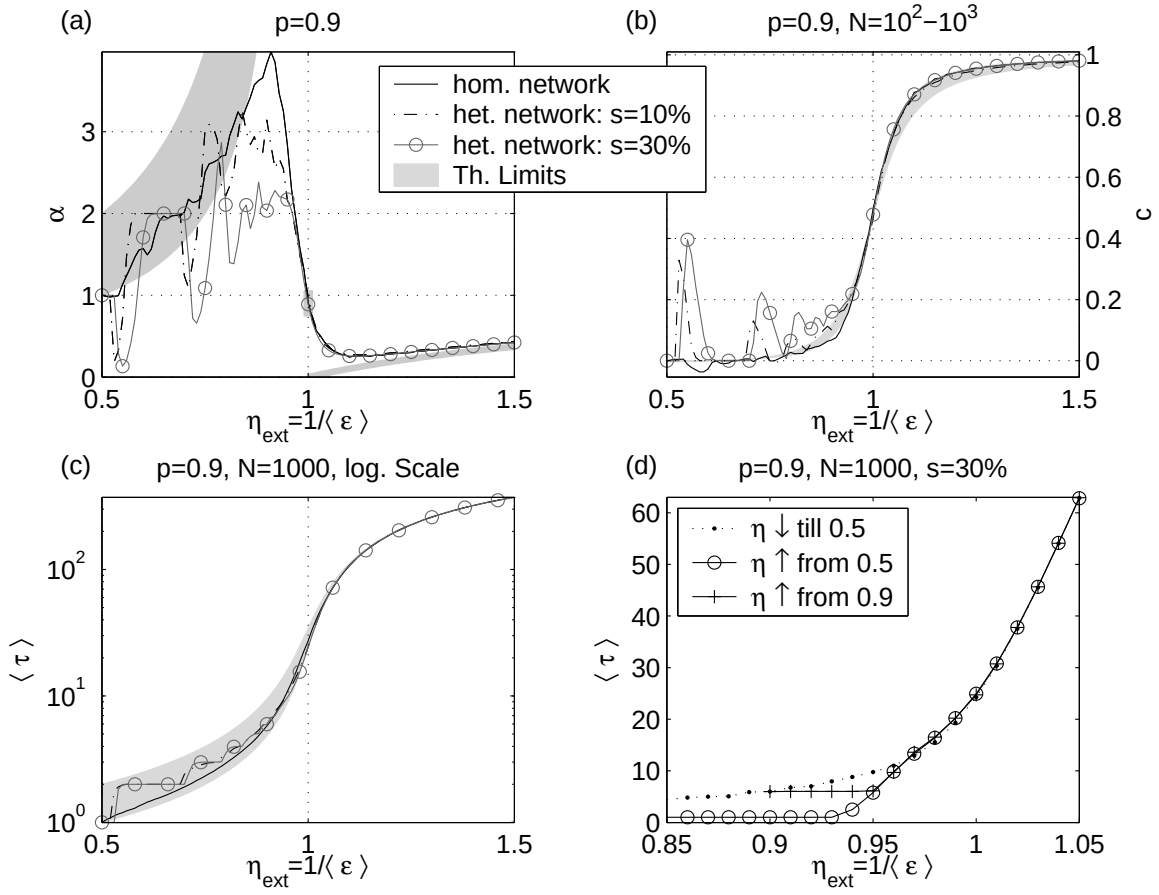

Figure 6.1: **(a)**, **(b)** and **(c)** compare the results of 1000 experiments with homogeneous and heterogeneous networks. **(a)** shows α and **(b)** c under the assumption that $\langle\tau\rangle = \alpha N^c$ for $N \in \{100, 200, \ldots 1000\}$. Coupling strengths and thresholds where taken from Gaussian distributions with deviations of 10% (dash-dotted line) and 30% (gray solid line with circles) of their means. The black solid lines (homogeneous network) coincide with the results shown in Figures 5.3 and 5.4, as well as the shaded areas, which represent in **(a)** the regions of possible values of α for $N \to \infty$ according to equations (5.20) and in **(b)** the region of possible values of c obtained using equations (5.10) and (5.11) for finite N as in the experiments. **(c)** Comparison only of the results for $N = 1000$. The mean ISIs $\langle\tau\rangle$ of the heterogeneous experiments lie within the gray area bounded by $\langle\tau\rangle_{min}$ (Eq. 5.10) and τ_{max} (Eq. 5.11). Compare with Figure 5.6c. We notice that the results obtained for the theoretical bounds of the ISI are also valid for heterogeneous networks. **(d)** Hysteresis in a heterogeneous network with $s = 30\%$. Compare with Figure 5.5. Hysteresis does also occur in heterogeneous networks, but vanishes there already at η slightly lower than 1.

6.2 Results for heterogeneous networks

We compare experiments with the generalized model with the results of chapter 5 for homogeneous networks. Figure 6.1 shows this comparison for the values of α (Figure 6.1a) and c (Figure 6.1b) of equation (5.1).

The only noticeable difference between experiments with homogeneous networks (solid black line) and the corresponding heterogeneous equivalents with deviations of 10% (dash-dotted line) and 30% of the mean value (gray solid line with circles) is that for $\eta \leq 1$ the curves show some irregular bumps which differ from the expected values (gray areas) of the theoretical analysis. A closer examination of the ISIs at $\eta < 1$ reveals that this bumps are provoked by jumps between integer values of the ISI, as can be observed in Figure 6.1c, which shows $\langle\tau\rangle$ for $N = 1000$. Contrary to intuition the smooth change of the mean ISI in the homogeneous case (black solid line) is more step-like in heterogeneous networks, meaning that for certain intervals of the coupling strength (i.e. the plateaus in Figure 6.1c) nearly all the experiments (with different networks) end up with the same ISI. The observed behavior, which is reproducible and robust despite the stochastic inputs and the heterogeneity of the network, is not fully understood, but might be of biological relevance and will be subject of future research. The locations of the steps depend on the ensemble size N, which causes the bumps in Figures 6.1a and 6.1b. In the thermodynamic limit, however, these bumps should disappear.

In spite of this effect, the upper and lower bounds for $\langle\tau\rangle$, given by equations (5.10) and(5.11) and represented by the gray area in Figure 6.1c, are valid even for high deviations of the underlying probability distributions. Also the hysteresis effect is present in the heterogeneous networks (Figure 6.1d), although it vanishes slightly before the critical coupling strength is reached at $\eta = 1$ (compare with Figure 5.5). This is caused by some neurons which receive less input compared with their threshold than the others. They need stochastic input to reach the threshold already slightly below $\eta = 1$, which can cause the end of self-sustained firing and an increase in the ISI of the ensemble.

Chapter 7

Sequential versus Parallel Dynamics

The results presented so far have been obtained using parallel updating of the units, meaning that at every time-step all units are updated. Sometimes sequential dynamics, where only a reduced number of neurons is updated at every time-step, are used to simulate neural dynamics instead (Herz and Marcus, 1993). It has been shown that sequential and parallel updating can lead to different behavior of the Hopfield model (Fontanari and Köberle, 1988) and multi-state Ising-type ferromagnets (Bolle and Blanco, 2004), which motivates us to investigate the dependence of our results on the type of updating.

7.1 Sequential model

We will use the most simple case of sequential updating, where only one neuron is updated at each time-step and modify the model presented in section 4.1 in the following way:

- One time-step of the original model is split up into N time-steps and at each new time-step only one neuron is updated. A specific neuron i is updated at every time-step t which fulfills $i \equiv t \mod N$.

- Given a synaptic delay δ^{seq} and a refractory period t_{ref}^{seq}, the neuron which is updated at time t receives all the spikes which have been sent within the interval $[t-N-\delta^{seq}, t-\delta^{seq})$ by the other neurons. In case that neuron i fired in the last update, the interval narrows to $[t-N-\delta^{seq}+t_{ref}^{seq}, t-\delta^{seq})$.

This modification implies that the synaptic delay is no longer homogeneous. An update of a post-synaptic unit occurs now the next time it is updated instead of the precise time-step when the spike would reach the unit. Therefore the effective delay is uniformly distributed between δ^{seq} and $\delta^{seq}+N$,

leading to an average delay of

$$\langle \delta^{seq} \rangle = \delta^{seq} + N/2. \tag{7.1}$$

7.2 Results with sequential updating

To compare simulations with sequential and parallel dynamics we have to set δ^{seq} accordingly to fulfill $N\delta = \langle \delta^{seq} \rangle$ where δ is the delay of the parallel dynamics. This leads to

$$\delta^{seq} = N\left(\delta - \frac{1}{2}\right). \tag{7.2}$$

The equations for upper (Eq. 5.11) and lower bounds (Eq. 5.10) obtained for the parallel dynamics are valid only if $t_{ref} \leq \delta$, which means that the only noticeable effect of t_{ref} on the ensemble dynamics is that the threshold L acts as an absorbing barrier. In other words: if the state of a certain unit i exceeds the threshold, this excess is absorbed and not used as the new state of the unit after reseting it. Nevertheless, spikes of other units which occur during the same time-step as the one of unit i are not absorbed if the delay δ of the message exchange is greater than or equal to the refractory period t_{ref}. This means that only a minimum amount of activity is absorbed in the parallel dynamics. To achieve

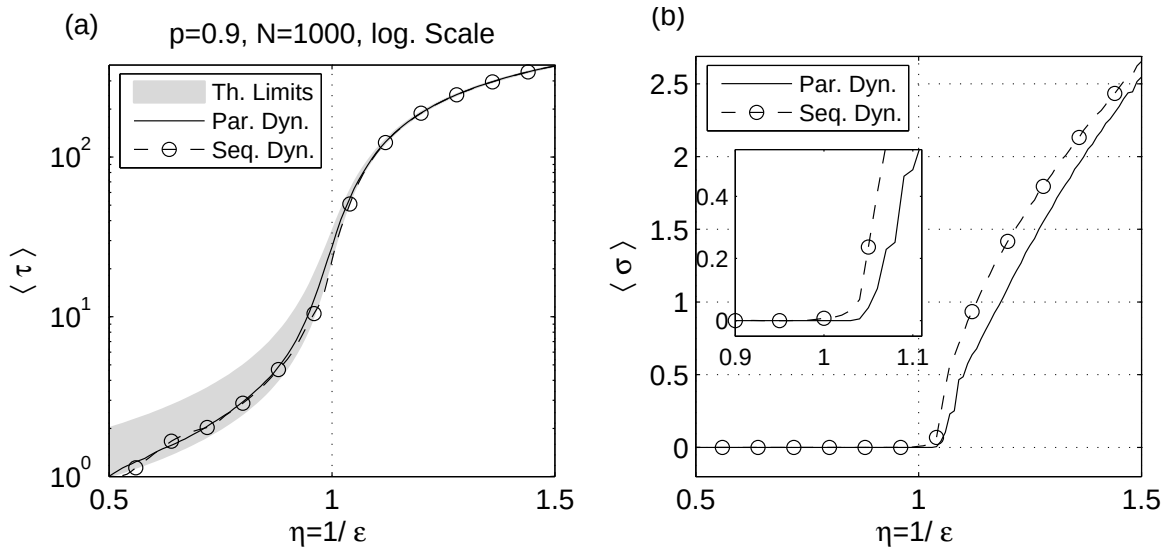

Figure 7.1: Comparison of 1000 experiments with parallel dynamics (continuous lines) and their equivalent with sequential updating (dashed lines with circles). Number of neurons $N = 1000$ equals threshold L and $p = 0.9$. The results for the sequential dynamics are rescaled by the factor 1000. **(a)** The mean ISIs $\langle\tau\rangle$ of both type of dynamics nearly coincide and lie within the gray area bounded by $\langle\tau\rangle_{min}$ (Eq. 5.10) and τ_{max} (Eq. 5.11). **(b)** The sequential dynamics show a slightly higher mean of deviation $\langle\sigma\rangle$ of the units ISIs with the same experiments as the parallel dynamics for $\eta \geq 1$ but also end up in phase-locked clusters at $\eta < 1$. The inset shows a zoom on the interesting region around $\eta = 1$.

the same effect of the refractory period in the sequential model we have to set t_{ref}^{seq} to a minimal value, i.e. $t_{ref}^{seq} = 1$. This guarantees that spikes from other units which arrive after the threshold crossing are not affected by the the refractory period. A t_{ref}^{seq} greater than 1 could lead to the absorption of those spikes and in consequence to a greater ISI of the ensemble than in the corresponding parallel experiments.

If we consider these two constraints we obtain similar results for both type of dynamics, as shown in Figure 7.1, where we compare simulations with increasing coupling strength for $N = 1000$ neurons and a noise rate $p = 0.9$. Since the delay δ of the parallel simulations equals 1, δ^{seq} was set to 500. This implies a mean delay $\langle \delta^{seq} \rangle$ of N, which is coherent with the rescaling of t to t/N. We observe in Figure 7.1a that after rescaling (i.e. dividing the ISI by the ensemble size) the mean ISI of the sequential dynamics (dashed line with circles) nearly coincides with the result of the parallel simulations (continuous line), and the bounds obtained in section 5.4 are valid also for this type of dynamics. Hysteresis can also be observed (data not shown). Units with sequential updating show due to the inhomogeneous delays a slightly greater deviation of their ISIs than their equivalents with parallel updating (see Figure 7.1b). This effect causes that phase-locked clusters, although observable also at $\eta = 1$, appear as a general phenomena (i.e. $\langle \sigma \rangle = 0$) for couplings slightly greater than the critical coupling strength as we can observe in the inset of Figure 7.1b.

Despite these small differences due to the enhanced dispersion of the ISIs we can conclude that the results derived in the previous chapters are also valid if sequential instead of parallel updating is used.

Chapter 8

Discussion of the results for neural networks

We analyzed, by varying its coupling strength ε, the behavior of an ensemble of stochastic, non-leaky integrate-and-fire neurons with delayed, excitatory global coupling and a small refractory period. Around a critical value of the coupling strength the behavior of the system undergoes a phase transition (Figure 5.3), which has three main consequences on the dynamics of the ensemble:

Transition from irregular to clustered spiking behavior: The units of the ensemble are homogeneous but show, due to a stochastic component in their evolution towards threshold, irregular spiking behavior if they are weakly coupled (Figure 4.1a). The coupling strength ε is inversely proportional to the parameter η (see equation 4.4), which describes the system and allows to fixate the phase transition at $\eta = 1$. For coupling greater than or equal to the coupling at $\eta = 1$ the population splits into several clusters. All neurons within a cluster spike in unison, although they still might show different trajectories towards the threshold. The clusters are phase-locked (Figure 4.1b) and have all exactly the same ISI, which is proportional to the number of clusters. This number decreases if the coupling is increased further (Figure 4.1c), but usually remains greater than 1 until a trivial case of only one cluster is reached at latest at $\eta < 0.5$. The activity at $\eta \leq 1$ is self-sustained in the sense that the stochastic inputs are not needed to maintain the clustered spiking activity.

Hysteresis: The phase transition is accompanied by a hysteresis effect (Figure 5.5). We applied a cyclic process to our system which consisted of two subprocesses: a concentration process where we increased ε and a dilution process where ε is decreased. Starting at an initial configuration with low coupling the process is reversible as long as we do not reach (at values of η slightly greater than 1) the onset of phase-locking. If we increase the coupling strength further the ISI τ of the concentration process decreases following rules explained below, whereas if we inverse the process (start the dilution process) the ISI remains frozen as long as $\eta \leq 1$.

Then it jumps up to a value fulfilling condition (5.21) and coincides again with the ISI of the concentration process at η slightly greater than 1.

Change in the dependence of the ISI on ensemble size and noise rate: For low coupling the mean ISI $\langle\tau\rangle$ of the ensemble in the concentration process depends linearly on the ensemble size N, at $\eta = 1$ there is a square root dependence on N, whereas for coupling greater than at $\eta = 1$ the mean ISI $\langle\tau\rangle$ does not depend on N nor on the rate of the stochastic component, which governs the dynamics for low coupling. Between $\eta = 1$ and $\eta = 0.5$ the ISI only depends on the coupling strength itself. For a coupling greater than at $\eta = 0.5$ the influence of ε on the ISI is also lost. The length of the time delay determines the length of the ISI in this regime.

To obtain analytical results we used a deterministic approach to the model dynamics which allowed us, using a simple condition (5.4), to derive upper and lower bounds (τ_{max} and $\langle\tau\rangle_{min}$) for the mean ISI $\langle\tau\rangle$ of the ensemble in the concentration process. The lower bound $\langle\tau\rangle_{min}$ is also an excellent approximation for $\langle\tau\rangle$, as can be observed in Figure 5.6d. Using the bounds we can calculate the behavior of the system at its thermodynamic limit (i.e. for $N \to \infty$) and characterize the phase transition analytically.

These theoretical results are also valid if sequential instead of parallel updating (Herz and Marcus, 1993) is used to simulate the dynamics (Figure 7.1). In this case the synaptic delay is no longer homogeneous, leading to a slightly higher deviation of the unit's ISIs and in consequence a slightly later onset of clustered spiking behavior in the concentration process.

The above explained effects could also be observed if, instead of an increase or decrease of the coupling strength, positive or negative external input were be added to the system. To calculate the critical point in this case we would have to add the external input to the denominator of equation (4.4) to get the appropriate value of η.

Using the hysteresis effect one can generate a simple memory by stimulating the system with a strong input, which leads the system to a value below $\eta = 1$. If the input is then substituted by a smaller one, which is just big enough to maintain the system below the critical couping strength and could represent the will to remember the first input, the ISI and the firing pattern of the ensemble will still be the same as if the strong input were still present. Once the system receives a short erase signal (e.g. in form of a negative input, or the absence of the small input), which allows it to reach a state corresponding to $\eta > 1$, the firing pattern produced by the strong input will disappear (i.e. the memory will be deleted). Such a mechanism might be a novel way to represent working memory functions (Wang, 2001), which are often modeled in the form of bistable dynamical attractor networks (Durstewitz, Seamans and Sejnowski, 2000). In our case it seems that we have multi-stability for coupling greater than the critical coupling strength, but further analysis is needed to verify this claim.

The main difference of our model to those used in earlier studies is the use of discrete time dynamics and that we combine delayed coupling with an implicit refractory period. Setting delay δ and refractory period t_{ref} identical and equal to 1 in the experiments does not represent a critical restriction on the presented results as can be seen in the theoretical analysis, which is valid in the general case as long as $\delta \geq t_{ref}$ and both are positive. We can observe as well from equations (5.15) and (5.17) that in a system with no delay, i.e. $\delta = 0$, the upper and lower bounds nearly coincide, leaving no space for clustering with more than one cluster and hysteresis. For a delay lower than the refractory period some of the inter-population messages would get absorbed, leading to different upper and lower bounds for the ISIs. Such a pair of bounds has been calculated for a system without stochastic input in van Vreeswijk and Abbott (1993) for the case of δ slightly lower than t_{ref}. We expect those results to be valid for our system at $\eta < 1$ in the thermodynamic limit. In the case of sequential dynamics the condition $\delta \geq t_{ref}$ translates into setting the refractory period to a minimum value.

It is straightforward to transfer the discrete time dynamics onto the continuous domain replacing the stochastic state transitions with a continuous increase of the state variable. This leads to continuous oscillators similar to the ones analyzed by Senn and Urbanczik (2000), but with the add-ons of delayed coupling and refractory period, which are both crucial to observe the reported phase transition and clustering phenomena. One can even maintain the stochastic dynamics using a continuous extension of the ISI distribution of a single uncoupled unit, a negative binomial distribution in our case (Rodríguez et al., 2001). Two different possibilities for such an extension have been presented by Gómez, Kaltenbrunner and López (2006), leading both to gamma distributions. The length of delay and refractory-period remain untouched by these extensions. An analysis of these models is object of current research using a novel event-driven modelling technique (Gómez et al., 2006) allowing to simulate such extended models (also with non-integer values for delay and refractory period) without precision errors and without determining the exact trajectories of the states of the units in the ensemble. The derived formulas for upper and lower bounds should, apart from some minor modifications, be valid in these extended systems as well.

For models with a leaky term (Mirollo and Strogatz, 1990) clustering phenomena have been reported by Ernst et al. (1998) if a delay is added, but these clusters turned out to be unstable for excitatory coupling if noise was added to the coupling strength. We conjecture that this behavior would change if a positive refractory period were included in the system. During the refractory period the threshold acts as an absorbing barrier allowing the system a certain tolerance against noise which is the higher the greater the amount of absorption is. The fact that Ernst et al. (1998) reports stability for inhibition is a clear evidence for this conjecture, since the reset state is a reflecting barrier in their model, allowing to absorb noisy negative coupling. It would also be interesting to observe

the effect of delay and refractory period for a model with a biological inspired phase response curve (PRC). For this type of PRC the existence of a phase transition in the case of one (Östborn, 2002) and two dimensional (Östborn et al., 2003) oscillator lattices has been reported.

Our study shows that synaptic delay changes significantly neural dynamics. It is crucial for the observed hysteresis effect and the appearance of several phase-locked clusters. Without it we would get a totally synchronized ensemble at the critical coupling strength. The lack of a leaky term makes our model biologically plausible only at the limit of high coupling where integration of synaptic inputs occurs over a time scale much shorter than the decay constant (Burkitt and Clark, 1999), which is exactly where we find the phase transition and hysteresis. We therefore conjecture that the phenomena described could be found as well in more complex, realistic neural models with delay. Even in a system with inhomogeneous delays we can find similar results as shown for the case of sequential dynamics, which demonstrates the robustness of the findings.

In a network consisting of heterogeneous neurons with different coupling strengths and thresholds drawn from Gaussian distributions the reported phenomena are also present (Figure 6.1). This may be of great importance if synaptic dynamics are added to the model. We conjecture that in this context, plasticity may act as a homeostatic mechanism to maintain the system in the regime around the critical coupling strength if it experiences perturbations. In the neighborhood of the critical state the system explores all possible clusters one after the other. Clusters that are phase-locked after crossing this point are then transient states and the system is ready to set in any of the phase-locked, periodic firing patterns as a reaction to an increase in the number of received messages. This could have potential applications in a wide range of engineering applications like image segmentation (Campbell, Wang and Jayaprakash, 1999; Rhouma and Frigui, 2001) or large scale sensor networks (Hong and Scaglione, 2005; Hu and Servetto, 2006), where clustering might be useful to optimize the information throughput. The application of the results to information processing in natural systems is the subject of current research.

As a final aspect we would like to highlight the application of our model (interpreted as a network of pulse-coupled oscillators with stochastic frequencies) to describe animal behavior, e.g. populations of flashing fireflies (Buck, 1988). For the North American firefly several types of synchronization have been reported (Copeland and Moiseff, 1995) and it seems that a certain number of flashing flies within a certain area is needed to observe synchronization. This would be in consonance with our model, where an increase in the number of units (fireflies) would decrease the coupling parameter η. For a certain number of units we would reach the critical point, where synchronization would appear. Apart form unison synchrony, wave synchrony has been observed, which might be explained by the clusters we report.

Part III

Human communication behavior

Chapter 9

Introduction into human communication dynamics

9.1 Motivation

Nowadays, an important part of human activity leaves electronic traces in form of server logs, e-mails, loan registers, credit card transactions, blogs, etc. This huge amount of generated data allows to observe human behavior and communication patterns at nearly no cost on a scale and dimension which would have been impossible some decades ago. A considerable amount of studies has emerged in recent years using some part of these data to investigate the time patterns of human activity. The studied temporal events are rather diverse and reach from directory listings and file transfers (FTP requests) (Paxson and Floyd, 1995), job submissions on a supercomputer (Kleban and Clearwater, 2003), arrival times of consecutive printing-job submissions (Harder and Paczuski, 2006) over trades in bond (Mainardi, Raberto, Gorenflo and Scalas, 2000) or currency futures (Masoliver, Montero and Weiss, 2003) to messages in Internet chat systems (Dewes, Wichmann and Feldmann, 2003), online games (Henderson and Bhatti, 2001), page downloads on a news site (Dezso et al., 2006) and e-mails (Johansen, 2004). A common characteristic of these studies is that the observed probability distributions for the waiting or inter-event times are heavy-tailed (Sigman, 1999). However, which type of heavy-tailed distribution provides the best explanation of the data is still an open problem. A recent study (Barabási, 2005) tries to illuminate these phenomena under the assumption that these heavy-tailed distributions can be well approximated by a power-law or at least by a power-law with an exponential cut-off (Newman, 2005). The cited study presents a model which seems to explain the distribution of e-mail response times and has been used later to account for the inter-event times of web-browsing, library loans, trade transactions and correspondence patterns of letters (Vázquez et al., 2006). However, the hypothesis of a power-law distribution is not generally accepted, at least in case of e-mail response times. Stouffer, Malmgren and Amaral (2006) claim that the data can be much better fitted with either a log-normal (LN) distribution (Crow and Shimizu, 1988; Limpert, Stahel

and Abbt, 2001) or the superposition of two LN, a double log-normal (DLN) distribution (Fowlkes, 1979). The debate power-law versus log-normal has been repeated across many areas of science for decades, as noticed by Mitzenmacher (2004). For log-normal event-time distributions in other areas of science see Lawrence (1988).

9.2 Slashdot

Here we extend the above mentioned debate to the temporal patterns of human communication in systems where social interaction occurs in a more complex manner than just person to person (one-to-one) communication. We think it is valuable to analyze the many-to-many social interaction on a technology-related news-website which supports user participation and have therefore chosen to investigate the communication patterns on Slashdot[1], a popular website for people interested in reading and discussing about technology and its ramifications. It gave name to the "Slashdot effect" (Adler, 1999), which refers to the phenomenon of a popular website linking to a small, under-powered one, causing a huge influx of traffic towards the hosted link during a short period of time, which may force the small website to slow down or even to temporarily collapse.

Slashdot was created at the end of 1997 and has ever since metamorphosed into a website that hosts a large interactive community capable of influencing public perceptions and awareness on the topics addressed. Its role can be metaphorically compared to that of commercial malls in developed markets, or hubs in intricate large networks. The site's interaction consists of short-story **posts** that often carry fresh news and links to sources of information with more details. These posts incite many readers to **comment** on them and provoke discussions that may trail for hours or even days. Most of the commentators register and comment under their nicknames, although a considerable amount participates anonymously.

Although Slashdot allows users to express their opinion freely, moderation and meta-moderation mechanisms are employed to judge comments and enable readers to filter them by quality. The moderation system was analyzed by Lampe and Resnick (2004), who concluded that it upholds the quality of discussions by discouraging spam and offending comments, marking a difference between Slashdot and regular discussion forums. This high quality social interaction has prompted several socio-analytical studies about Slashdot. Poor (2005) and Baoill (2000) have both conducted independent inquiries on the extent to which the site represents an online public sphere as defined by Habermas (1962/1989).

Given that a great amount of users with different interests and motivations participates in discussions about very different topics, one would expect to observe a high degree of heterogeneity on

[1] http://www.slashdot.org

a site like Slashdot. However, what if the posts and comments were analyzed just as imprints of an occurring information exchange, with no regard to semantic aspects? Is there a homogeneous behavior pattern underlying heterogeneity? To answer these and related questions we collected and studied one year's worth of interchanged messages along with the associated meta-data from Slashdot. We show here that the temporal patterns of the comments provoked by a post are very similar, indicating that homogeneity is the rule not the exception. The temporal patterns of the social activity fit accurately log-normal distributions, thus giving empirical evidence of our hypothesis and establishing a link with previous studies where social interaction occurs in a simpler way. The quality of the LN-fit depends on the publishing hour of a post. This dependency can be eliminated and therefore the quality of the fit can be improved by using double log-normal distributions, i.e. a mixture of two independent log-normals, as for example used in (Stouffer et al., 2006) to explain the waiting time in email conversation, or by multiplying a log-normal distribution with a periodic function. The best results are obtained if both methods are combined.

Our analysis allows more insight into questions such as: is there a time-scale common to all discussions, or are they scale-free? What does incite a user to write a comment, is it the relevance of the topic, or maybe just the hour of the day? Can we predict the amount of activity a post will trigger already some minutes after it has been written? Which type of applications can we devise on the basis of using these conclusions?

Even though Slashdot holds much closer ties to web based bulletin board systems (BBS) and newsgroups, we can find some related studies about the comments to posts on weblogs (Mishne and Glance, 2006; Duarte, Mattos, Bestavros, Almeida and Almeida, 2007). It was shown that the amounts of comments per post and per blog follow heavy-tailed distributions, but only 30% of the blogs (15% percent of the posts) received comments (Mishne and Glance, 2006). According to Duarte et al. (2007), 55% of the discussions appearing in these blogs can be classified as many-to-many communication. Among other temporal patterns of the comments, their study also analyzes the aggregate of all PCI-distributions, which is fit by a Weibull distribution. The number of comments per user in a BBS was shown to be distributed according to a truncated LN distribution (Naruse and Kubo, 2006), which coincides with our results.

9.3 Statistical preliminaries

In this section we briefly give a formal characterization of heavy-tailed distributions, the densities of the probability distributions used for fitting the data and explain the principle of the statistical test used to measure the quality of the fits.

9.3.1 Definition of heavy-tailed distributions

According with (Sigman, 1999) we give the following formal definition for the class of heavy-tailed distribution:

Definition 2 *Given a non-negative random variable X, its distribution is said to be heavy-tailed if its cumulative distribution function $F(x) = P(X \leq x)$ fulfills*

$$\lim_{x \leftarrow \infty} P(X > x+y | X > x) = \lim_{x \leftarrow \infty} \frac{1-F(x+y)}{1-F(x)} = 1 \tag{9.1}$$

for $y \geq 0$.

In other words, if X ever exceeds a large value it is likely to exceed any larger value as well. An important subclass of the heavy-tailed distributions are the so called subexponential distributions (Goldie and Kluppelberg, 1998), whose tail $1-F(x)$ tend to zero slower than any exponential $e^{-\varepsilon x}$. Several important distributions belong to this class. Those of them which we will use in this study are described in more detail hereafter.

9.3.2 Log-normal and double log-normal distributions

If a random variable Y follows a Gaussian distribution then $X = \exp(Y)$ is log-normally distributed. This implies that a **log-normal (LN)** distribution has the following probability density function (pdf):

$$f_{LN}(t;\mu,\sigma) = \frac{1}{t\sigma\sqrt{2\pi}} \exp\left(\frac{-(\ln(t)-\mu)^2}{2\sigma^2}\right) \tag{9.2}$$

and its cumulative distribution function (cdf) is given by:

$$F_{LN}(t;\mu,\sigma) = \frac{1}{2} + \frac{1}{2}\mathrm{erf}\left(\frac{\ln(t)-\mu}{\sqrt{2}\sigma}\right), \tag{9.3}$$

where erf(x) is the Gauss error function being defined as

$$\mathrm{erf}(x) = \frac{2}{\sqrt{\pi}} \int_0^x \exp(-u^2) du. \tag{9.4}$$

And a **double log-normal (DLN)** distribution, which is a superposition of two independent LN-distributions and has the following pdf:

$$\begin{aligned} f_{DLN}(t;\theta) &= c\, f_{LN}(t;\mu_1,\sigma_1) + (1-c)\, f_{LN}(t;\mu_2,\sigma_2) \\ \text{where } \theta &= (\mu_1,\sigma_1,c,\mu_2,\sigma_2). \end{aligned} \tag{9.5}$$

The corresponding cdf can be easily derived from equations (9.3) and (9.5).

9.3.3 Power law distributions

The tail of a heavy-tailed distributed random variable X is often tried to fit with a function of the form of a power law

$$P(X = t) = Ct^{-\alpha} \text{ for } t \geq t_{min}. \tag{9.6}$$

Such distributions are also referred to as Pareto distributions or Zipf's laws (Newman, 2005). The value of C depends on the lower bound for the powerlaw behavior t_{min}, the exponent α and on whether we are modelling discrete or continuous data. Here we are only interested in the discrete **power law (PL)** distribution, whose pdf is given by

$$f_{PL}(t;\alpha,t_{min}) = \frac{t^{-\alpha}}{\zeta(\alpha,t_{min})} \tag{9.7}$$

and its cdf by

$$F_{PL}(t;\alpha,t_{min}) = 1 - \frac{\zeta(\alpha,t)}{\zeta(\alpha,t_{min})} \tag{9.8}$$

where

$$\zeta(\alpha,t) = \sum_{n=0}^{\infty}(n+t)^{-\alpha} \tag{9.9}$$

is the generalized or Hurwitz zeta function (Adamchik and Srivastava, 1998).

To find the optimal value for t_{min} to fit a dataset a recent study (Clauset, Shalizi and Newman, 2007) proposes a method based on finding the t_{min} for which the distance between the cdf of data and a PL-fit (using maximum likelihood estimation) takes a minimum value, which in most cases is equivalent with maximizing the p-value of a Kolmogorov-Smirnov test, which is described hereafter.

9.3.4 Kolmogorov-Smirnov test

To test whether a given dataset is distributed according to a certain model distribution F, we use the Kolmogorov-Smirnov (KS) test with the following hypotheses:

H_0**:** The data is a sample of distribution F.

H_1**:** The hypothesis H_0 is not true.

The test is based on finding the maximal difference D between the cdf of data and model distribution. With this maximum and the number of samples (i.e. the number of comments in our case) we can calculate the p-value of the KS-test. It gives us the probability of obtaining a result as different from F as the data. In other words: the greater the p-value, the closer is the fit with the test distribution. The hypothesis H_0 is accepted if the p-value is greater than the chosen level of significance α_0 (usually

set to 0.05 or 0.01). Using the following formula one can calculate the p-value, given the number n of elements in the dataset:

$$p = 2\sum_{i=1}^{\infty}(-1)^{i-1}\exp\left(-2i^2\left(\sqrt{n}+0.12+0.11/\sqrt{n}\right)^2 D^2\right). \tag{9.10}$$

Usually a summation up to $i = 100$ is enough to obtain reliable results (Press, Flannery, Teukolsky and Vetterling, 1992). For more details see for example (DeGroot and Schervish, 2002).

Note that the KS-test is designed to test distributions whose parameters are independent of the dataset used. In other words: if we use the dataset to calculate the parameters of the distribution, e.g.. through maximum likelihood estimation, we introduce a bias towards higher p-values (Goldstein, Morris and Yen, 2004). One could use instead an equivalent to the Lilliefors test for normal distribution (Abdi and Molin, 2007). However, this implies a huge amount of Monte Carlo simulations to obtain reliable results. Since we are mainly interested in describing the quality of a fit, we use the p-values of the much simpler KS-test as a measure of approximation quality rather than as statistical proof of the origin of the underlying data.

Chapter 10

The dataset

In this chapter we explain the methods used for data retrieval and the analysis of Slashdot. We give then some basic quantities of the retrieved data and an overview of the global activity looking at the data on different temporal scales.

10.1 Data retrieval process

The crawled[1] data correspond to posts and comments published between August 26th, 2005 and August 31th, 2006. We divided the crawling process into two stages. The first stage included crawling the main HTML (posts) and first level comments and the second stage covered all additional comment pages. Crawling all the data took 4.5 days and produced approximately 4.54 GB of data. Post-processing caused by the presence of duplicated comments was necessary (due to an error of representation on the website). This explains discrepancies in the total number of comments between our study and Slashdot for certain posts.

Although a high amount of information was extracted from the raw HTML (sub-domains, title, topics, hierarchical relations between comments) we concentrated only on a minimal amount of information: **type** of contribution (either post or comment), its **identifier**, **author**'s identifier and **time-stamp** or date of publishing. The selected information was extracted to XML-files and imported into Matlab where the statistical analysis was performed. Table 10.1 shows the main quantities of the crawling process.

Figure 10.1 shows an example of a post (blue dashed box) with 4 of its comments (black dash-dotted box). The time-stamps of post and comments (indicated by red boxes in Figure 10.1) can be obtained from Slashdot with minute-precision and corresponded to the EDT time zone (= GMT−4 hours). They allow to calculate the following two quantities:

[1] Software used: wget, Perl scripts, and Tidy on a GNU/Linux, Ubuntu 6.0.6 OS.

Period covered	26-8-05 – 31-8-06
Time needed for crawling	4.5 days
Amount of data mined	4.54 GB

Table 10.1: Main quantities of the crawling

The **Post-Comment-Interval (PCI)** stands for the difference between the time-stamps of a comment and its corresponding post. The PCIs of Figure 10.1 are symbolized by the dimensioning.

The **Inter-Comment-Interval (ICI)** refers to the difference between the time-stamps of two consecutive comments of the same user (no matter what post he/she comments on).

The **Inter-Comment-Interval (ICI_1)** refers to the difference between the time-stamps of two consecutive comments of the same user to different post, i.e. only the first comments of a users to a post is considered in its calculation.

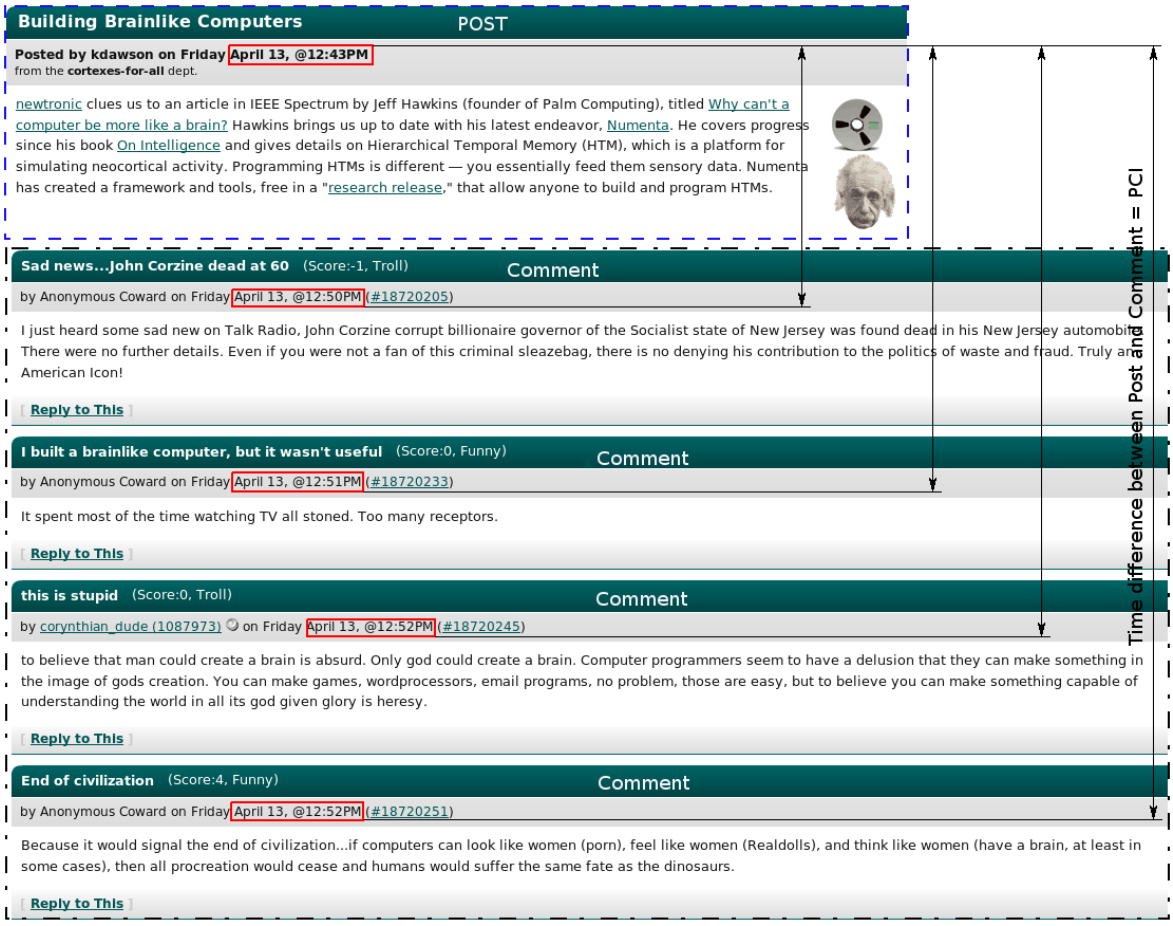

Figure 10.1: Example for a post (blue dashed) and a few of its comments (black dash-dotted box).

10.2 Basic quantities of the retrieved data

The data analyzed contain about 10^4 news posts which received a total of $2 \cdot 10^6$ comments. We found nearly 10^5 distinguishable users (commentators) responsible for this comments. The exact numbers are shown in Table 10.2. Approximately 18.6% of the comments were given by anonymous users. Assuming that many users comment anonymously, most of the anonymous users do not posses a registered user-name and the number of comments per anonymous user is similar to those of the registered ones, we can suppose that the actual number of commentators is about 20% higher. Nevertheless, for our purposes the exact identification of unique user-names is only interesting in chapter 12 where we have to eliminate the comments of the anonymous users. In the rest of the study the fact that a comment is anonymous does not entail any restrictions on our analysis and we can use the entire dataset.

Posts	10016
Comments	2075085
Anonymous comments	18.6%
Commentators	93636

Table 10.2: Main quantities of retrieved data

The distribution of the number of comments per post is quite heterogeneous. It is shown in the form of a histogram in Figure 10.2. Half of the posts provoke more than 160 comments and some of them even trigger more than 1000. In the next section we analyze the time-distribution of these comments and in the next chapter we study the distribution of their post-comment intervals (PCIs).

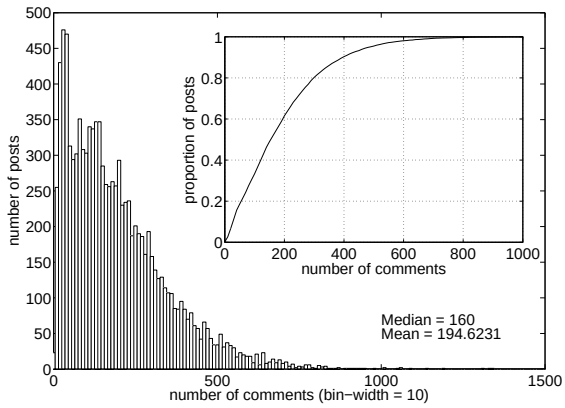

Figure 10.2: Histogram of the number of comments per post (inset shows the corresponding cdf).

10.3 Activity cycles on Slashdot

In this section we analyze the time-series generated by the post- and commenting activity on Slashdot. Figure 10.3a shows these two time-series[2] grouped into 10 five week periods. The amounts of posts (blue continuous) and comments (black continuous lines) per hour show clearly daily and weakly cyclic behavior. Figures 10.3b-d represent the mean and standard deviations (gray areas) of the post and comment activity shown in Figures 10.3a over different timescales. In Figure 10.3b we can observe the average daily cycles of the time series of Figure 10.3a, while Figure 10.3c shows the average over these time series. Figure 10.3d finally shows average and standard deviation over the cycles of Figure 10.3d. The low values of the standard deviations indicate that the activity cycles do not change much during the year, they are relatively stable over time especially in the case of the comments.

[2] A correction to account for changes in the activity rhythm caused by the Daylight Saving Time (DST) has to be applied, since the DST is not reflected in the raw data obtained from Slashdot. We used the DST-period of the USA, which slightly differs from the schedule in the European Union.

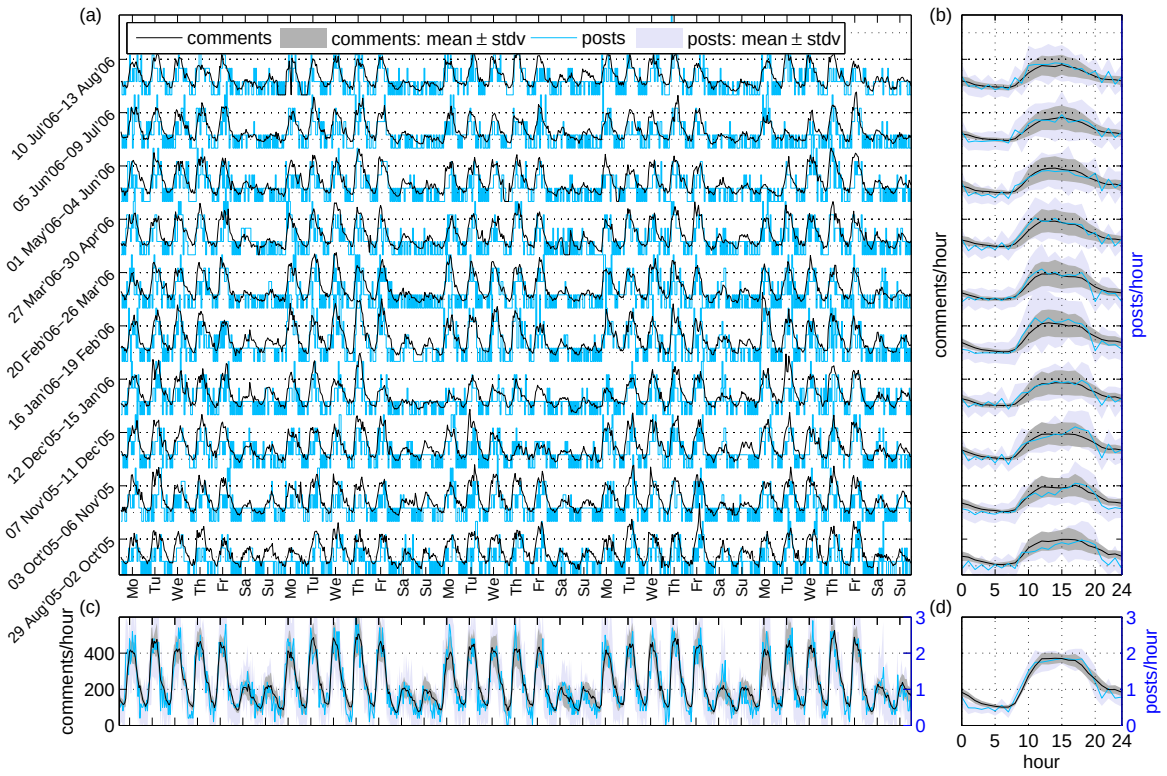

Figure 10.3: Post and comment activity on Slashdot throughout the year. **(a)** Evolution of the number of post and comments per hour. **(b)** Mean and standard deviations of the daily activity cycles for the 10 time-series shown in (a). **(c)** Mean and standard deviation over the time-series shown in (a). **(d)** Mean and standard deviation of the daily activity cycles of (b). We observe daily and weakly activity cycles which are relatively stable throughout the year of mined activity.

Interestingly, although post activity shows more fluctuations and higher standard deviations than comment activity, there is little discrepancy between their mean temporal profiles. This difference in the deviations is not surprising since the number of posts is 3 magnitudes smaller than the number of comments (see Table 10.2). This is further confirmed by Figure 10.4 which shows the mean number of posts and comments per hour, now with the standard deviation of all the data. It illustrates patterns

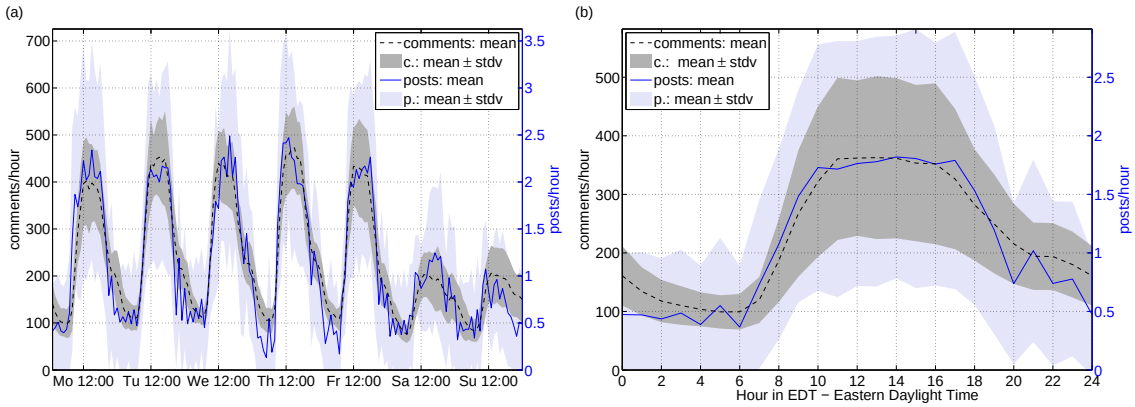

Figure 10.4: **(a)** Weekly and **(b)** daily activity cycles

which are in agreement with the social activity outside the public sphere. Figure 10.4a shows high activity working days which slows down during weekends. This weekly cycle is interleaved by daily oscillations illustrated in Figure 10.4b. The daily activity cycle reaches its maximum between 11am and 2pm approximately and its minimum during the night between 5am and 6am. At weekends and holidays (compare also with Figure 10.3 the maximum of the daily activity cycle reduces to 50% of its value during working days, while the minimum does not show much variations. We can conclude that there is a certain stock of activity which is maintained independent of hour and weekday and that, although Slashdot is open to public access around the world, its activity profile is clearly biased towards the American time-schedule.

Chapter 11

Analysis of Post-induced activity

In this chapter we focus on the time-distribution of the activity (comments) a single post induces on Slashdot. The distribution of the number of comments per posts was shown Figure 10.2. To analyze the time-distribution of these comments we study their post-comment intervals (PCIs). We are especially interested in the resulting probability distribution of all the PCIs of a certain post, which gives us the probability of a post to receive a comment t minutes after it has been published. These distributions are approximated with different types of heavy-tailed probability distributions. To measure the quality of those approximations we use the p-value of a KS-test.

11.1 Approximation with log-normal (LN) distributions

We start by analyzing the PCI-distribution of some example posts and use LN-distributions as a first guess to approximate them. Figures 11.1a and 11.1b show in linear and logarithmic scale the PCI-distribution of a post, let us call it post1, which triggered 1341 comments. We notice (Figure 11.1a) that the activity starts directly after the post has been published, reaches its maximum after around 30 minutes and decays then successively. Some fluctuations around this general behavior can be observed. The characteristic shape of the probability density function (pdf) resembles a LN-distribution, which becomes even more visible in its bell shape in logarithmic scale of Figure 11.1b. However, to averaged out the fluctuations of the pdf a better picture can be obtained from the cumulative probability distribution (cdf) which is shown in Figures 11.1c and 11.1d, again in both linear and logarithmic scale. The fit with a LN-distribution (dashed) closely resembles the data (continuous line) and it is thus not surprising that a KS-test gives us a high p-value of 0.637 an we would accept the LN-fit as a valid hypothesis to explain the PCI-distribution of this post. The parameters μ and σ of the LN-distribution are obtained simply by calculating the mean and standard deviation of the logarithm of the PCIs in the dataset.

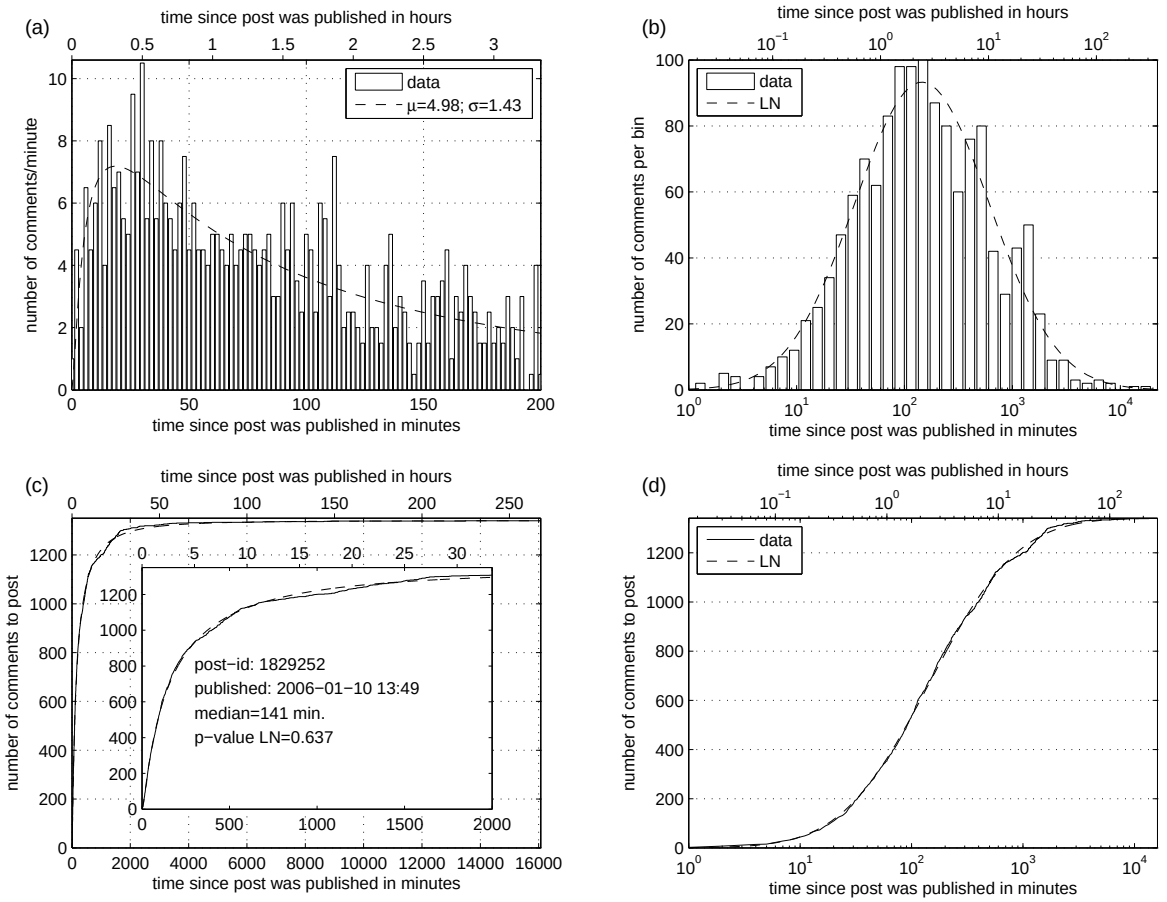

Figure 11.1: LN approximation (dashed lines) of the PCI-distribution (solid lines and bars) of **post1** which received 1341 comments. **(a)** Comments per minutes (bin-with= 2 for better visualization) for the first few hours after the post has been published. **(b)** Same as (a) in logarithmic scale. **(c)** The cumulative distribution of the data shown in (a). Inset shows a zoom on the first 2000 minutes. **(d)** Same as (c) in logarithmic scale.

The PCI-cdf of three more posts and their LN-fits are show in Figure 11.2. The top two sub-figures show good fits with p-values of 0.3 and 0.99 respectively, both much greater than the usual criteria of rejection. The topmost Figure on the right shows that even for a post with a smaller number of comments the PCI-distributions is well approximated with a LN-distributions. The question is now whether all posts show this LN-pattern in the time-distribution of their comments. The answer is no, the LN-fit is not accurate for all posts. E.g. the PCIs of the post shown in Figure 11.2 (bottom), post2 from now on, start to show considerable different behavior from the LN-approximation about 3 hours after its publication around midnight. The activity is lower than the LN would predict, but starts to increase again at about 8am in the morning the following day. At around 10:30pm it increases further to recover the lost activity during the night. More such oscillations of activity can be observed during the subsequent days. The time-spans of variations in activity coincide quite exactly with the average

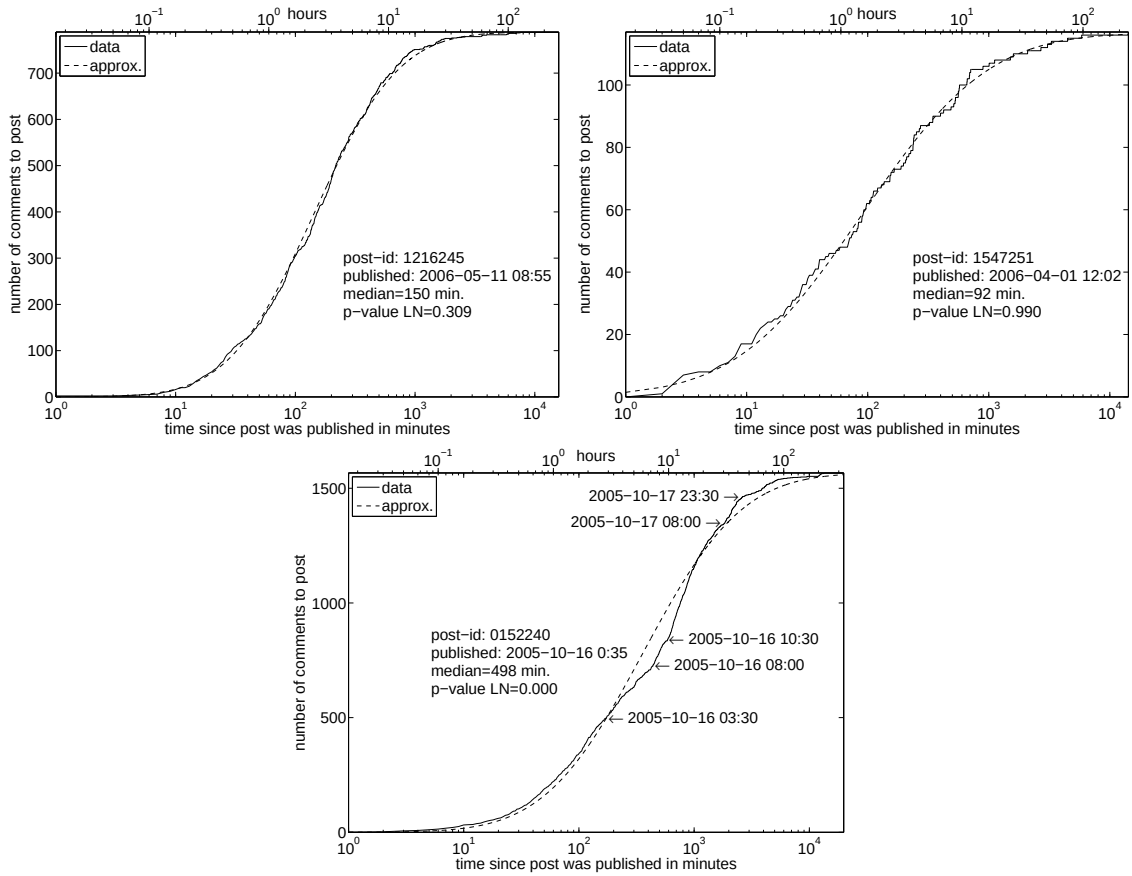

Figure 11.2: LN-approximation of the PCI-distribution of 3 different posts.

daily activity cycle shown in Figure 10.4b, which suggests that it may be the cause for the aberration of the LN-behavior. We will investigate this further in section 11.5, but first we try to improve the fit in those cases.

11.2 Approximation with double log-normal (DLN) distributions

To approximate PCIs of posts like post2 (Figure 11.2 bottom) for which a LN-fit gives bad results, we can use a double log-normal distribution (DLN), i.e. a superposition of two LN-distributions (See subsection 9.3.2). To find their parameters and especially their mixing coefficient we use maximum likelihood estimation (MLE) (Stouffer et al., 2006; DeGroot and Schervish, 2002), which is performed by minimizing the negative logarithm of the likelihood function with `fminsearch` in MATLAB. Since the DLN has five parameters compared to only two of the LN, it should lead to better results.

In Figure 11.3 we compare LN and DLN approximation of the the PCI-distribution (black continuous line) of post2, shown previously in Figure 11.2 bottom. The red and blue lines indicate the two

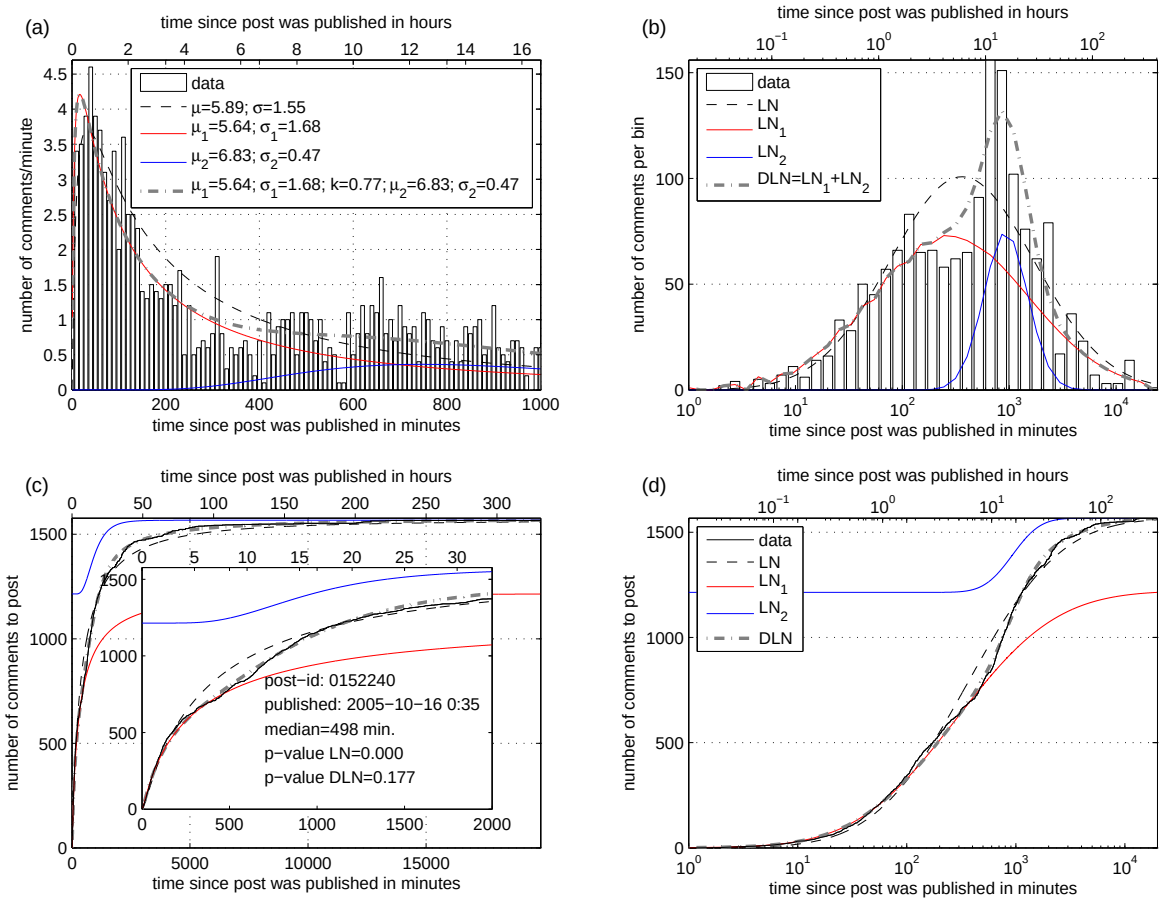

Figure 11.3: Comparison of LN and DLN-approximations (dashed-dotted lines) of the PCI-distribution (solid lines and bars) of a post which received 1567 comments. The DLN-distribution is a superposition of LN_1 and LN_2, which in the above figure are rescaled according to the coefficient k of the DLN. Rest of legend as in Figure 11.1.

log-normals (LN_1 an LN_2) rescaled according to the mixing parameter k. Their superposition results in a DLN (gray, dash-dotted), which clearly outperforms the previous LN (black, dashed) approach. The p-value of the DLN approximation is 0.177, which is above the usual level of significance. We would therefore accept the DLN-distribution as a valid model of the PCI-distribution in this case, while the LN hypothesis is rejected with a p-value below 10^{-10}. The two LN-distributions which form the DLN can be interpreted as two waves of activity. The first one (LN_1, red line)) starts directly after a post has been published and approximates well the first 8 hours of activity. Then the activity increases due to the rise in the circadian activity cycle (compare also with Figure 10.4b and the text labels in Figure 11.2 bottom). The second wave (LN_2, blue line) accounts for the extra of activity due to this rise and therefore the DLN-approximation reflects the first bump in the PCI-cdf and fits well the data. However, a second bump in the cdf, caused by the subsequent oscillation of activity due to the circadian circle during the following day is not reproduced by the DLN-approximation. Since

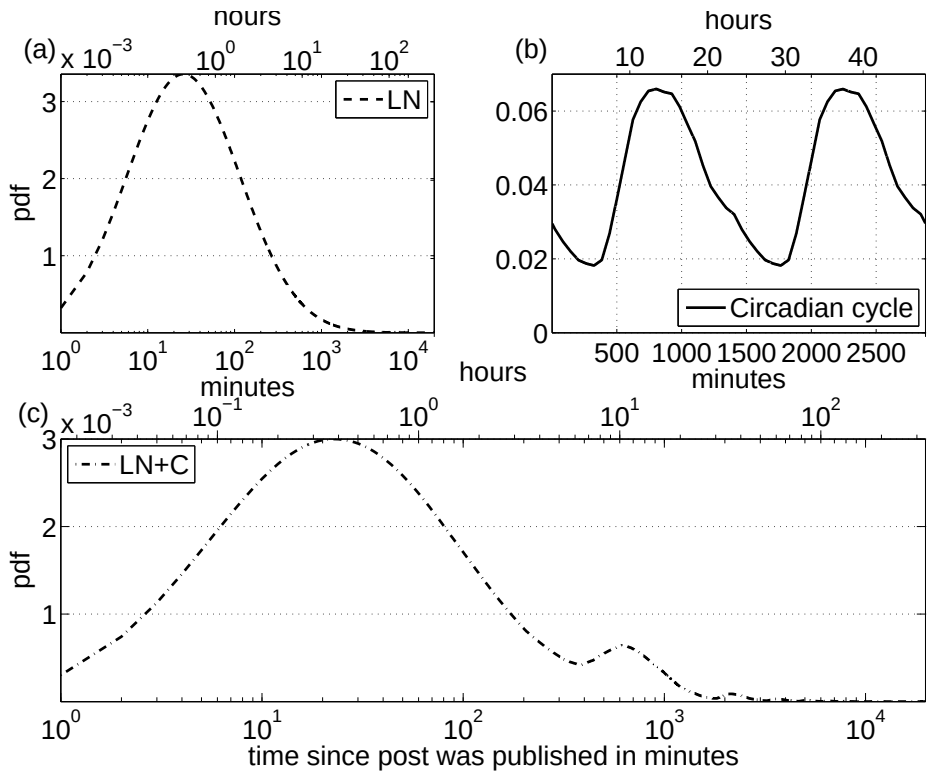

Figure 11.4: Transformation of LN into LNxC.

its amplitude is low compared to the rest of activity triggered by the post, it is not strong enough to force us to reject the DLN-hypothesis in the KS-test. Nevertheless, in the following section we try to approximate this minor bumps as well.

11.3 Approximation with LN and DLN distributions combined with the circadian cycle

Another possibility to improve the LN-fits is the use of modified LN and DLN distributions which incorporate fluctuations which account for the activity changes due to the circadian rhythm. We denominate them LNxC and DLNxC and describe them in more detail in what follows.

11.3.1 Definition of LNxC and DLNxC

The distributions LNxC and DLNxC are generated by point-wise multiplication[1] of the LN or DLN pdf with a periodic continuation of an “ad hoc” circadian cycle as shown in Figure 11.4b. The circadian cycle is approximated by the normalized mean number of comments per hour of the day,

[1]Note that we use a discretized version of the pdfs, since we model discrete data with minute precision.

which is then linearly interpolated to achieve minute resolution. Alternatively, higher dimensional interpolation could be used, but the differences are negligible for our purposes.

The starting point of the periodic function coincides with the moment the post is published. After the multiplication we have to normalize to obtain the final pdf. We denominate the two resulting probability distributions LNxC and DLNxC. This procedure is visualized in Figure 11.4. Figure 11.4a shows an example of a LN-pdf. After multiplying it with the periodic continuation of the circadian activity cycle (Figure 11.4b) and a renormalization we obtain the LNxC-pdf (Figure 11.4c). In order to find the parameters of the above described distributions which best approximate a given post we use again MLE.

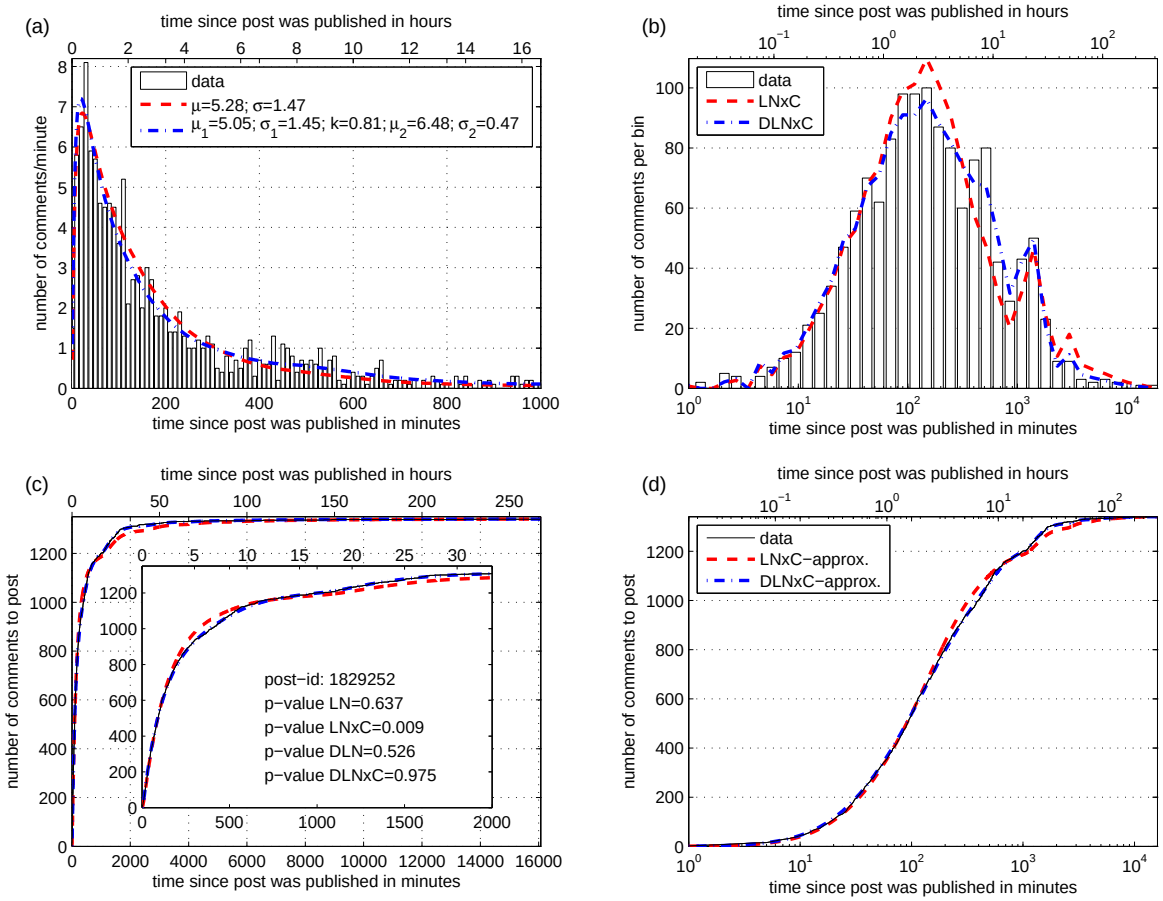

Figure 11.5: Approximation with LNxC (red dashed line) and DLNxC (blue dashed doted) of the PCI-distribution (solid lines and bars). **(a)** Comments per minute (bin-with=2) for the first 1000 minutes after the post's publishing. **(b)** Same as (a) but in logarithmic scale. **(c)** The cumulative distribution of the data shown in (a). Inset shows a zoom on the first 2000 minutes. **(d)** Same as (c) but in logarithmic scale.

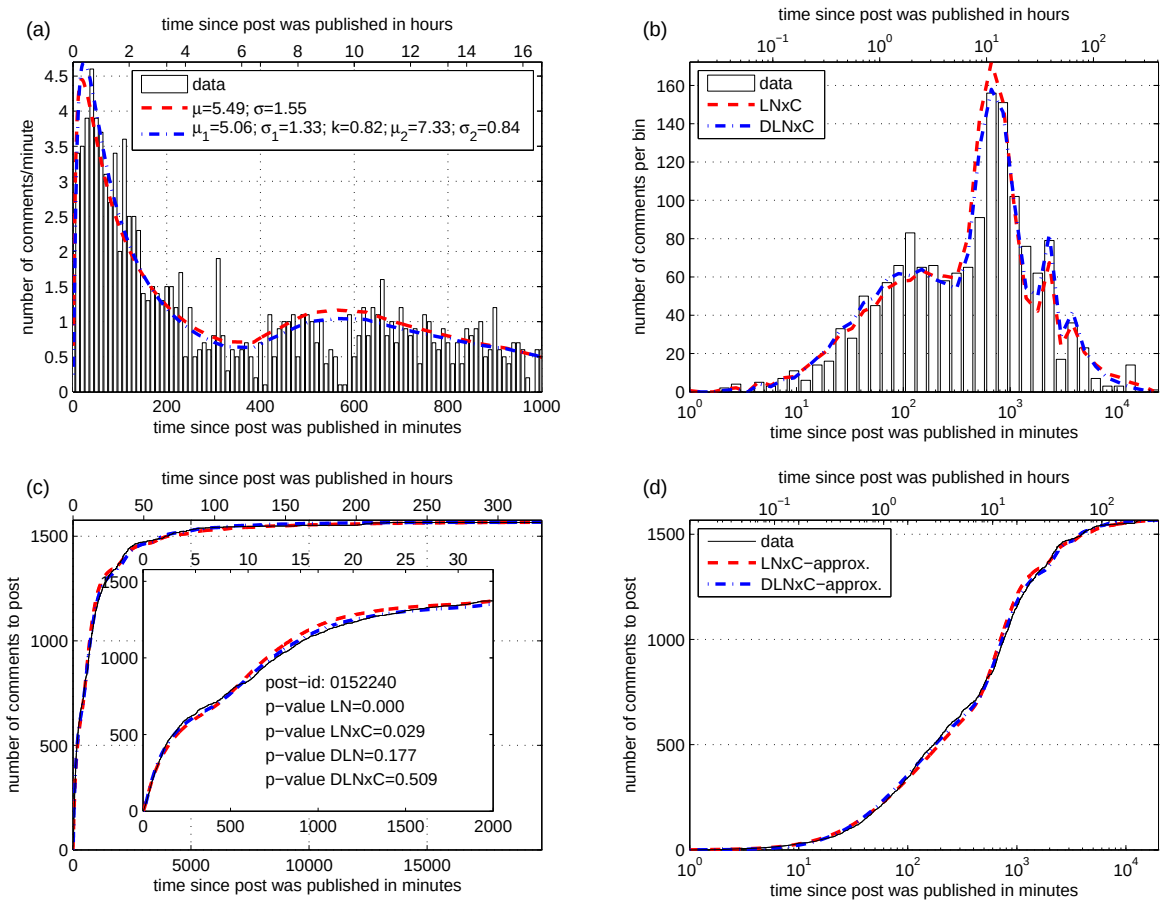

Figure 11.6: Example of improvement of fit with DLNxC. Legend as in Figure 11.5.

11.3.2 Two example posts

We use the PCI-distributions of post1 and post2 to show the quality of the LNxC or a DLNxC-approximation in comparison with the LN and DLN-fits. We start with the PCI-distribution of post1 which was well approximated by a plain LN distribution ($p = 0.637$ in Figure 11.1). Figure 11.5 shows the fits with LNxC (red dashed) and DLNxC (blue dash-doted line) distributions. The later improves the LN-fit and adjusts very well even the small bumps in the cdf after about 1000 minutes of activity (Figure 11.5c and Figure 11.5d). This implies the high p-value of 0.975, meaning a nearly perfect fit. On the contrary the LNxC, although it also adapts its shape to the bumps, shows worse results than the simple LN distribution. It achieves only a p-value of 0.009, which is below the usual choices for the level of significance, which implies the rejection of the null hypothesis . Although the p-values of the three other distributions of the LN family are much greater than those significance levels, they indicate that the DLNxC-fit is the closest to the data.

Moreover, the DLNxC leads to excellent results even for those cases where the KS-test rejects the LN-hypothesis. We show this in Figure 11.6 on the example of post2, which was published late in

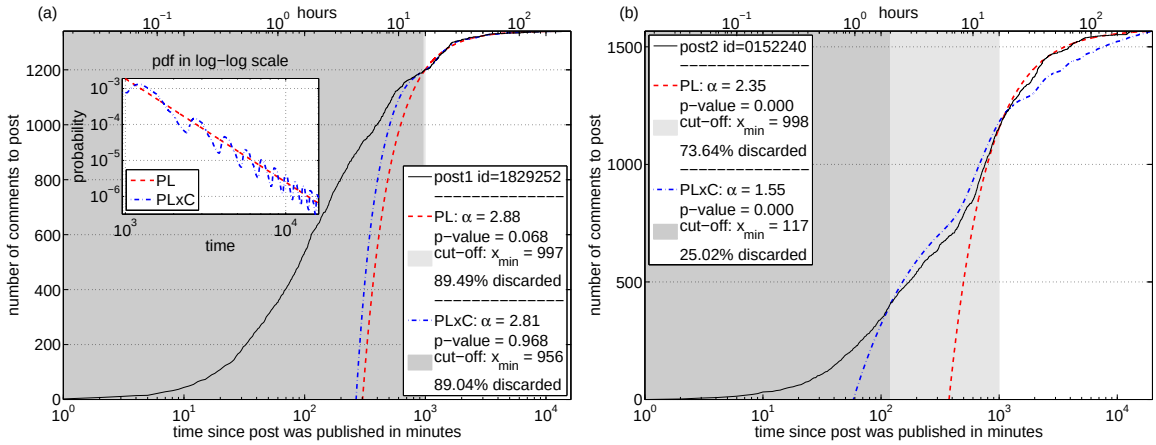

Figure 11.7: Two examples of the approximation of the tail of PCI-distribution with power-laws (PL). The PCI-cdf of **(a)** post1 **(b)** post2 is shown in logarithmic scale. The gray areas correspond to the amount of discarded data for the PL-fits. Inset in (a) shows the pdf of the two variants of PL used.

the evening and suffers thus distortions due to the circadian cycle. The LN-hypothesis is rejected (p-value $< 10^{-10}$), but a DLNxC-fit would be accepted with a p-value of 0.509. Also the DLN variant has a p-value (0.177) which is above the thresholds of rejection. The outcome of the KS-test for the LNxC depends on the chosen value of the significance level α_0, since the corresponding p-value of 0.029 can either lead to acceptance ($\alpha_0 = 0.01$) or rejection ($\alpha_0 = 0.05$). Although the LNxC represents an improvement compared to the simple LN for post2, it does not reach the quality of the DLN or the DLNxC. If we compare the approximation quality of LNxC and DLNxC visually we note that both LNxC and DLNxC seem to adjust well the PCI-pdf (Figures 11.6a and 11.6b), but the corresponding PCI-cdf (Figures 11.6c and 11.6d) shows us that the DLNxC is closer to the data. For the two example post analyzed in this section we notice that the DLNxC adapts very well to the oscillations of activity. A more general comparison of the quality of the four different distributions of the LN family involving all posts will be given in section 11.5.

11.4 Approximation with power-law (PL) distributions

As explained in subsection 9.3.3 the tail of heavy tailed distributions is often fit with a power-law. We will try this as well for the PCI-distributions of the posts on Slashdot and give in this section two examples for these fits. Apart from the power-law (PL) distribution we also use a powerlaw distribution modified by the circadian cycle (PLxC) which we generate in the same way as the LNxC and DLNxC multiplying a PL-distribution with a periodic extension of the circadian cycle. The inset in Figure 11.7a illustrates the relationship between the pdfs of PL (red dash-dotted line) and PLxC (blue dashed curve) in a log-log plot.

We take as example, as in the previous sections, the PCI-distributions of post1 and post2, whose

cdfs are shown in Figure 11.7 together with their approximation in log-scale. We use the methodology explained in subsection 9.3.3 to find the optimal value for the cut-off parameter x_{min}. Only PCI greater than x_{min} are considered for the fits. We set the maximal cut-off at 1000 minutes to guarantee at least one magnitude of data for the fit. The discarded PCI-data is represented by the gray areas in Figure 11.7 (dark gray for the PLxC and light gray for the PL-distribution). For post1 we have to cut-off more than 89% of the comments to achieve the best fits. Both post show p-values above the levels of significance, although the PL ($p = 0.086$) is very close to rejection. For post2 both p-values are 0. We would have to allow higher values for x_{min} to achieve better results in this case, which then of course would imply an even greater percentage of discarded data.

In the next section we will show that this is the general problem of trying to fit power-laws with the tails of the PCI-distributions. The more data one discards the easier becomes a powerlaw fit, but the less significant is it to explain the data.

11.5 Comparison of all six approximation variants

After these analysis of some example posts we will try to achieve a general picture by performing KS-tests for all posts and all six types of distributions presented earlier. We then compare their p-values to analyze their overall approximation quality. The higher the p-value the better is the approximation.

11.5.1 Overall performance of the approximations

The cdfs of the p-values of these tests are shown in Figure 11.8a. The axes are interchanged so that the x-axis gives the proportion of posts whose p-value is lower than or equal to the corresponding $y-$coordinate of a curve. This implies that the closer a curve of a probability distribution is to the top border of the plot, the better it approximates the data "on average".

First we compare only the four different variants of log-normal distributions, which we will refer to in what follows as the LN-family. We observe that the LN (dashed line) gives the worst results of all tested distributions, it is the closest curve to the bottom of the plot. A significant improvement is achieved if we use a log-normal plus circadian cycle (LNxC)-distribution (black continuous line). And as expected from the results for the example-posts, the best performance is obtained by the two double log-normal distributions. For both, DLN and DLNxC, fits the proportion of posts which low p-values is much smaller than those of their single LN counterparts. However, the improvement achieved by using the circadian cycle is very small, the curves of DLNxC (dash-dotted line) and DLN-curve (gray continuous line with circles) nearly coincide.

The same ranking of the distributions can be observed if we fix the significance level α_0 of the

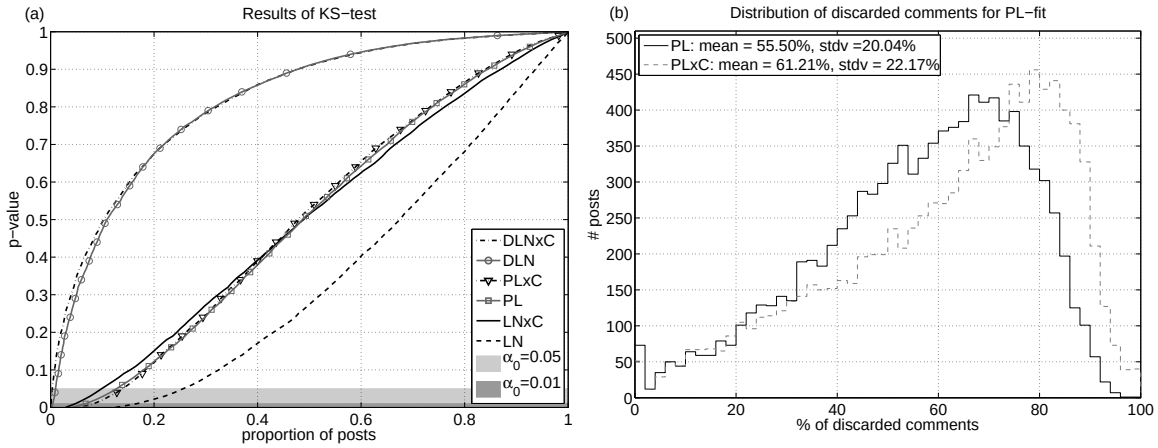

Figure 11.8: **(a)** Result of KS-test of all posts for different approximations. **(b)** Percentage of discarded comments for the PL and PLxC-fits.

KS-test with either 0.01 or 0.05 (shown as gray areas in Figure 11.8a). We can then quantify the percentage of posts for which the KS-test rejects the null hypothesis. The corresponding number can be found in Table 11.1. We observe that while a single LN-distribution can only explain in 83% of the cases the activity provoked by a post, both double log-normal variants are a valid model of the data for more than 99.5% of all posts. The best results are obtained for DLNxC which is only rejected for 11 of 10016 posts ($\alpha_0 = 0.01$). We can conclude that both DLN and DLNxC are valid models to explain the activity provoked by the posts on Slashdot.

To compare our results with other studies which favor power-laws to fit heavy tailed distributions, we also analyzed the approximation quality of two classes of PL-distributions. The corresponding results of the KS-tests are similar to those of the LNxC in Figure 11.8a. However, we have to stress out that we cannot compare the distributions of the p-values of the PL with those of the LN-family directly, since the PL-variants only approximate a fraction of the PCI-distribution. A large number of comments, those with the lowest PCIs, have to be discarded to achieve reasonable results in approximating the tail of the PCI-distribution. In other words: we have to make the heavy tail very short to fit it with a PL. The distribution of the percentage of discarded comments is shown in Figure 11.8b.

	$\alpha_0 = 0.01$	$\alpha_0 = 0.05$	PCIs used
LN	16.68%	25.62%	100%
LNxC	4.80%	9.88%	100%
PL	6.79%	12.77%	44.50%($\pm$20.04%)
PLxC	8.36%	13.94%	38.79%($\pm$22.17%)
DLN	0.44%	0.96%	100%
DLNxC	0.11%	0.33%	100%

Table 11.1: Percentage of rejected 0-hypotheses and data used for the PCI-approximation.

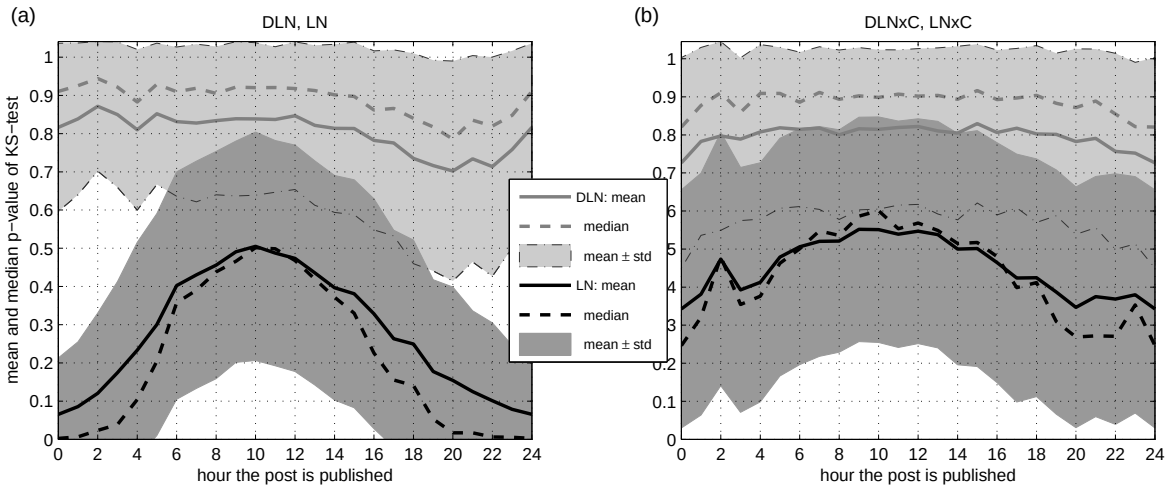

Figure 11.9: Results of KS-tests per publishing hour of post of **(a)** DLN and LN, **(b)** DLNxC and LNxC.

On average 55.5% of the comments have to be discarded in the case of a simple PL and even 61.21% when we approximate with PLxC. In Figure 11.8a we observe that in the case of DLN and DLNxC, the performance of PL (gray continuous line with squares) and PLxC (dash-dotted line with triangles) are very similar, although here the PL is slightly better than its oscillatory variant as can be seen in Table 11.1. A PL allows to explain 93% of the tails of the PCI-distribution versus the 91% of PLxC. We observe that the PLxC does not lead to an improvement of the results of the PL distribution, since the PL explains more data and achieves better approximations of the tails of the PCI-distributions.

However, it is no surprise that parts of LN-distributed data can be fit by PLs (Newman, 2005). A LN-distribution is a quadratic curve in log scales and a quadratic curve looks straight (i.e a PL in log scale) if looked on a sufficient small portion of it[2], which can represent a relatively large portion of its range depending on the parameters of the LN. The same is true for DLN distributions. This, together with the fact that the LN-family is able to explain the entire PCI-distribution with similar (LNxC) or even much better quality (DLN and DLNxC) than a PL, motivates us to concentrate only on the LN-family in what follows.

11.5.2 Dependency of the approximation quality on the circadian cycle

The analysis of the example posts in section 11.1 suggested that the publishing hour of a post influences the quality of a LN-fit of their PCI-distributions. Here we will investigate whether there exist a dependency of the outcome of the KS-tests on the hour of the day. To do so we arrange the posts in 24 groups according to their publishing hour. Figure 11.9 shows mean (continuous), median

[2]The exponent α of the corresponding PL-fit of this portion would depend then on which part of the data we were approximating and only secondarily, over the parameters of the LN, on the data itself.

(dashed lines) and standard deviations (gray areas) of the *p*-values for each of the groups and the four distributions of the LN-family. We observe that the quality of LN (black lines in Figure 11.9a) and LNxC-approximation (black lines in Figure 11.9b) depends on the publishing hour, although this dependence diminishes in the case of LNxC. Posts published during the phase of increased activity of the circadian cycle (see Figure 10.4) achieve significantly higher *p*-values than those made public outside of this time-span. This explains the bad approximation of post2 (see Figure 11.3), published around midnight, with LN and LNxC distributions.

On the contrary, both types of double log-normal distributions show only minor variations due to the publishing hour of the post. Although the DLNxC (gray lines in Figure 11.9b) is slightly more constant than DLN (gray lines in Figure 11.9a) we can conclude that both DLN-variants, account for the main part of the variations in the activity patterns caused by the circadian rhythm.

11.6 Approximation parameters

After having analyzed the quality of different approximations of the PCI-distributions, we now take a look on the parameters of two of this approximations.

We start with the LN-distribution which, when it leads to good approximation results, allows to describe the activity triggered by a post with only two parameters: the median [3] and the geometric standard deviation σ_g of the LN. Both quantities are commonly used to compare log-normally distributed data (Limpert et al., 2001). The median and σ_g relate to the parameters μ and σ of a LN-distribution in the following way:

$$\text{median} = \exp(\mu)\ , \qquad \sigma_g = \exp(\sigma); \tag{11.1}$$

Estimates for the values of μ and σ are given by the mean and standard deviation of the logarithm of the PCIs.

Figure 11.10a shows the distribution of the medians of the LN-fits of all posts. The medians are rather short (for 50% of the posts they are below 2.5 hours, for 90% below 6 hours) compared to the maximum PCI (approx. 14 days), which implies that, although the activity a post generates covers a large time span, the major part of it happens within the first few hours after the post's publication. We can use the median of the LN-approximation as a measure for the "half-life" of a discussion, which is an indicator of how fast after the publication of a post the mayor part of its comments have been put online. The geometric standard deviation σ_g, on the other hand, gives us an idea of how dispersed in time the activity is. Its distribution, which is centered around 4.5 (stdv= 0.91), is shown in the inset of Figure 11.10a. The lower the value of σ_g the more peaked is the discussion, i.e the faster is

[3] Note that the median coincides with the geometric mean for a log-normally distributed random variable.

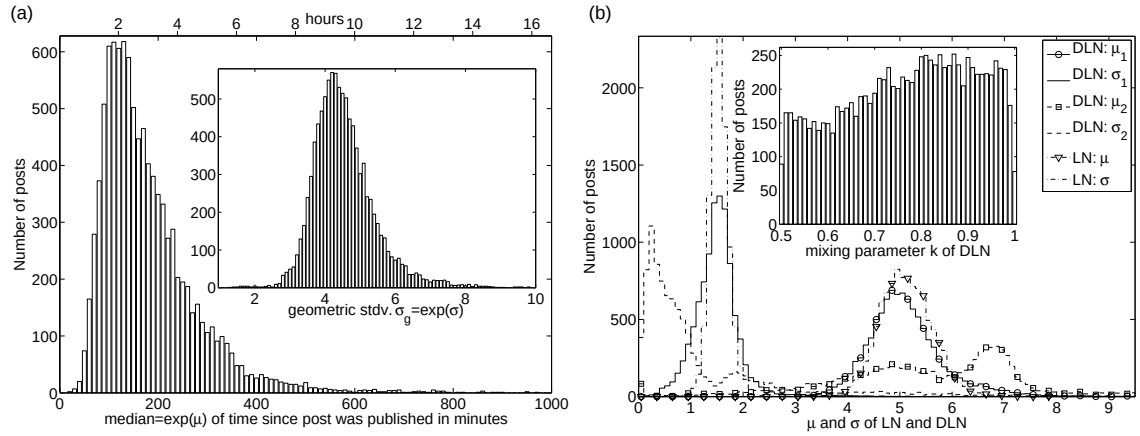

Figure 11.10: **(a)** Histograms of the estimates of medians (bin-width $= 10$) and geometric standard deviations (inset, bin-width $= 0.1$) of the PCI-distributions. **(b)** Parameters of LN and DLN-approximations. Bin-width=0.1 for μ and σ, 0.01 for k (inset).

the decay of activity once the median has been reached, while a large σ_g indicates a tail with slowly decreasing activity. It is interesting to note that no significant correlation between the median and σ_g could be found (correlation coefficient $= 0.0076$), making this two parameters independent indicators which allow to describe the reaction of the community to a certain news post.

When we use a DLN-distribution to approximate the data we need five parameters to describe the activity. Their distributions together with those of the parameters σ and μ of the LN-approximation can be observed in Figure 11.10b. For better visualization we choose a stair plot instead of a bar-graph and relabel the parameters when necessary to ensure a value of the mixing coefficient $k \geq 0.5$. Clearly, the regions of μ_1 (continuous line with circles) and σ_1 (continuous line) are very similar to those of the parameters of LN-approximations (dashed-dotted lines), indicating that the first one of the two log-normal distributions used to generate the DLN is similar to the LN-approximation. The parameters μ_2 (dashed with squares) and σ_2 (dashed), on the other hand, show an interesting bimodal distribution. The first of its two peaks lies within the regions of the values of μ_1 or σ_1 respectively, corresponding to posts for which the two superposed log-normal distributions are very similar and the data fits well already a single LN. However, the second peak in the μ_2-distribution represents posts which trigger a second wave of activity starting after the next increase of the circadian cycle. In those cases the parameter σ_2 is usually smaller than σ_1, which indicates that the second wave of activity is less extended than the first one.

Finally, we observe in the inset of Figure 11.10b the distribution of the mixing parameter k, which is nearly uniform except that values in $[0.7, 1]$ are slightly more likely than lower ones. To get a better picture of the distribution of k and the other parameters we analyze in the following section aggregate distributions of several posts.

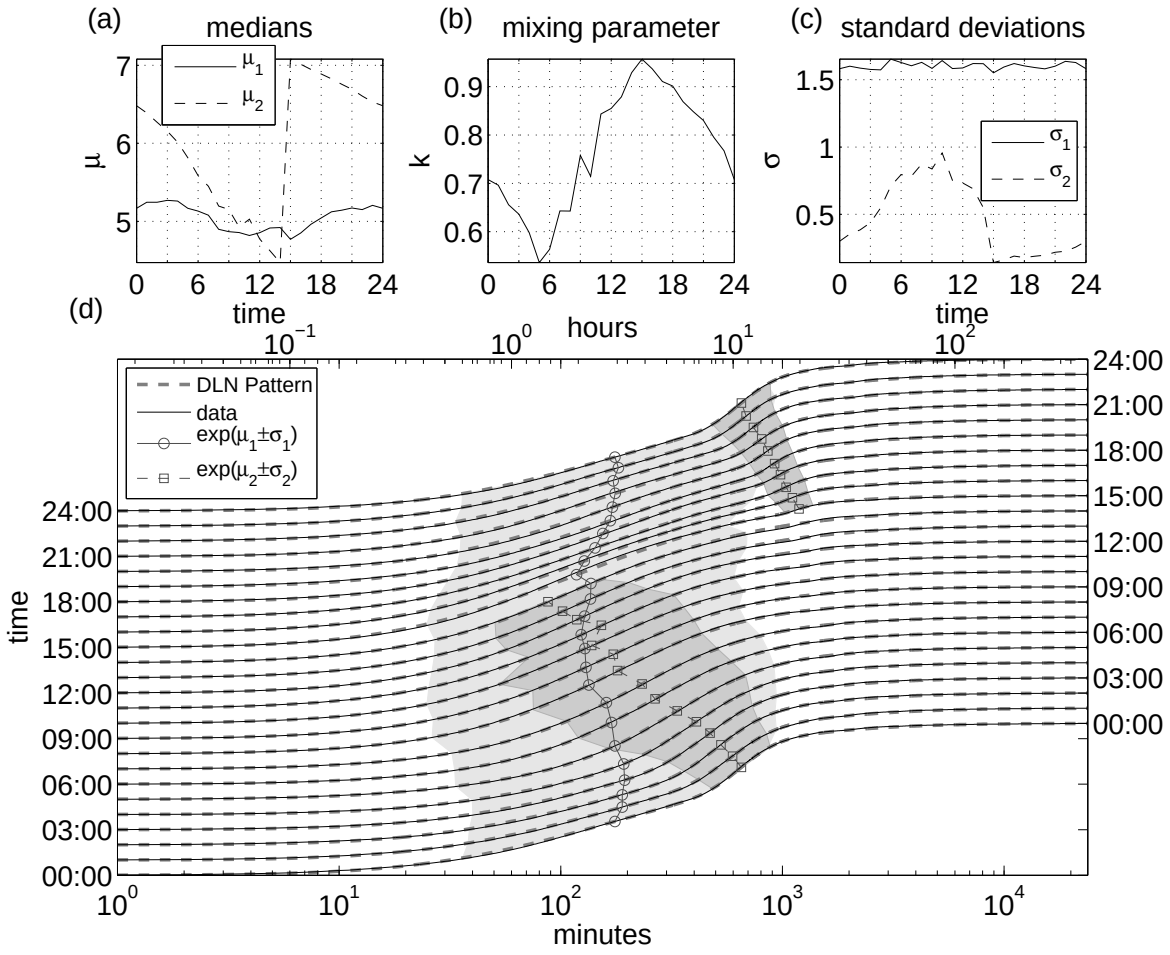

Figure 11.11: PCI of aggregate posts and parameters of DLN approx. by publication hour.

11.7 Two waves of activity

As explained already in section 11.2 the fact that a DLN, a combination of two LN distributions (LN_1 and LN_2), allows to approximate well the PCI-distributions suggests that the activity triggered by a post consists of two major waves, each one represented by one of the two LNs. To verify this claim we combine the PCIs of all posts of our dataset which have been published during the same hour of the day into an aggregate post. For example, to obtain the first aggregate post we generate the distribution of the PCIs of the posts published between 1am and 2am. In this way we obtain 24 aggregate posts, which we approximate with DLN-distributions. The normalized PCI-cdfs of those aggregates (black solid lines) and their DLN-approximations (gray dashed lines) are shown in Figure 11.11d. The shift on the *y*-axis of the curves corresponds to the hour, which the aggregate post represents.

The parameters of these 24 DLN-approximations can be observed in the top three subplots of

Figure 11.11. We notice that the parameters μ_1 and σ_1 (continuous lines in Figures 11.11a and 11.11c) of the first LN-distribution (LN_1), which corresponds to the first wave of activity, experience only minor variations due to the hour of publication. The mixing parameter k, μ_2 and σ_2 (dashed lines), on the other hand, vary significantly.

Figure 11.11b shows that k experiences a cyclic behavior, similar to the circadian activity cycle (Figure 11.4b). The location in time of the maximums and minimums of both cycles approximately coincide. The value of k reaches its maximum around 3pm, which indicates that for posts published at this time of the day most of the activity can be modelled only by LN_1. At the same time μ_2 reaches its maximum and σ_2 its minimum. The difference between the medians $\exp(\mu_1)$ and $\exp(\mu_2)$ of LN_1 and LN_2 is of about 16 hours. This connotes hat LN_2 models the activity of those users which comment the post during the following day, i.e. during the next high-phase of the circadian cycle. For publishing times later than 15pm the value of k decreases successively, while σ_2 increases, which implies that the proportion of the total number of comments received during this second wave of activity increases as well. Parallel to this rise, μ_2 decays likewise to the decrease of the time-difference between the publishing of the post and the next rise of activity. This trend stops in the morning around 5am when the proportion of comments provided by the first wave of activity increases again. Between 9am and 14pm, during the high-phase of activity, the values of μ_1 and μ_2 are very similar, making a separation of the two waves and the interpretation of their parameters very difficult. During this time window the DLN leads only to minor improvements compared to a single LN distribution as it is also the case in the approximation of the aggregate post of 3pm which leads us back to the beginning of the paragraph and closes the cycle.

The gray areas in Figure 11.11d representing the activity within $\exp(\mu_{1,2} \pm \sigma_{1,2})$, visualize the influence of the above described two waves of activity in the composition of the DLN-approximation. We observe the relative evenness of LN_1 (line with circle marks and light gray area) and the strong variations of LN_2 (dashed line with squares and dark gray area), which corresponds to the second wave of activity.

This analysis gives us further insight why posts like post1 (Figure 11.5), published during the high-phase of activity on Slashdot, can be well approximated by a single LN distribution, while posts similar to post2 (Figure 11.5), published late at night, need a DLN or (a DLNxC) to approximate their PCI-distribution.

Chapter 12

User Dynamics

In this chapter we analyze the activity on Slashdot taking the authorship of the comments into account. We first study the distribution of activity among all the users participating in the debates and then focus on the temporal activity patterns of single users. For obvious reasons we do not consider the anonymous comments, which represent 18.6% of the total amount of comments (see section 10.2 for more details), in this chapter.

12.1 Global user activity

To illustrate the activity of a users we use the number of his comments. The resulting distribution of the number of comments per user, which we refer to as the activity distribution in the following, is heavy tailed and gives a quite hetereogenous picture of the Slashdot-users. It is shown as black dots in double-logarithmic scale in Figure 12.1a. Most of the approximately 10^5 unique users we identified write a low number of comments (53% write 3 or less) during the time-span which is covered by our data (approximately a year). Nevertheless, a considerable amount of user writes more then 10 comments (24.85%) and the small number of 93 users (0.1%) writes even more than 1000 comments. See Table 12.1 for more details. It is interesting to note that, although only 3.4% of the users write more than 100 comments, these approximately 3200 users generate more than 51% of all the comments in our dataset, whereas the 53% of the users which write 3 or less are responsible only for 4.6% of the total amount of interaction on the site.

Contrary to the PCI-distributions analyzed in the previous chapter, the lower limit of the support of the activity distribution has highest probability, which then (apart from some fluctuations in the tail decays successively for higher numbers of comments per user. Such a decay, which at first sight resembles linear in log-log scale, has been frequently modeled with a power-law (PL) probability distribution (see subsection 9.3.3). Indeed, after applying linear regression as in other studies

# comments per user	% of users	% of comments
1	30.90%	1.71%
$(1,10]$	44.25%	10.53%
$(10,100]$	21.43%	36.39%
$(100,1000]$	3.32%	43.57%
$(1000,\infty)$	0.10%	7.80%
$[1,\infty)$	100.00%	100.00%
$(100,\infty)$	3.42%	51.37%
$(50,\infty)$	7.00%	65.32%
$(10,\infty)$	24.85%	87.76%
$(0,3]$	52.99%	4.62%

Table 12.1: Percentage of users (second column) which write a certain number of comments (first column) and the percentage of the total number of comments (third column) produced by these users.

(Faloutsos, Faloutsos and Faloutsos, 1999; Albert, Jeong and Barabási, 1999) we obtain a quite large correlation coefficient $R^2 = -0.97$ for an exponent of $\alpha = 1.79$. However, if we apply rigorous statistical analysis as proposed in Goldstein et al. (2004) the picture changes. First, we estimate the power-law exponent computing the less biased maximum likelihood estimator (MLE). The resulting PL with exponent $\alpha = 1.48$ differs significantly from the previous one and is illustrated in Figure 12.1 as dark gray dashed line. Although this PL-fit of the pdf in Figure 12.1a is tempting to accept the PL hypothesis, the cdf shown in Figure 12.1b clearly discards it. It is thus not surprising that the Kolmogorov-Smirnov (KS) test forces us to reject the PL fit. This does not change if we apply the method of Clauset et al. (2007) and approximate only the tail of the distribution with a PL. The resulting distribution, which is shown as blue dashed line in Figure 12.1 is only a minor improvement. We have to discard more than 95% of the users, represented by the gray areas in Figure 12.1 to achieve at least a good optical fit of the cdf. Nevertheless, the p-value of a KS-test remains small ($p < 10^{-8}$)

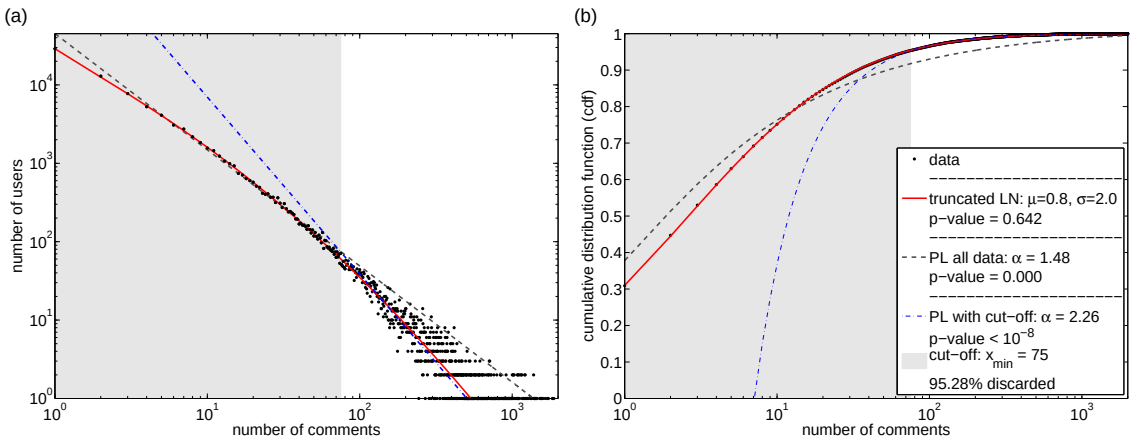

Figure 12.1: **(a)** Histogram of the number of comments per user and **(b)** and its corresponding cdf.

and we are forced to reject the PL-fit of the tail as well.

As an alternative hypothesis to describe the data we propose a truncated LN probability distribution, shown in Figure 12.1 as red solid-line. Its parameters are found using MLE. Clearly, the fit is much better using this hypothesis and a KS-test accepts the fit (p-value$= 0.64$) of the entire data-set.

We can thus conclude that the distribution of activity among the Slashdot-users is not scale free, which implies that the parameters of the LN-fit may depend on the size of the dataset[1]. We have only made a momentary picture of the distribution, which may change if for example a second year of activity would be considered. This findings coincide with those of Naruse and Kubo (2006), who found that the number of articles submitted by individuals to public distributions bulletin board system is also distributed like a LN. Truncated LN distributions give also good fits of the distribution of different parameters describing the communication threads and the social network on Slashdot, as will be shown in Gómez, Kaltenbrunner and López (2008).

12.2 Single user dynamics

After characterizing the user activity at a general level, we investigate the temporal behavior patterns of single users. First we analyze some example users and give than an overview of all users.

12.2.1 Four examples of single users

The following analysis concentrates on the temporal activity patterns of four users, to protect their privacy we refer to them as user1, user2, etc. In Table 12.2 we can find the number of comments these users have published during the time-span covered by our data and how many post have been commented by them. The temporal patterns of the users we analyze are the distributions of the PCIs

	user1	user2	user3	user4
commented posts	1189	1306	64	113
comments	3642	3350	73	163

Table 12.2: Contributions of the two most active users.

of their comments as well their inter-comment-interval (ICI) distributions, i.e. the time-differences between two subsequent comments of the same user.

First we focus only on the two most active users in our dataset (user1 and user2). Figure 12.2a shows the PCI-cdf of user1 (light grey continuous) and user2 (dark gray continuous). We observe a great similarity to the PCI-distributions of the posts analyzed in chapter 11, which motivates us to use

[1]For example, if the LN were the results of the multiplication of identical random variables X_i, one for every time-step i, the parameters of the LN would be determined according to the central limit theorem by number of time-steps.

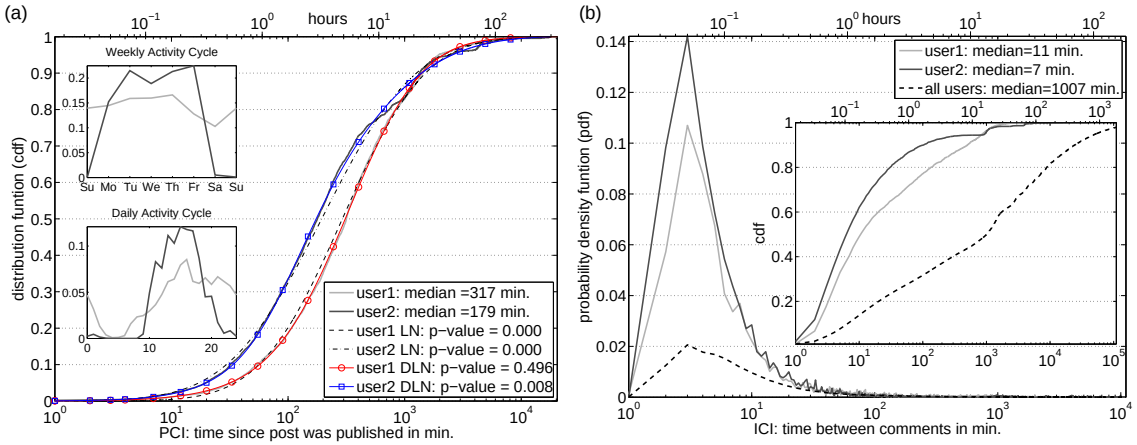

Figure 12.2: Activity patterns of the two most active users: **(a)** PCI-distributions, insets shows daily and weekly activity cycles. **(b)** Distribution of the inter-comment intervals (ICI) compared with the whole population (dashed line).

here as well LN and DLN-approximations. The LN-fits are shown as dashed (users1) and dashed-dotted lines (user2) in Figure 12.2a, and the DLN-fits as red curve with circle markers (user1) and blue curve with box markers (user2) ibid. To measure the approximation quality we use again the p-value of a KS-test. While the LN shows bad performance in approximating the PCI-distribution ($p = 0$ for both users), a DLN is a good explanation of the PCIs at least for user1, for which it achieves a p-value of approximately 0.5. For user2 the p-value of the DLN-fit is below the usual choices of the level of significance, which implies that the it is rejected for this user. Nevertheless, we observe that the first 8 hours of his PCI-cdf are well approximated by a DLN, then the activity decays relative to the approximation but increases again after 16 hours. This bump in the cdf, causing the rejection of the DLN-hypothesis, is originated by the activity cycle of user2, whose participation on Slashdot concentrate almost exclusively on the working hours from Monday to Friday, as can be observed in the insets of Figure 12.2a. User1, on the other hand, whose daily and especially weekly activity cycles are much more balanced than those of user2, does not show such prominent bumps and the time difference between his comments and the corresponding posts are hence easier to approximate by a DLN.

The DLN does not account for the alteration due to the circadian cycle in the PCI-distribution of user2, since we mix here all posts, independent of their publishing hour, which makes it difficult to isolate the exact influence of the circadian cycle on the distribution. To get a better picture we would have to investigate only the comments of user2 to posts published at the same hour of the day. Unfortunately the number of his comments (as well those of the other users) in the dataset is too low to achieve reliable information from such an analysis. We will therefore perform the observations in

this section without considering this aspect[2].

The influence of the activity cycle becomes even more evident in the ICI-distribution, which for user1 (light grey) and user2 (dark gray curve) is illustrated in Figure 12.2b. The ICI-cdf, shown in the inset of Figure 12.2b, of user2 reveals an even more pronounced increase as in the PCI-cdf around an ICI-length of 16 hours, which is clearly caused by the 8h of inactivity in the activity cycle of user2. We further notice that the ICI-pdf peaks for both users as well as for the whole population (dashes curve) at 3 minutes. This is probably caused by an anti-troll filter (Malda, 2002), which should prevent a user from commenting more than once within 120 seconds. The medians of the ICI-distributions of user1 and user2 are rather short (11 and 7 minutes respectively) compared to the median of the whole population (about 17 hours), indicating that the two users engage in discussions frequently during their activity phase.

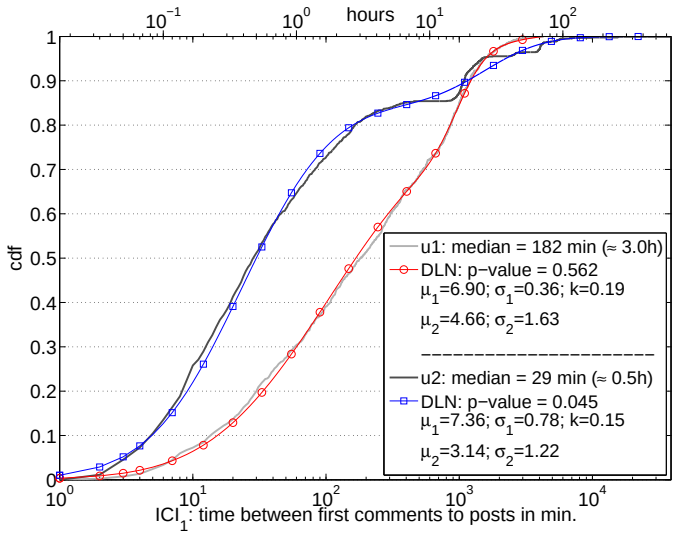

Figure 12.3: DLN fit of the distribution of the inter-post intervals (ICI_1) of user1 and user2 between their first comments to different posts.

An approximation of the ICI-distribution with LN or DLN does not lead to good results, since a user may write more than one comment to a post during a short time interval, bounded below by the anti-troll filter, which leads to an abundance of short ICIs. However, if we group the activity into sessions as proposed by Duarte et al. (2007), we achieve much better results. We consider the first comment to a post as the beginning of a new session and the subsequent comments to the post as within the same session.

To refer to the time difference between two sessions we use the abbreviation ICI_1, which corresponds to the time-difference between two subsequent first comments of the same user to different posts. The cdf of the resulting ICI_1-distributions of user1 and user2 is shown in Figure 12.3. As in the

[2]However, one has to keep in mind that a similar study using a greater dataset could probably obtain better results, if the publishing hour of the post were considered.

case of the PCI-distribution the LN approximation does not lead to good results (data not shown) and the DLN-approximation is acceptable for user1. For user2 the outcome of the KS-test depends on the choice of the significance level α_o. The resulting p-value of 0.045 accepts the DLN-hypothesis for $\alpha_0 = 0.01$, but rejects it for $\alpha_0 = 0.05$.

If we compare the medians of the ICI (Figure 12.2b) and the ICI_1-distributions (Figure 12.3) of user1 and user2, we observe that although their ICI-medians are quite similar the two users show different behavior, when looking on their ICI_1s. User2 changes the post very frequently (median $\approx$ 0.5h), while user1 is more persistent to the post's subject (median $\approx$ 3h).

In Figure 12.4 we show the temporal patterns of two more users (user3 and user4), which are less active than those analyzed previously. For both users we can approximate their ICI_1 as well as their PCI-distributions with DLNs, as is shown in Figure 12.4 (see Figure legend for the corresponding p-values). The daily activity cycle of user2 is similar to the one of user4 (compare insets of Figure 12.4a and Figure 12.2a). Nevertheless, since about 95% of all the comments of user4 are given within the first 16 hours after the publishing of the respective posts, no bumps affecting the outcome of the KS-tests can be observed in the activity distributions of this user.

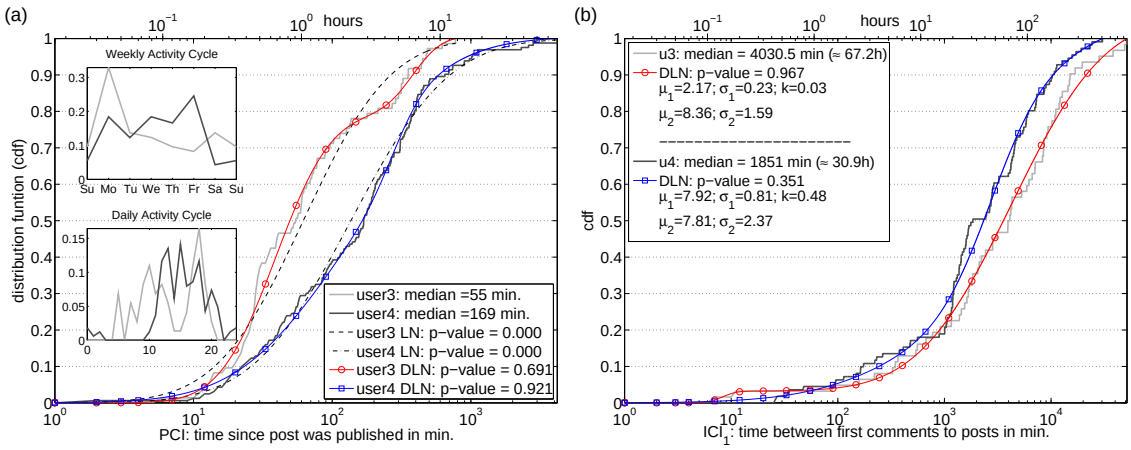

Figure 12.4: Activity patterns of user3 and user4: **(a)** PCI-distributions, insets show daily and weekly activity cycles. **(b)** Distribution of the inter-comment intervals (ICI_1) of the first comment to a post.

User3 shows an even more complicated activity pattern. His daily activity cycle shows a bimodal behavior, with an second phase of reduced activity around lunch time (light gray curves in the lower inset of Figure 12.4a). This causes decreased activity in the PCI-distribution between 2 and 4 hours after the posts are published. It is interesting to note that in this case we are able to approximate the bump well with a DLN-distribution. When comparing the medians of PCI and ICI_1 distribution we note as a second interesting fact that although user3 is faster in the respond to a new post than user4, the latter has a shorter ICI_1. It seems thus that we observe two independent parameters which will allow us to describe the activity of the users. A more detailed analysis on this subject will be given at

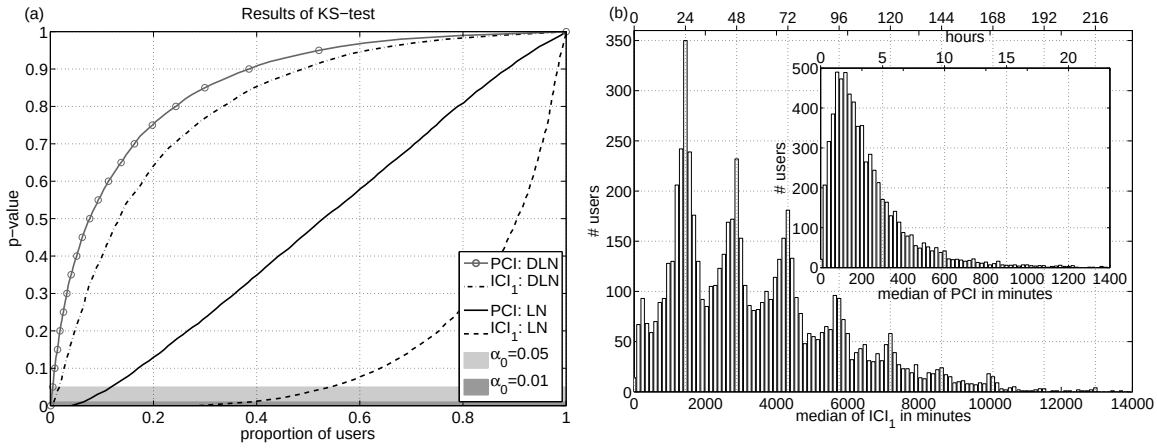

Figure 12.5: **(a)** Results of KS-test of PCI- and ICI_1-distributions for users which write more than 50 comments. **(b)** Medians of their PCI (inset) and ICI_1-distributions.

the end of this chapter.

12.2.2 Description of the activity patterns the most active users

After having analyzed the activity patterns of some users in detail, we will now compare the approximation quality of the patters of the most active part of the users as well as present parameters which allow to describe their activity.

Approximation Quality

We concentrate on the 6736 users for which we can identify more than 50 comments in our dataset and analyze the quality of LN and DLN-approximations of their PCI and ICI_1-distributions. To measure the approximation quality we use, as in the case of the PCI-distributions of single posts, the *p*-values of KS-tests.

Figure 12.5a shows the cdf of the resulting *p*-values. We notice that a DLN allows to approximate the activity patterns of most of the users. The result is slightly better for the PCI-distributions, where the DLN approximation ins rejected for only 12 users with a level of significance $\alpha_0 = 0.01$, whereas in the case of the ICI we reject it for 44. This corresponds to 0.18% and 0.66% of the total amount of

		$\alpha_0 = 0.01$	$\alpha_0 = 0.05$
ICI_1:	LN	38.89%	54.38%
	DLN	0.66%	1.77%
PCI:	LN	6.43%	11.79%
	DLN	0.18%	0.48%

Table 12.3: Percentage of users with rejected 0-hypotheses of their PCI and ICI_1-approximations.

users investigated. The LN distribution does not give good results for the ICI, but we can still explain the reaction times to a post, i.e. the PCI-distribution, of more than 93% of the users (see Table 12.3).

We can conclude that a DLN is a valid explanation for the activity patterns of single users, since it allows to fit the reaction time distribution (PCI) as well as the distribution of the time differences between two consecutive comments to different post (ICI_1) of more than 99% of the investigated users. Again, the DLN shows to be very flexible in accounting for the alterations in these distributions caused by the activity cycles of single users.

Characterization of single users

As insinuated in the previous subsection we will use the medians[3] of PCI and ICI_1 distribution to characterize the activity of single users. We concentrate again on the users which wrote more than 50 comments.

The distribution of the two medians of these users can be observed in Figure 12.5b. While the PCI-medians, shown in the inset of Figure 12.5b, are distributed in an right skewed unimodal distribution, the medians of the ICI_1s give rise to an interesting multi-modal distribution, which peaks around time differences between the comments of 24, 48, etc. hours. This is caused by activity cycles of users with very narrow peaks. Such users comment mainly during a very short time interval, e.g. once a day, what then naturally results in time differences of a least 24h between comments, weekends and casual absence of commenting can cause the peaks at multiples of 24h.

Only a very small correlation (correlation coefficient $= 0.082$) can be found between the two medians, which allows to use these largely independent quantities for user characterization. The median of the PCI-distribution gives us a measure of how fast a user reacts to a new post, and the ICI_1 median tells us how frequent a user joins a new discussion about another subject.

[3]Since we deal with heavy tailed distributions we use as descriptive parameter the median instead of the mean, to avoid dependency on a few very large large values in the tail.

Chapter 13

Discussion of the results for human communication

The special architecture of the technology-related news website Slashdot allowed us to analyze the temporal communication patterns of an online society without considering semantic aspects. The interactions on the site are driven by news-posts which provoke communication activity in the form of comments.

The number of comments per user (Figure 12.1 and Table 12.1) indicates a high amount of heterogeneity in the behavior of Slashdot users. The vast majority of the users writes only a very reduced number of comments while a small nucleus of "hard-core" commentators is responsible for the main part of the comments. We can fit the distribution of the number of comments well with a truncated log-normal (LN) distribution. A similar result has been obtained on a much smaller scale by Naruse and Kubo (2006) analyzing the number of comments per individual in web based bulletin board systems.

Despite the heterogeneity in the distribution of activity among the users and the diversity of themes (games, politics, science, books, etc.) simple homogeneous patterns can be identified on Slashdot, which repeat themselves over and over again. These patterns appear in the reaction time of both community and single users to new posts as well as in the time difference between consecutive comments to different posts of single users.

We show with a The distribution of the time differences between a post and its comments (the PCIs) can be well approximated by a LN distribution for most of the posts. The only remarkable deviations from these approximations are caused by oscillatory daily and weekly activity patterns (Figure 10.4) on the site, which become less noticeable if a post is published early in the morning (Figure 11.9). A significant improvement of the approximation can be achieved using a superposition of two log-normal distributions. Such a double log-normal (DLN) accounts for the first vacillation of activity caused by the circadian cycle and can be interpreted as two independent waves of activity (Figure 11.11), one starting directly after a post has been published, and the second at the next increase

of activity due to the circadian rhythm. Although more such vacillations may occur during the life-time of a post, their amplitude is low compared to the first one, suggesting that a combination of more than two LN-distributions would only increase the complexity of parameter-finding (via MLE) without improving significantly the approximation quality. Nevertheless, a combination of a DLN-distribution with an oscillatory function (DLNxC) emulating the circadian cycle leads to slightly better results without affecting the complexity of MLE.

In single user behavior akin patterns appear in the PCI-distribution of all comments a user writes (to several posts) and in the ICI_1-distribution of single-users, i.e. the time-span between two consecutive comments of a certain user to different posts. Both distributions can be well approximated for nearly all users by DLNs, which again are able to account for the deviations from a simple LN pattern caused now by the individual circadian activity cycles of the users.

We would expect that the time-spans between publishing and reading of a post, or in other words the number of readers of a post per time-interval, also follow log-normal patterns. This is supported by a study of visits of news-pages on an Hungarian website (Dezso et al., 2006), which revealed patters quite similar to the PCI-distribution on Slashdot. To verify our claim one could for example check the server logs of Slashdot or the access-times of an external homepage linked by a Slashdot post. Such a study has been performed to show the Slashdot effect (Adler, 1999), but the scale of the data presented does not allow to draw significant conclusions. Further investigation on this issue is needed.

Log-normal and DLN temporal patterns similar to those described above for many-to-many communication were found in the waiting and inter-event times of single users in person-to-person e-mail communication by Stouffer et al. (2006). The temporal patterns of the e-mail data were previously claimed to show power-law (PL) behavior, which could be explained by a queuing model (Barabási, 2005). Although the model of Barabási might allow insight into temporal patterns of other types of human activity (Vázquez et al., 2006) it is not able to account for the observed log-normal behavior patterns in e-mail conversations (Stouffer et al., 2006). The same is true for the temporal patterns in Slashdot, as we show for the posts' PCI-distributions. Only after discarding on average more than 50% of the comments can the tail of the PCI-distributions be explained by PLs. The multiplication of a PL with an oscillatory function, in analogy to the DLNxC, only deteriorates the fit. One can conclude that the temporal patterns of human communication investigated are not scale-free and thus not covered by the model of Barabási. We hope therefore to encourage further research towards a theoretical understanding of the underlying phenomena responsible for this apparently quite general human behavior patterns.

The medians (Figure 11.10) of the PCI-distributions are very small compared to the overall duration of the activity provoked by a post. Although the posts might be available for commenting

for more than 10 days, the first few hours decide whether they will become highly debated or just receive some sporadic comments. We would therefore expect that the simplicity of the approximation together with the high initial activity should make an accurate prediction of the expected user behavior feasible at an early phase after a post has been put online. The accuracy of such forecasting methods is subject of current research and will be published elsewhere (Kaltenbrunner, Gómez and López, 2007a).

An early characterization of the activity triggered by a post could be applied, for instance, on dynamic pricing or placing of online advertisements or on the improvement of online marketing. The success of a campaign might be predicted already after a short time-period, thus allowing an early adaptation of the strategy of information diffusion. In this context the viral marketing concept (Leskovec, Adamic and Huberman, 2006) which relies on personal communication might be the most promising field.

In our opinion, the regular communication activity patterns described in this work may be relevant in two aspects. The first, simpler one, is related to applications where a better understanding of information trade in the web translates easily into a better description, and even quantification, of Internet audience. But a second, more complex, aspect is related to the human "communicative" behavior uncovered at present time: Internet based communication capabilities. We face a new, large scale, all-to-all public space in which a novel kind of social behavior arises, a scenario that we do not yet fully understand. However, we should not forget that the new activity is being largely recorded and the data can be available for research. The work presented in this contribution is a good example of how those data can be collected and analyzed to give, at least, a quantitative description of the behavior. This is a first step towards a more ambitious target: to develop "ab initio" models for the population dynamics of message interchange, which is also the goal of our current research.

Conclusions and Future Research

Conclusions

We have presented two different aspects of the dynamics of message interchange between stochastic units. Both can be considered as two subclasses of animal communication, one at a high cognitive level of human communication and the other at the basic level of intra-cellular communication in the form of pulsed spikes between neurons.

We found that a network of non-leaky integrate-and-fire neurons with delayed, pulsed coupling experiences a phase transition around a critical value of the coupling strength. For sub-critical coupling the neurons can be considered as nearly independent and are mainly governed by external stochastic input to the system. If, on the contrary, the coupling is greater than the critical value (supercritical) we observe a self-organization phenomena, where the communication between units becomes dominant. The neurons group into phase-locked clusters with an ISI, which is independent of the number of neurons or the stochastic input. It only depends on the coupling strength. Hysteresis can be observed in the supercritical region and theoretical limits for the ISI and its expectation, valid of the entire parameter range of the system are given.

We conclude that synaptic delay changes significantly the dynamics of neural networks. It is crucial for the observed hysteresis effect and the appearance of several phase-locked clusters. Our results are also valid for networks of neurons with heterogeneous thresholds and coupling strengths or if the updating is changed form parallel to sequential. The later implies heterogeneous delays. This robustness of the findings allows us to conjecture that the phenomena described could be found as well in more complex, realistic neural models with delay.

In the case of human communication we analyzed the temporal patterns of discussions triggered by the tech-news website Slashdot. We identified daily and weekly activity cycles and analyzed the distributions of the time differences between the publishing of a new news-post and the comments it triggers. These distributions were approximated with several different heavy-tailed distributions based on either power-law and log-normal distributions. Although in some cases good fits can be

achieved with a single log-normal distribution, the best approximation quality was reached by a superposition of two log-normal distributions (a double log-normal), which can be interpreted as two waves of activity, one starting directly after a post has been published, and the second at the next increase of the activity cycle. The double log-normal (DLN) distribution accounts for the variations caused by the daily activity cycle. We obtained similar results for the reaction time of single users to a new posts and expect a double log-normal distributions to be a good approximation for the temporal patterns of other types of human communication behavior, e. g. in the time-spans between publishing and reading of news articles. This hypothesis is supported by an analysis of e-mail communication by Stouffer et al. (2006)

Unlike most studies which fit similar data-sets with power-law distributions, double log-normal distributions approximate the entire data. We do not have to cut-off an important (if not the mayor) part of the probability mass on the left hand side of the distribution to achieve good fits (Clauset et al., 2007). The fits with DLN distributions are even better than those of power-laws with cutoff. These cutoffs (apart from the weaker quality of the fits) present a mayor drawback for some recent models which try explain temporal patterns in human behavior using power-law distributions (Barabási, 2005; Vázquez, 2005), and leave the question for a theoretical explanation of this behavior open.

Future Research

Most of the approaches we have introduced here can still be improved. Moreover, they generate new perspectives of work and have other possible applications. We outline plans for future research and some for each of the subjects involved in this thesis:

PART II: Neural populations

- Extension to other models of pulse coupled oscillators:

The main results of Part II is the existence of a phase transition in a network of stochastic, pulse-coupled, non-leaky integrate-and-fire neurons around a critical value of the coupling strength where the system transforms from an ensemble of asynchronous oscillators to a system of stable phase-locked clusters. We conjecture that this result is restricted to our special model configuration, but is a general property that can be observed in a wide range of different models, as long as they incorporate a delayed coupling and an explicit refractory period.
Candidates for an occurrence of the phenomena would be:

- The leaky integrate-and-fire oscillator of Mirollo and Strogatz (1990).
- The linear, non-leaky-integrate and fire oscillator used by Senn and Urbanczik (2000).
- Oscillators with biological inspired phase response curves like the one used by Östborn (2002).
- Models where the coupling is defined via alpha functions like by van Vreeswijk (1996) instead of point processes.

- Detecting synchronization between populations of stochastic spiking neurons:

We plan to used two networks of coupled populations of stochastic spiking neurons as used in this thesis to generate pairs of time series. We will then try to uncovered the direction of coupling

with standard methods of nonlinear time series analysis (Quiroga, Arnhold and Grassberger, 2000; Smirnov and Andrzejak, 2005) which are in the two previously cited studies used to analyze coupling between chaotic oscillators. The stochasticity in our model allows the application of those methods.

- Provide a more detailed prediction of the mean period of the system:

In Rodríguez et al. (2002) an approximation for the distribution of the ISI at the critical coupling strength was given. We plan to extend this approximation to the complete domain of possible coupling strengths.. As a first step we will derive this distribution for a network of deterministic neurons starting at random initial conditions with low coupling and receiving adiabatic increases of the coupling strength.

- Application of the Hysteresis as a simple memory mechanism:

The hysteresis effect might be used to generate a simple memory of a strong stimulus, which leads the system below the critical point around which the phase transition occurs. If the strong stimulus would be substituted by a weaker but sufficient strong one to maintain the system below the critical point, the system would still evolve as if the strong stimulus would still be present ("remembered") due to the hysteresis. The memory could be erased by removing the weaker input or a short negative input leading the system back to a sub-critical behavior.

- Perform a stability analysis of the system:

Working memory function are often modeled in the form of bistable dynamical attractor networks (Durstewitz et al., 2000). We would expect the system analyzed here to be multi-stable in the region of supercritical coupling in the where hysteresis occurs, since it can choose there between a large amount of different, apparently quite stable periodic firing patterns, with different amounts of neurons in the clusters or even different amount of clusters. A formal stability analysis of these firing patterns should be performed. The result will be interesting to compare with the unstable attractors found in networks of pulse coupled oscillators with delayed coupling (Timme et al., 2002; Ashwin and Timme, 2005).

PART III: Human communication behavior

- Develop a model which generates the log-normal behavior:

Develop a model similar to those explained in section 2.3 which is able to reproduce the log-normal distributions in the reaction time of the community to a news item.

- Predict the activity on Slashdot:

Using the excellent approximation quality of the PCI-distributions we will develop an algorithm which allows the prediction of expected server-loads.

- Analyze the nesting of the comments:

The comments a news-post receives on Slashdot are threaded and nested. We plan to investigate two aspects of the structure of the nesting tree.

- *Analysis of the social network of Slashdot users:* We consider that two users (user1 and user2) are related when user1 replies to a comment of user2. Using this we can generate a social network, which can be analyzed with standard measures (Newman, 2003) like clustering coefficient, average path length, etc. We expect the number of links per user to follow a heavy-tailed distribution similar to the one of the number of posts per user (see Figure 12.2).

- *Measure the controversy caused by a certain post:* Using an adapted version of the *h*-index of Hirsch (2005), commonly used to characterize the scientific output of researchers, we can generate a measure to quantify the amount of controversy generated by a certain post. We order the comments of a post in nesting levels, Top-level comments which reply directly to the post are in level one, replies to these comments in level two and so fort. The h-index h of a post is then the maximum nesting level i which has at least $h > i$ comments, or in other words, $h+1$ is the first nesting level i which has less then i comments. This measure should be more robust than just the maximum nesting level, which might reach high values, for example, due to debates between only two users for on post which otherwise does not initiate much discussions in the community.

- Use the content of the comments:

Standard methods of text classification (Joachims, 2002) and clustering will be applied on the content of the comments to analyze how useful the comments are to identify the topic of the post and to generate clusters of users with similar characteristics.

Appendix

Appendix A

Proof of Periodic Pattern Condition 5.4

In the following analysis we use the deterministic rule (5.3) instead of the stochastic state transitions (4.1) and restrict ourself to the case of $\delta \geq t_{ref}$. A unit with ISI τ can make $\tau - 1 - t_{ref}$ transitions due to this rule before reaching the threshold. The term t_{ref} corresponds to the refractory period where no increase of the state of an unit is allowed and the -1 to the last time-step when the threshold is reached. We have therefore a contribution of $p(\tau - 1 - t_{ref})\Theta(\tau - 1 - t_{ref})$ because of rule (5.3) to the total evolution of a neuron before its threshold is reached[1].

With this result we can calculate the mean minimum cluster size of a system of κ clusters. We call the clusters K_i ($i \in \{1, \ldots, \kappa\}$) and set the number of elements of every cluster $|K_i| = k_i$. The clusters are ordered according to their spiking time. At every time-step one cluster reaches threshold starting with cluster K_1. After cluster K_κ spikes the cycle starts again with cluster K_1. When cluster K_i reaches threshold, the elements of cluster K_{i+1} (or of K_1 in case of $i = \kappa$) have received the inputs of all clusters except cluster K_i and an increase of $p(\tau - 1 - t_{ref})$ due to rule (5.3). This leads to the following condition:

$$1 + \Big(-1 + \sum_{\substack{j=1 \\ j \neq i}}^{\kappa} k_j \Big)\varepsilon + p(\tau - 1 - t_{ref})\Theta(\tau - 1 - t_{ref}) < L. \tag{A.1}$$

Which due to $\sum_{j=1}^{\kappa} k_j = N$ is equivalent to

$$k_i > k_{min} = N - 1 + \frac{1 + p(\tau - 1 - t_{ref})\Theta(\tau - 1 - t_{ref}) - L}{\varepsilon} \qquad \text{for all } i \in \{1, \ldots, \kappa\}. \tag{A.2}$$

Written in terms of η this is equal to

$$k_i > k_{min}(\tau) = (N-1)(1-\eta) + \frac{p(\tau - 1 - t_{ref})\Theta(\tau - 1 - t_{ref})}{\varepsilon}\,. \tag{A.3}$$

We have proved the periodic pattern condition (5.4).

[1] Note the use of the Heaviside step function to have a valid formula also for the case of $\tau < t_{ref} + 1$.

Appendix B

Bounds for τ

In this Appendix we derive bounds for the ISI τ of the ensemble and the mean ISI $\langle\tau\rangle$ of several experiments. Again we will use the deterministic rule (5.3) instead of the stochastic dynamics (4.1). We will obtain two absolute bounds such that $\tau_{min} \leq \tau \leq \tau_{max}$ for all possible ISIs of the system, and a lower bound for the mean value $\langle\tau\rangle$ over all possible initial conditions which we call $\langle\tau\rangle_{min}$. We get thus

$$\langle\tau\rangle_{min} \leq \langle\tau\rangle \leq \tau_{max} \; . \tag{B.1}$$

B.1 Maximum ISI τ_{max}

First we derive the maximum possible ISI τ_{max} of the system. It is obvious that the mean cluster size $\bar{k}(\tau) \geq k_{min}$, which can be written using equations (5.6) and (A.3) as

$$\bar{k}(\tau) = \frac{N\delta}{\tau} \geq (N-1)(1-\eta) + \frac{p(\tau-1-t_{ref})\Theta(\tau-1-t_{ref})}{\varepsilon} \; . \tag{B.2}$$

This results in an inequality of degree 2 for τ which has the only solution

$$\tau \leq \tau_{max} = \frac{(N-1)\varepsilon(\eta-1)}{2p} + \frac{1+t_{ref}}{2} + \sqrt{\left(\frac{(N-1)\varepsilon(\eta-1)}{2p} + \frac{1+t_{ref}}{2}\right)^2 + \frac{N\varepsilon\delta}{p}} \; . \tag{B.3}$$

compatible with the condition $\tau \geq 0$. We omitted the $\Theta(\tau-1-t_{ref})$ term to calculate (B.3). This can be done if $\tau \geq 1+t_{ref}$. Inequality (B.2) permits us to calculate the minimum value of η for which a certain ISI τ is possible. We get

$$\eta \geq \eta_{min}(\tau) = \frac{p(\tau-1-t_{ref})\Theta(\tau-1-t_{ref})}{(N-1)\varepsilon} + 1 - \frac{N\delta}{(N-1)\tau} \; . \tag{B.4}$$

It is sufficient to calculate $\eta_{min}(2\delta)$ since we assume that $\delta \geq t_{ref} \geq 1$ and the system will be fully synchronized ($\tau = \delta$), i.e. it consists of only one cluster, for values of η below this limit, which we

call η_{sync}. We get

$$\eta \geq \eta_{sync} = 0.5 - \frac{1}{2(N-1)} + \frac{p(2\delta - 1 - t_{ref})\Theta(2\delta - 1 - t_{ref})}{(N-1)\varepsilon} \,. \tag{B.5}$$

For the limit of large N this transforms into

$$\lim_{N\to\infty} \eta_{sync} = 0.5 \,. \tag{B.6}$$

Condition (B.3) is therefore valid if $\eta \geq 0.5$.

B.2 Minimum ISI τ_{min}

If, instead of looking at the state of a neuron before the threshold is reached as in the proof of the periodic pattern condition in Appendix A, we observe the state of a neuron just after it has passed the threshold, we can derive a condition for the minimum possible ISI. We use that a neuron with an ISI of length τ increases its state due to the deterministic rule (5.3) by $p(\tau - t_{ref})$ during every ISI. Moreover, since the ensemble is homogeneous we expect that during an ISI of a single neuron all other neurons fire once, which translates into an increase of the activation state by $(N-1)\varepsilon$ due to the ensemble dynamics. Combining the two terms we get

$$L \leq 1 + (N-1)\varepsilon + p(\tau - t_{ref}), \tag{B.7}$$

which we can transform into a condition for τ

$$\tau \geq \hat{\tau}_{min} = t_{ref} + \frac{L - 1 - (N-1)\varepsilon}{p} = t_{ref} + \frac{(N-1)\varepsilon(\eta - 1)}{p} \,. \tag{B.8}$$

Comparing this result with equation (4.5), we observe that $\hat{\tau}_{min} = \tau_{mf}$ and have thus found that the formulas (4.5) are a lower bound for the ISI τ. This bound of course can be improved for for $\eta < 1$, since there $\hat{\tau}_{min}$ is negative, although τ can never be smaller than t_{ref}. We use therefore the Heaviside step function and get

$$\tau_{min} = t_{ref} + \Theta\left(\frac{(N-1)\varepsilon(\eta - 1)}{p}\right), \tag{B.9}$$

which is a lower bound for τ valid for all values of η.

B.3 Minimum mean ISI $\langle\tau\rangle_{min}$

To derive a lower bound for $\langle\tau\rangle$ we start with

$$\begin{aligned} \frac{N\delta}{\tau} &= g(\tau)\,\lfloor k_{min}(\tau) + 1 \rfloor \\ &\leq g(\tau)\left((N-1)(1-\eta) + \frac{p(\tau - 1 - t_{ref})\Theta(\tau - 1 - t_{ref})}{\varepsilon} + 1\right), \end{aligned} \tag{B.10}$$

which can be obtained from (5.6), (5.7) and (A.3). We calculate the mean of the left and right hand side according to the probabilities $P(\tau)$, which denominate the probability of the system ending up in a system with ISI τ.

$$\sum_{i=1}^{\tau_{max}} \frac{N\delta}{i} P(i) \leq \sum_{i=1}^{\tau_{max}} g(i) \left((N-1)(1-\eta) + \frac{p(i-1-t_{ref})\Theta(i-1-t_{ref})}{\varepsilon} + 1 \right) P(i) \,. \tag{B.11}$$

We set $1/\tau = f$ where f is the spiking-frequency, use $P(\tau) = P(f) = P(g(\tau))$, eliminate the terms of the summation which equal 0 and get

$$\begin{aligned} N\langle f\rangle\delta &\leq \langle g\rangle \left((N-1)(1-\eta) + 1 - \frac{(1+t_{ref})p}{\varepsilon} \right) + \\ &\quad + \frac{p}{\varepsilon} \left(\sum_{i=1}^{1+t_{ref}} g(i)P(i) + \sum_{i=2+t_{ref}}^{\tau_{max}} g(i)iP(i) \right). \end{aligned} \tag{B.12}$$

Using the following identity $\langle XY\rangle = \langle X\rangle\langle Y\rangle + \mathrm{Cov}(X,Y)$ for two random variables X and Y we achieve

$$\begin{aligned} N\langle f\rangle\delta &\leq \langle g\rangle \left((N-1)(1-\eta) + 1 - \frac{(1+t_{ref})p}{\varepsilon} \right) + \\ &\quad + \frac{p}{\varepsilon} \left(\langle g\rangle\langle\tau\rangle + \mathrm{Cov}(g(\tau),\tau) - \sum_{i=2}^{1+t_{ref}} g(i)(i-1)P(i) \right). \end{aligned} \tag{B.13}$$

From (B.10) it is easy to see that $\mathrm{Cov}(g(\tau),\tau) \leq 0$ since an increase of τ translates into a decrease of $g(\tau)$ and vice versa. Because of this fact and $g(\tau) \geq 0$ we can eliminate the two leftmost terms of inequality (B.13) by weakening the inequality.

$$N\langle f\rangle\delta \leq \langle g\rangle \left((N-1)(1-\eta) + 1 + \frac{p(\langle\tau\rangle - 1 - t_{ref})}{\varepsilon} \right). \tag{B.14}$$

The mean frequency $\langle f\rangle$ is equal to the inverse of the harmonic mean $h(\tau)$. Since for a set of positive numbers its harmonic mean is never greater than its arithmetic mean (Bullen, 2003) we have $\frac{1}{\langle\tau\rangle} \leq \frac{1}{h(\tau)} = \langle f\rangle$. Applying this on inequality (B.14) leads to

$$\frac{N\delta}{\langle\tau\rangle} \leq \langle g\rangle \left((N-1)(1-\eta) + 1 + \frac{p(\langle\tau\rangle - 1 - t_{ref})}{\varepsilon} \right). \tag{B.15}$$

We can transform this into a quadratic inequality of $\langle\tau\rangle$ since $\langle\tau\rangle > 0$. It has the only positive solution

$$\begin{aligned} \langle\tau\rangle \geq \langle\tau\rangle_{min} &= \frac{(N-1)\varepsilon(\eta-1) - \varepsilon}{2p} + \frac{1+t_{ref}}{2} + \\ &\quad + \sqrt{\left(\frac{(N-1)\varepsilon(\eta-1) - \varepsilon}{2p} + \frac{1+t_{ref}}{2} \right)^2 + \frac{N\varepsilon\delta}{p\langle g\rangle}} \,. \end{aligned} \tag{B.16}$$

We have found a lower bound for the mean value of our ISI distribution.

Appendix C

Thermodynamic limits of $\langle\tau\rangle_{min}$ and τ_{max}

In this Appendix we will calculate the thermodynamic limit (i.e. the behavior for $N \to \infty$) of $\langle\tau\rangle$ for the different regions of η. We first calculate the thermodynamic limits of the bounds $\langle\tau\rangle_{min}$ and τ_{max} of $\langle\tau\rangle$ calculated in Appendix B and then situate the thermodynamic limit of $\langle\tau\rangle$ between the limits of the bounds.

We start with the limit for $\langle\tau\rangle_{min}$ using (B.16):

- $\eta > 1$

$$\begin{aligned}\lim_{N\to\infty}\frac{\langle\tau\rangle_{min}}{N} &= \lim_{N\to\infty}\frac{\varepsilon(\eta-1)}{2p}-\frac{\varepsilon(\eta-1)}{2pN}+\frac{1+t_{ref}}{2N}+\\ &\quad+\sqrt{\left(\frac{\varepsilon(\eta-1)}{2p}-\frac{\varepsilon(\eta-1)}{2pN}+\frac{1+t_{ref}}{2N}\right)^2+\frac{\varepsilon\delta}{p\langle g\rangle N}}\\ &= \frac{\varepsilon(\eta-1)}{2p}+\left|\frac{\varepsilon(\eta-1)}{2p}\right|, \end{aligned} \tag{C.1}$$

  which for $\eta > 1$ is

$$\lim_{N\to\infty}\frac{\langle\tau\rangle_{min}}{N} = \frac{\varepsilon(\eta-1)}{p}\,. \tag{C.2}$$

  This coincides with the limit of τ_{mf}/N (See equation (4.5)).

- $\eta = 1$

  Setting $\eta = 1$ in (B.16) leads to

$$\lim_{N\to\infty}\frac{\langle\tau\rangle_{min}}{\sqrt{N}} = \lim_{N\to\infty}\frac{1+t_{ref}}{2\sqrt{N}}-\frac{\varepsilon}{2p\sqrt{N}}+\sqrt{\frac{1}{4N}\left(1+t_{ref}-\frac{\varepsilon}{p}\right)^2+\frac{\varepsilon\delta}{p\langle g\rangle}} = \sqrt{\frac{\varepsilon\delta}{p\langle g\rangle}}. \tag{C.3}$$

- $\eta < 1$

  Equation (C.1) for $\eta < 1$ leads to $\lim_{N\to\infty}\langle\tau\rangle_{min}/N = 0$, but we can improve this result. We

transform (B.16) slightly and calculate

$$\lim_{N\to\infty}\langle\tau\rangle_{min} = \lim_{N\to\infty}\frac{1+t_{ref}}{2}-\frac{(N-1)\varepsilon(1-\eta)+\varepsilon}{2p}+ \\ +\sqrt{\left(\frac{(N-1)\varepsilon(1-\eta)+\varepsilon}{2p}-\frac{1+t_{ref}}{2}\right)^2+\frac{N\varepsilon\delta}{p\langle g\rangle}}\,.$$

Applying $-a+b=\frac{-a^2+b^2}{a+b}$ we get

$$\begin{aligned}\lim_{N\to\infty}\langle\tau\rangle_{min} &= \lim_{N\to\infty}\frac{\frac{N\varepsilon\delta}{p\langle g\rangle}}{\frac{(N-1)\varepsilon(1-\eta)+\varepsilon}{2p}-\frac{1+t_{ref}}{2}+\sqrt{\left(\frac{(N-1)\varepsilon(1-\eta)+\varepsilon}{2p}-\frac{1+t_{ref}}{2}\right)^2+\frac{N\varepsilon\delta}{p\langle g\rangle}}} \\ &= \delta\left(\frac{\langle g\rangle(1-\eta)}{2}+\left|\frac{\langle g\rangle(1-\eta)}{2}\right|\right)^{-1} \qquad \text{(C.4)}\end{aligned}$$

and have therefore for $\eta<1$

$$\lim_{N\to\infty}\langle\tau\rangle_{min}=\frac{\delta}{\langle g\rangle(1-\eta)}\,. \qquad \text{(C.5)}$$

The limits for τ_{max} can be calculated analogously from equation (B.3). Combining the limits for both bounds with the result of equation (B.6) that the system has an ISI of δ for $\eta<0.5$ we obtain

$$\begin{aligned}\lim_{N\to\infty}\langle\tau\rangle &= \delta && \text{if } \eta<0.5\,,\\ \frac{\delta}{\langle g\rangle(1-\eta)}\le\lim_{N\to\infty}\langle\tau\rangle &\le\frac{\delta}{(1-\eta)} && \text{if } 0.5\le\eta<1\,,\\ \sqrt{\frac{\varepsilon\delta}{p\langle g\rangle}}\le\lim_{N\to\infty}\frac{\langle\tau\rangle}{\sqrt{N}} &\le\sqrt{\frac{\varepsilon\delta}{p}} && \text{if } \eta=1\,,\\ \lim_{N\to\infty}\frac{\langle\tau\rangle}{N} &= \frac{\varepsilon(\eta-1)}{p} && \text{if } \eta>1\,. \qquad \text{(C.6)}\end{aligned}$$

Appendix D

Graphical interpretation of the bounds for $\langle\tau\rangle$

In this part of the Appendix we will present a graphical interpretation for $\langle\tau\rangle_{min}$ and τ_{max}. The special form of the formula for $\langle\tau\rangle_{min}$ (See equation 5.10 and Appendix B for derivation)

$$\langle\tau\rangle_{min} = \frac{(N-1)\varepsilon(\eta-1)-\varepsilon}{2p} + \frac{1+t_{ref}}{2} + \sqrt{\left(\frac{(N-1)\varepsilon(\eta-1)-\varepsilon}{2p} + \frac{1+t_{ref}}{2}\right)^2 + \frac{N\varepsilon\delta}{p\langle g\rangle}} \tag{D.1}$$

suggests that it might be interpreted as shown in Figure D.1 in the form of a right triangle.

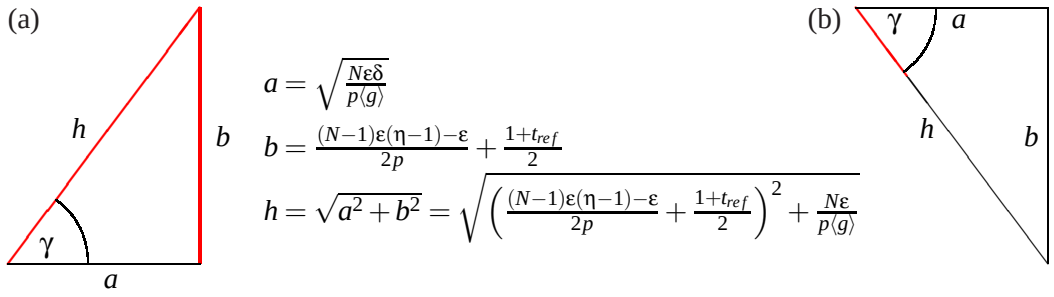

Figure D.1: Graphical interpretation of equation (D.1) for $\langle\tau\rangle_{min}$ for different regions of η. **(a)** $\eta > 1$: The sum of the lengths of the thick red lines h and b is equivalent to $\langle\tau\rangle_{min}$. **(b)** $\eta < 1$: The length of the thick red line is equivalent to $h - |b|$ which is approximately equal to $\langle\tau\rangle_{min}$

Figure D.1a represents the interpretation for $\eta > 1$ and Figure D.1a for $\eta < 1$. Each of the sides a, b and h of the triangle represents a part of equation D.1. The definitions for a, b and h are shown in Figure D.1. Since $a^2 + b^2 = h^2$ the triangle is right-angled. With the variables of the geometrical interpretation equation D.1 for $\langle\tau\rangle_{min}$ reduces to

$$\langle\tau\rangle_{min} = b + h = b + \sqrt{a^2+b^2}. \tag{D.2}$$

The thick red lines in Figure D.1 represent this equation. Using the absolute value $|b|$ instead of b,

equation (D.2) can be approximately written as

$$\langle\tau\rangle_{min} \approx \begin{cases} h-|b| & \text{for } \eta < 1 \\ a & \text{for } \eta = 1 \\ h+|b| & \text{for } \eta > 1 \end{cases} \tag{D.3}$$

Note: In this part of the Appendix we don not take care of the fact that the formula for $\langle\tau\rangle_{min}$ does not lead to correct results for $\eta < 0.5$. We are only interested in its geometrical interpretation which is valid for $\eta \geq 0.5$.

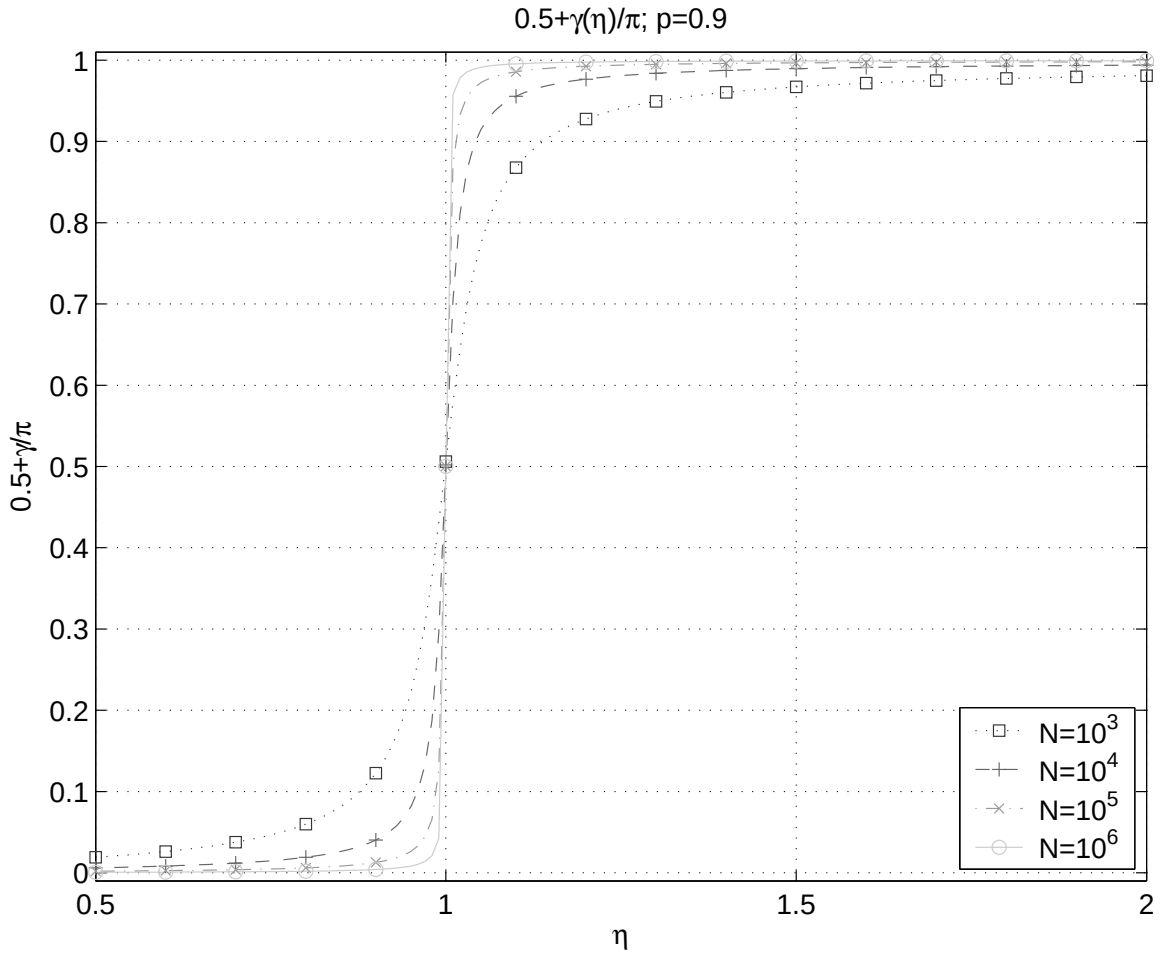

Figure D.2: Phase transition of γ at the critical coupling strength $\eta = 1$ for different N. $N = L$, $p = 0.9$ and $\langle g\rangle = 2$. and in all cases. The interval $[-\frac{\pi}{2}, \frac{\pi}{2}]$ was transformed into $[0,1]$ using $0.5 + \frac{\gamma}{\pi}$. We observe that γ undergoes a phase transition at $\eta = 1$ for $N \to \infty$.

D.1 Dependency on the angle γ

A way to determine the sign of b is to use the angle γ between the hypotenuse h and on-cathetus a of the triangle. γ can be calculated by

$$\tan(\gamma) = \frac{b}{a}, \tag{D.4}$$

which transforms into

$$\gamma = \arctan\left(\frac{(N-1)(\eta-1)-1}{2}\sqrt{\frac{\varepsilon\langle g\rangle}{Np\delta}} + \frac{1+t_{ref}}{2}\sqrt{\frac{p\langle g\rangle}{N\varepsilon\delta}}\right). \tag{D.5}$$

We can determine the sign of γ approximately according to the value of η if we do not fixate on the small fluctuations due to the constant term $1+t_{ref}-\varepsilon/p$ of b

$$\begin{aligned} \gamma &< 0 \quad \text{for } \eta < 1\,, \\ \gamma &= 0 \quad \text{for } \eta = 1\,, \\ \gamma &> 0 \quad \text{for } \eta > 1\,. \end{aligned} \tag{D.6}$$

With γ we can, using some trigonometric identities, calculate $\langle\tau\rangle_{min}$. Due to

$$b = a\tan(\gamma), \tag{D.7}$$

$$h = \frac{a}{\cos(\gamma)}, \tag{D.8}$$

we get

$$\langle\tau\rangle_{min} = b + h = a\left(\tan(\gamma) + \frac{1}{\cos(\gamma)}\right), \tag{D.9}$$

which since $\frac{1}{\cos(\gamma)} = \sqrt{1+\tan^2(\gamma)}$ is equivalent to

$$\langle\tau\rangle_{min} = a\left(\tan(\gamma) + \sqrt{1+\tan^2(\gamma)}\right). \tag{D.10}$$

The angle γ encodes the phase transition as can be seen in Figures D.2 and D.3. In order to show the similarity with the parameter c of Figure 5.3 the transformation $0.5+\frac{\gamma}{\pi}$ was used to transforms the interval $[-\frac{\pi}{2},\frac{\pi}{2}]$ into $[0,1]$ in both figures. The value of g has been set equal to its empirical limit 2.
Figure D.2 shows γ in relation to η for different values of N. If we compare the slope at $\eta = 1$ of the curves for $N = 10^3$ (dotted line with $\square$ markers) and $N = 10^6$ (solid line with circles) we observe that the higher the value of N the more abrupt is the change of the value of γ at $\eta = 1$. The curve for $N = 10^6$ is already very close at the thermodynamic limit where γ experiences a phase transition at the critical coupling strength $\eta = 1$.
The influence of the probability p of a stochastic state transition on γ can be seen in Figure D.3 in relation to the value of η. The curve for $p = 0.9$ (solid line with circles) has a lower slope at $\eta = 1$ than the curve for $p = 0.1$ (dashed line with $+$ markers). We observe thus that lowering p has a similar effect as increasing N. The jump from 0 to 1 at $\eta = 1$ is more abrupt.

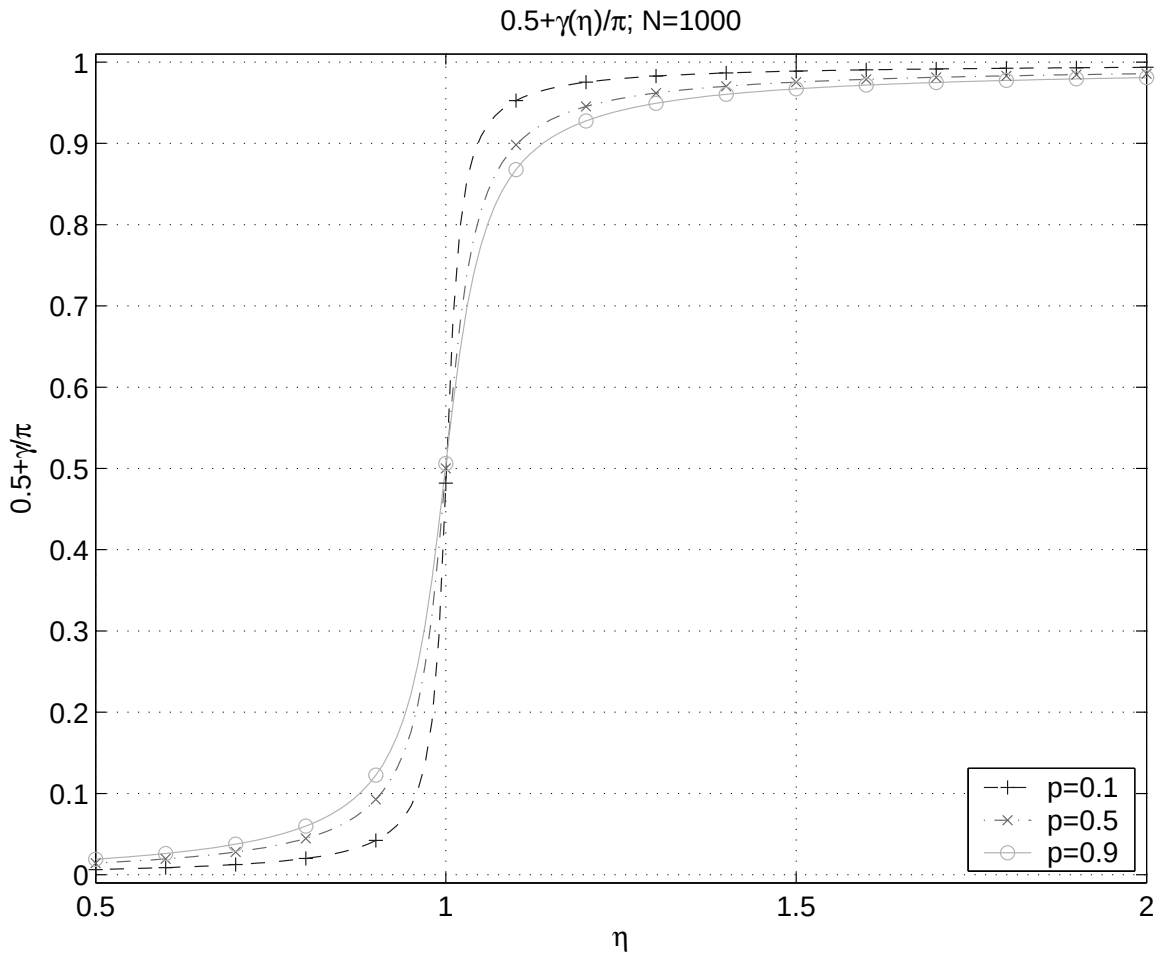

Figure D.3: Phase transition of γ for different p. $N = L = 1000$ and $\langle g\rangle = 2$ in all cases. The interval $[-\frac{\pi}{2}, \frac{\pi}{2}]$ was transformed into $[0,1]$ using $0.5 + \frac{\gamma}{\pi}$. We can observe that the lower the value of p, the greater is the expression of the phase transition at $\eta = 1$.

D.2 Conclusions of the graphical interpretation

The value of the angle γ represents the degree of interaction between two forces, which are represented by the catheti a and b of a right triangle. If γ is close to $\frac{\pi}{2}$ the system is governed by b, which means it acts approximately as predicted by the mean field formulas (4.5). If $\gamma \approx 0$, the dynamics of the system are governed by a which represents the solution of the period for $\eta = 1$. For γ close to $-\frac{\pi}{2}$ the value of h is again dominated by b, but since b has negative sign for negative γ, the value of $\langle\tau\rangle_{min}$ is equal to $h - |b|$. This leads to the cancellation of h if it is dominated by b. In other words $\langle\tau\rangle_{min}$ is of $o(1)$ if γ is close to $-\frac{\pi}{2}$.

A similar interpretation can be done with τ_{max}.

Bibliography

Abdi, H. and Molin, P. (2007). Lilliefors test of normality. In N. Salkind (Ed.), *Encyclopedia of measurement and statistics* (p. 540-544). Thousand Oaks, CA, USA: Sage. 66

Abeles, M. (1991). *Corticonics: Neural circuits of the cerebral cortex*. Cambridge, UK: Cambridge University Press. 22

Adamchik, V. and Srivastava, H. (1998). Some series of the zeta and related functions. *Analysis*, *18*, 131–144. 65

Adler, S. (1999). *The slashdot effect, an analysis of three internet publications.* (Published online) 62, 98

Albert, R., Jeong, H. and Barabási, A.-L. (1999). The diameter of the world wide web. *Nature*, *401*, 130. 90

Ashwin, P. and Timme, M. (2005). Unstable attractors: existence and robustness in networks of oscillators with delayed pulse coupling. *Nonlinearity*, *18*, 2035–2060. 22, 106

Baoill, A. Ó. (2000). Slashdot and the public sphere. *First Monday*, *5*(9). 62

Barabási, A. L. (2005). The origin of bursts and heavy tails in human dynamics. *Nature*, *435*, 207-211. 61, 98, 104

Bienenstock, E. (1995). A model of neocortex. *Network-Computation In Neural Systems*, *6*, 179-224. 21, 22

Bolle, D. and Blanco, J. B. (2004). Two-cycles in spin-systems: sequential versus synchronous updating in multi-state ising-type ferromagnets. *European Physical Journal B*, *42*, 397-406. 51

Brunel, N. and Hakim, V. (1999). Fast global oscillations in networks of integrate-and-fire neurons with low firing rates. *Neural Computation*, *11*, 1621-1671. 23

Brunel, N. and Hansel, D. (2006). How noise affects the synchronization properties of recurrent networks of inhibitory neurons. *Neural Computation*, *18*, 1066-1110. 23

Buck, J. (1988). Synchronous rhythmic flashing of fireflies .II. *Quarterly Review Of Biology*, *63*, 265-289. 21, 58

Bullen, P. S. (2003). *Handbook of means and their inequalities*. Dordrecht, The Netherlands: Kluwer. 115

Burkitt, A. N. (2006). A review of the integrate-and-fire neuron model: I. homogeneous synaptic input. *Biological Cybernetics*, *95*(1), 1–19. 11, 12, 22

Burkitt, A. N. and Clark, G. M. (1999). Analysis of integrate-and-fire neurons: Synchronization of synaptic input and spike output. *Neural Computation*, *11*(4), 871-901. 58

Campbell, S. R., Wang, D. L. L. and Jayaprakash, C. (1999). Synchrony and desynchrony in integrate-and-fire oscillators. *Neural Computation*, *11*, 1595-1619. 58

Canavier, C. C. and Achuthan, S. (2007). Pulse coupled oscillators. *Scholarpedia*, 11641. 10

Chen, C. C. (1994). Threshold effects on synchronization of pulse-coupled oscillators. *Physical Review E*, *49*, 2668-2672. 21

Clauset, A., Shalizi, C. R. and Newman, M. E. J. (2007). *Power-law distributions in empirical data.* (e-print arXiv:0706.1062) 65, 90, 104

Copeland, J. and Moiseff, A. (1995). The occurrence of synchrony in the north-american firefly photinus-carolinus (coleoptera, lampyridae). *Journal Of Insect Behavior*, *8*, 381-394. 21, 23, 58

Cox, D. and Miller, H. (1965). *The theory of stochastic processes*. London: Methuen. 11, 15

Crow, E. L. and Shimizu, K. (Eds.). (1988). *Lognormal Distributions: Theory and Applications*. New York: Marcel Dekker, Inc. 62

DeGroot, M. H. and Schervish, M. J. (2002). *Probability and statistics* (3rd ed.). New York: Addison-Wesley. 66, 75

Dewes, C., Wichmann, A. and Feldmann, A. (2003). An analysis of internet chat systems. In *IMC '03: Proceedings of the 3rd ACM SIGCOMM conference on Internet measurement* (pp. 51–64). New York, NY, USA: ACM Press. 61

Dezso, Z., Almaas, E., Lukacs, A., Racz, B., Szakadat, I. and Barabási, A. L. (2006). Dynamics of information access on the web. *Physical Review E*, *73*, 066132. 61, 98

Diesmann, M., Gewaltig, M. O. and Aertsen, A. (1999). Stable propagation of synchronous spiking in cortical neural networks. *Nature*, *402*, 529-533. 22

Dorogovtsev, S. N., Goltsev, A. V. and Mendes, J. F. F. (2007). *Critical phenomena in complex networks.* (e-print arXiv:0705.0010) 22

Duarte, F., Mattos, B., Bestavros, A., Almeida, V. and Almeida, J. (2007). Traffic Characteristics and Communication Patterns in Blogosphere. In *Proceedings of the 1st International Conference on Weblogs and Social Media (ICWSM'06).* Boulder, Colorado, USA. 63, 93

Durstewitz, D., Seamans, J. K. and Sejnowski, T. J. (2000). Neurocomputational models of working memory. *Nature Neuroscience Supplement*, *3*, 1184-1191. 56, 106

Ernst, U., Pawelzik, K. and Geisel, T. (1995). Synchronization induced by temporal delays in pulse-coupled oscillators. *Physical Review Letters*, *74*, 1570-1573. 21

Ernst, U., Pawelzik, K. and Geisel, T. (1998). Delay-induced multistable synchronization of biological oscillators. *Physical Review E*, *57*, 2150-2162. 21, 57

Faloutsos, M., Faloutsos, P. and Faloutsos, C. (1999). On Power-law Relationships of the Internet Topology. In *SIGCOMM '99: Proceedings of the conference on Applications, technologies, architectures, and protocols for computer communication* (pp. 251–262). New York, NY, USA: ACM Press. 90

Fontanari, J. F. and Köberle, R. (1988). Information-processing in synchronous neural networks. *Journal de Physique*, *49*, 13-23. 51

Fowlkes, E. B. (1979). Some methods for studying the mixture of two normal (lognormal) distributions. *Journal of the American Statistical Association*, *74*, 561-575. 62

Fusi, S. and Mattia, M. (1999). Collective behavior of networks with linear (vlsi) integrate and fire neurons. *Neural Computation*, *11*, 633-652. 22

Gerstein, G. L. and Mandelbrot, B. (1964). Random walk models for the spike activity of a single neuron. *Biophys J*, *4*, 41–68. 15, 17, 22

Gerstner, W. (1996). Rapid phase locking in systems of pulse-coupled oscillators with delays. *Physical Review Letters*, *76*, 1755-1758. 21

Gerstner, W. (2000). Population dynamics of spiking neurons: Fast transients, asynchronous states, and locking. *Neural Computation*, *12*, 43-89. 23

Goldie, C. and Kluppelberg, C. (1998). Subexponential distributions. In R. Adler, R. Feldman and M. Taqqu (Eds.), *Practical guide to heavy tails: Statistical techniques for analysing heavy tails* (pp. 435–459). Basel, Switzerland: Birkhauser. 64

Goldstein, M. L., Morris, S. A. and Yen, G. G. (2004). Problems with fitting to the power-law distribution. *The European Physical Journal B*, *41*(2), 255-258. 66, 90

Gómez, V., Kaltenbrunner, A. and López, V. (2006). Event modeling of message interchange in stochastic neural ensembles. In *IJCNN'06 proceedings* (p. 81-88). Vancouver, BC, Canada: IEEE World Congress of Computational Intelligence. 57

Gómez, V., Kaltenbrunner, A. and López, V. (2008). Statistical analysis of the social network and discussion threads in Slashdot. In *17th International World Wide Web Conference (WWW2008)*. Beijing, China: ACM Digital Library. (in prepartion) 91

Gong, P. L. and van Leeuwen, C. (2007). Dynamically maintained spike timing sequences in networks of pulse-coupled oscillators with delays. *Physical Review Letters*, *98*, 048104. 22

Habermas, J. (1962/1989). *The structural transformation of the public sphere : Inquiry into a category of bourgeois society*. Cambridge, MA, USA: MIT Press. 62

Harder, U. and Paczuski, M. (2006). Correlated dynamics in human printing behavior. *Physica A, 361*, 329-336. 61

Henderson, T. and Bhatti, S. (2001). Modelling user behaviour in networked games. In *MULTIMEDIA '01: Proceedings of the 9th ACM International Conference on Multimedia* (pp. 212–220). New York, NY, USA: ACM Press. 61

Herz, A. V. M. and Marcus, C. M. (1993). Distributed dynamics in neural networks. *Physical Review E, 47*, 2155-2161. 51, 56

Hirsch, J. E. (2005). An index to quantify an individual's scientific research output. *Proceedings of the National Academy of Sciences, 102*, 16569. 107

Hong, Y. W. and Scaglione, A. (2005). A scalable synchronization protocol for large scale sensor networks and its applications. *IEEE Journal On Selected Areas In Communications, 23*, 1085-1099. 58

Hoppensteadt, F. C. and Izhikevich, E. M. (1997). *Weakly connected neural networks*. Secaucus, NJ, USA: Springer-Verlag New York, Inc. 8

Hu, A. S. and Servetto, S. D. (2006). On the scalability of cooperative time synchronization in pulse-connected networks. *IEEE Transactions On Information Theory, 52*, 2725-2748. 58

Ikegaya, Y., Aaron, G., Cossart, R., Aronov, D., Lampl, I., Ferster, D. et al. (2004). Synfire chains and cortical songs: Temporal modules of cortical activity. *Science, 304*, 559-564. 22

Izhikevich, E. M. (2006). Polychronization: Computation with spikes. *Neural Computation, 18*, 245–282. 22

Izhikevich, E. M. (2007). *Dynamical systems in neuroscience: The geometry of excitability and bursting*. Cambridge, MA, USA: The MIT press. 7, 8, 9

Izhikevich, E. M., Gally, J. A. and Edelman, G. M. (2004). Spike-timing dynamics of neuronal groups. *Cerebral Cortex, 14*, 933-944. 22

Joachims, T. (2002). *Learning to classify text using support vector machines – methods, theory, and algorithms*. Norwell, MA, USA: Kluwer Academic Publishers. 107

Johansen, A. (2004). Probing human response times. *PHYSICA A, 338*, 286. 61

Kaltenbrunner, A., Gómez, V. and López, V. (2007a). Description and prediction of slashdot activity. In *Proceedings of the 5th Latin American Web Congress (LA-WEB 2007)*. Santiago de Chile: IEEE Computer Society. 99

Kaltenbrunner, A., Gómez, V. and López, V. (2007b). Phase transition and hysteresis in an ensemble of stochastic spiking neurons. *Neural Computation, 19*(11), 3011–3050.

Kaltenbrunner, A., Gómez, V., Moghnieh, A., Meza, R., Blat, J. and López, V. (2007). Homogeneous

temporal activity patterns in a large online communication space. In *Proceedings of the BIS 2007 Workshop on Social Aspects of the Web (SAW 2007)*. Poznan, Poland: CEUR-WS.

Kaneko, K. (1990). Clustering, coding, switching, hierarchical ordering, and control in a network of chaotic elements. *Physica D*, *41*, 137-172. 22

Kirk, V. and Stone, E. (1997). Effect of a refractory period on the entrainment of pulse-coupled integrate-and-fire oscillators. *Physics Letters A*, *232*, 70-76. 21

Kleban, S. D. and Clearwater, S. H. (2003). Hierarchical dynamics, interarrival times, and performance. In *SC '03: Proceedings of the 2003 ACM/IEEE conference on Supercomputing* (p. 28). Washington, DC, USA: IEEE Computer Society. 61

Kuramoto, Y. (1984). *Chemical oscillations, waves and turbulence*. Berlin: Springer. 8, 22

Lampe, C. and Resnick, P. (2004). Slash(dot) and burn: Distributed moderation in a large online conversation space. In *CHI '04: Proceedings of the SIGCHI conference on Human factors in computing systems* (pp. 543–550). New York, NY, USA: ACM Press. 62

Lawrence, R. (1988). The Lognormal as Event-Time Distribution. In E. L. Crow and K. Shimizu (Eds.), *Lognormal Distributions: Theory and Applications* (p. 211-228). New York: Marcel Dekker, Inc. 62

Leskovec, J., Adamic, L. A. and Huberman, B. A. (2006). The dynamics of viral marketing. In *EC '06: Proceedings of the 7th ACM conference on Electronic commerce* (pp. 228–237). New York, NY, USA: ACM Press. 99

Limpert, E., Stahel, W. A. and Abbt, M. (2001). Log-normal distributions across the sciences: Keys and clues. *Bioscience*, *51*, 341-352. 62, 84

Lindner, B. (2004). Interspike interval statistics of neurons driven by colored noise. *Physical Review E*, *69*, 022901. 22

Mainardi, F., Raberto, M., Gorenflo, R. and Scalas, E. (2000). Fractional calculus and continuous-time finance ii: the waiting-time distribution. *Physica A*, *287*, 468-481. 61

Malda, R. (2002). *Slashdot FAQ: Comments and Moderation.* (http://slashdot.org/faq/com-mod.shtml#cm2000) 93

Masoliver, J., Montero, M. and Weiss, G. H. (2003). Continuous-time random-walk model for financial distributions. *Physical Review E*, *67*, 021112. 61

McMillen, D. and Kopell, N. (2003). Noise-stabilized long-distance synchronization in populations of model neurons. *Journal of Computational Neuroscience*, *15*, 143-157. 23

Middleton, J. W., Chacron, M. J., Lindner, B. and Longtin, A. (2003). Firing statistics of a neuron model driven by long-range correlated noise. *Physical Review E*, *68*, 021920. 22

Mirollo, R. E. and Strogatz, S. H. (1990). Synchronization of pulse-coupled biological oscillators. *SIAM Journal on Applied Mathematics*, *50*(6), 1645–1662. 16, 21, 57, 105

Mishne, G. and Glance, N. (2006). Leave a reply: An analysis of weblog comments. In *Www2006, 3rd annual workshop on the weblogging ecosystem*. Edinburgh, UK. 63

Mitzenmacher, M. (2004). A brief history of generative models for power law and lognormal distributions. *Internet Mathematics*, *1*(2), 226-251. 62

Naruse, K. and Kubo, M. (2006). Lognormal distribution of bbs articles and its social and generative mechanism. In *WI'06: Proceedings of the 2006 IEEE/WIC/ACM International Conference on Web Intelligence* (pp. 103–112). Washington, DC, USA: IEEE Computer Society. 63, 91, 97

Néda, Z., Ravasz, E., Brechet, Y., Vicsek, T. and Barabási, A. L. (2000). The sound of many hands clapping - tumultuous applause can transform itself into waves of synchronized clapping. *Nature*, *403*, 849-850. 21

Newman, M. E. J. (2003). The structure and function of complex networks. *SIAM Review*, *45*, 167. 107

Newman, M. E. J. (2005). Power laws, pareto distributions and zipf's law. *Contemporary Physics*, *46*, 323-351. 61, 65, 83

Östborn, P. (2002). Phase transition to frequency entrainment in a long chain of pulse-coupled oscillators. *Physical Review E*, *66*, 016105. 22, 58, 105

Östborn, P., Åberg, S. and Ohlén, G. (2003). Phase transitions towards frequency entrainment in large oscillator lattices. *Physical Review E*, *68*, 015004. 22, 58

Paxson, V. and Floyd, S. (1995). Wide area traffic: The failure of Poisson modeling. *IEEE-ACM Transactions On Networking*, *3*, 226-244. 61

Peskin, C. (1975). *Mathematical aspects of heart physiology*. New York: Courant Institute of Mathematical Sciences, New York University. 16, 21

Pikovsky, A., Rosenblum, M. and Kurths, J. (2001). *Synchronization: A universal concept in nonlinear sciences*. Cambridge, UK: Cambridge University Press. 7, 8, 10

Poor, N. (2005). Mechanisms of online public sphere: The web site Slashdot. *Journal of Computer-Mediated Communication*, *10*(2). 62

Press, W. H., Flannery, B. P., Teukolsky, S. A. and Vetterling, W. T. (1992). *Numerical Recipes in C: The Art of Scientific Computing* (2nd ed.). Cambridge, UK: Cambridge University Press. 66

Quiroga, R. Q., Arnhold, J. and Grassberger, P. (2000). Learning driver-response relationships from synchronization patterns. *Physical Review E*, *61*, 5142-5148. 106

Ratcliff, R. and Smith, P. L. (2004, April). A comparison of sequential sampling models for two-choice reaction time. *Psychol Rev*, *111*(2), 333–367. 12, 13

Redner, S. (2001). *A guide to first-passage processes*. Cambridge, UK: Cambridge University Press. 15

Rhouma, M. B. H. and Frigui, H. (2001). Self-organization of pulse-coupled oscillators with ap-

plication to clustering. *IEEE Transactions On Pattern Analysis And Machine Intelligence*, *23*, 180-195. 58

Rodríguez, F., Suárez, A. and López, V. (2001). Period focusing induced by network feedback in populations of noisy integrate-and-fire neurons. *Neural Computation*, *13*, 2495–2516. 16, 23, 25, 26, 27, 28, 44, 45, 57

Rodríguez, F., Suárez, A. and López, V. (2002). A discrete model of neural ensembles. *Philosophical Transactions of The Royal Society: Mathematical, Physical and Engineering Sciences*, *360*, 559–573. 17, 27, 106

Ross, S. M. (2003). *Introduction to probability models* (8th ed.). Orlando, FL, USA: Academic Press, Inc. 11

Salinas, E. and Sejnowski, T. J. (2002). Integrate-and-fire neurons driven by correlated stochastic input. *Neural Computation*, *14*, 2111-2155. 22

Senn, W. and Urbanczik, R. (2000). Similar nonleaky integrate-and-fire neurons with instantaneous couplings always synchronize. *SIAM Journal On Applied Mathematics*, *61*, 1143-1155. 21, 39, 57, 105

Sigman, K. (1999). Appendix: A primer on heavy-tailed distributions. *Queueing Systems*, *33*, 261-275. 61, 64

Smirnov, D. A. and Andrzejak, R. G. (2005). Detection of weak directional coupling: Phase-dynamics approach versus state-space approach. *Physical Review E*, *71*, 036207. 106

Smith, P. L. (2000). Stochastic dynamic models of response time and accuracy: a foundational primer. *J. Math. Psychol.*, *44*(3), 408–463. 11, 12, 13

Smith, P. L. and Ratcliff, R. (2004). Psychology and neurobiology of simple decisions. *Trends in Neuroscience*, *27*, 161–168. 12

Stein, R. B. (1965). A theoretical analysis of neuronal variability. *Biophys J*, *5*, 173–194. 15

Stein, R. B. (1967). Some models of neuronal variability. *Biophysical Journal*, *7*, 37-68. 22

Stouffer, D. B., Malmgren, R. D. and Amaral, L. A. N. (2006). *Log-normal statistics in e-mail communication patterns.* (e-print physics/0605027) 61, 63, 75, 98, 104

Timme, M., Wolf, F. and Geisel, T. (2002). Prevalence of unstable attractors in networks of pulse-coupled oscillators. *Physical Review Letters*, *89*(15), 154105. 22, 106

Tuckwell, H. C. (1988). *Introduction to theoretical neurobiology: Volume 2, nonlinear and stochastic theories.* Cambridge, UK: Cambridge University Press. 22

Uhlenbeck, G. E. and Ornstein, L. S. (1930). On the theory of brownian motion. *Phys. Rev.*, *36*, 823-841. 15

van Vreeswijk, C. (1996). Partial synchronization in populations of pulse-coupled oscillators. *Physical Review E*, *54*, 5522-5537. 22, 105

van Vreeswijk, C. and Abbott, L. F. (1993). Self-sustained firing in populations of integrate-and-fire neurons. *SIAM Journal On Applied Mathematics*, *53*, 253-264. 16, 23, 25, 43, 57

Vázquez, A. (2005). Exact results for the barabási model of human dynamics. *Physical Review Letters*, *95*, 248701. 104

Vázquez, A., Oliveira, J. G., Dezso, Z., Goh, K. I., Kondor, I. and Barabási, A. L. (2006). Modeling bursts and heavy tails in human dynamics. *Physical Review E*, *73*, 036127. 61, 98

Wang, X. J. (2001). Synaptic reverberation underlying mnemonic persistent activity. *Trends In Neurosciences*, *24*, 455-463. 23, 56

Winfree, A. T. (1967). Biological rhythms and the behavior of populations of coupled oscillators. *J. Theoret. Biol.*, *16*, 15-42. 22

Winfree, A. T. (2001). *The geometry of biological time* (2nd ed.). New York, USA: Springer. 15